

**CARBON CAPTURE PERFORMANCE AND
PROPERTIES OF CEMENTITIOUS MATERIAL WITH
LOCAL WASTE BIOCHAR**

PRISCILLA GUNN FONG ERN

**FACULTY OF ENGINEERING
UNIVERSITI MALAYA
KUALA LUMPUR**

2024

**CARBON CAPTURE PERFORMANCE AND
PROPERTIES OF CEMENTITIOUS MATERIAL WITH
LOCAL WASTE BIOCHAR**

PRISCILLA GUNN FONG ERN

**DISSERTATION SUBMITTED IN FULFILMENT OF
THE REQUIREMENTS FOR THE DEGREE OF MASTER
OF ENGINEERING SCIENCE**

**FACULTY OF ENGINEERING
UNIVERSITI MALAYA
KUALA LUMPUR**

2024

UNIVERSITI MALAYA
ORIGINAL LITERARY WORK DECLARATION

Name of Candidate: Priscilla Gunn Fong Ern

Matric No: S2199059/1

Name of Degree: Master of Engineering Science

Title of Dissertation ("this Work"): Carbon Capture Performance and Properties of Cementitious Material with Waste Biochar

Field of Study: Civil Engineering (Engineering and Engineering Trades)

I do solemnly and sincerely declare that:

- (1) I am the sole author/writer of this Work;
- (2) This Work is original;
- (3) Any use of any work in which copyright exists was done by way of fair dealing and for permitted purposes and any excerpt or extract from, or reference to or reproduction of any copyright work has been disclosed expressly and sufficiently and the title of the Work and its authorship have been acknowledged in this Work;
- (4) I do not have any actual knowledge nor do I ought reasonably to know that the making of this work constitutes an infringement of any copyright work;
- (5) I hereby assign all and every rights in the copyright to this Work to the Universiti Malaya ("UM"), who henceforth shall be owner of the copyright in this Work and that any reproduction or use in any form or by any means whatsoever is prohibited without the written consent of UM having been first had and obtained;
- (6) I am fully aware that if in the course of making this Work I have infringed any copyright whether intentionally or otherwise, I may be subject to legal action or any other action as may be determined by UM.

Candidate's Signature

Date: 01 – 12 – 2024

Subscribed and solemnly declared before,

Witness's Signature

Date: 03-12-2024

Name:

Designation:

CARBON CAPTURE PERFORMANCE AND PROPERTIES OF CEMENTITIOUS MATERIAL WITH LOCAL WASTE BIOCHAR

ABSTRACT

Considerable attention has been devoted to investigating the viability of utilizing sustainable alternatives derived from agricultural waste to partially replace cement in the construction industry. The shift to alternatives is primarily driven by the significant pollution generated by the industries over the years. Malaysia is known for its extensive plantations of various crops, which is a significant contribution to the economy of the country. The crop plantation in Malaysia produced a large amount of waste, posing challenges in waste utilization and disposal. The waste may be valorized by converting into biochar and incorporating into cement concrete products. Biochar is known for its potential in carbon sequestration, making it a prominent subject of study for environmental benefits. Four types of biochar were obtained and studied for its characterization, properties and carbon sequestration potential. These four types of biochar include rice husk biochar (RHB), palm kernel shell biochar (PKS), coconut husk biochar (CHB), and bamboo biochar (BB). Upon characterization of the biochar, RHB and PKS which had the best carbon sequestration ability were selected for more comprehensive investigation in cement mortar.

This study presents experimental investigations on high dosage of locally produced RHB and PKS as cement replacement, specifically at 10, 20, 30 and 40% by volume. The incorporation of biochar as a partial replacement in cementitious material presents a means to mitigate the adverse effect of carbon dioxide (CO₂) emissions resulting from cement production. Comprehensive assessments were done to study the porosity, strength, microstructure, and thermal characterization of the PKS and RHB-added mortar composites as an initial phase to develop eco-friendly concretes. All these efforts were undertaken with the aim of maximizing waste valorization and carbon uptake of the

produced mortars. The incorporation of biochar caused a change in porosity of the matrix, which is favorable for carbon sequestration. The porosity of the mortar increased by 52.9% after the integration of biochar.

The experiment also focuses on enhancing the carbon sequestration ability of biochar-added cement composite through carbonation curing. Qualitative and quantitative carbonation tests were carried out to determine the carbonation rate of the RHB and PKS-added mortar. The addition of biochar has been shown to facilitate the carbonation process, as evidenced by the increase in carbonation depth and degree of carbonation. PKS-added mortars had a higher CO₂ uptake compared to RHB-added mortars. Saturated PKS-added mortar demonstrated the highest CO₂ uptake of 24.8% (i.e. 248 gCO₂/kg PKS-added mortar), greater than unsaturated PKS-added mortar. Besides, the carbonated mortars exhibited higher strength than the water-cured mortars, resolving the strength issue with higher biochar addition. The improvement in strength due to carbonation curing ranges from 26.7 – 87.0%. Overall, the optimum replacement of PKS at 30% by volume contributes to higher carbon uptake and an improved strength in cement mortar through carbonation curing. The findings evaluated the potential of biochar to be effectively used as an additive in cement mortar. Biochar not only reduces environmental impact, but also has the capability to sequester a significant amount of carbon in civil infrastructure.

Keywords: Biochar; High volume replacement; Carbonation curing; Compressive strength; Saturated biochar.

PRESTASI PENANGKAPAN KARBON DAN SIFAT BAHAN SIMEN DENGAN SISA BIO-ARANG

ABSTRAK

Tumpuan yang besar telah diberikan untuk menyelidik kesesuaian menggunakan alternatif lestari yang diperoleh daripada sisa pertanian untuk menggantikan sebahagian simen dalam industri pembinaan. Peralihan ini didorong terutamanya oleh pencemaran yang ketara yang dihasilkan oleh industri tersebut selama bertahun-tahun. Malaysia dikenali sebagai pengeluar bahan pertanian, yang secara signifikan menyumbang kepada ekonomi negara. Aktiviti-aktiviti pertanian di Malaysia menghasilkan banyak sisa setiap tahun dan hal ini menimbulkan cabaran dalam pelupusannya. Sisa-sisa ini boleh dijadikan bernilai dengan ditukarkan menjadi bio-arang dan ditambahkan ke dalam produk konkrit simen. Bio-arang dikenali dengan potensinya dalam penyerapan karbon dan sering dijadikannya subjek utama dalam pengkajian untuk alam sekitar. Empat jenis bio-arang telah dikaji untuk mendapatkan penilaian, sifat dan potensi penyerapan karbonnya. Empat jenis bio-arang ini termasuk bio-arang sekam padi (RHB), bio-arang kulit biji sawit (PKS), bio-arang kulit kelapa (CHB), dan bio-arang buluh (BB). Selepas pencirian biochar, RHB dan PKS yang mempunyai keupayaan penyerapan karbon terbaik telah dipilih untuk penyiasatan yang lebih komprehensif dalam mortar simen.

Kajian ini menyampaikan penyelidikan eksperimen menggunakan RHB dan PKS tempatan sebagai pengganti simen dalam dos tinggi, khususnya pada 10, 20, 30 dan 40% mengikut isipadu. Penggunaan bio-arang sebagai pengganti sebahagian dalam bahan simen merupakan cara untuk mengurangkan kesan negatif pelepasan karbon dioksida (CO_2) akibat pengeluaran simen. Penilaian yang menyeluruh telah dijalankan untuk mengkaji porositi, kekuatan, struktur mikro, dan ciri-ciri haba komposit mortar PKS dan RHB sebagai fasa awal untuk menghasilkan konkrit mesra alam. Pelbagai usaha telah dilaksanakan untuk matlamat menjadikan sisa-sisa bernilai dan memaksimumkan

penyerapan karbon untuk menghasilkan alternatif hijau yang mesra alam. Penggunaan bio-arang akan menyebabkan perubahan dalam porositi matriks, yang bermanfaat untuk penyerapan karbon. Porositi mortar meningkat sebanyak 52.9% selepas penyepaduan biochar.

Eksperimen ini juga memberi tumpuan pada peningkatan penyerapan karbon komposit bio-arang simen melalui pengawetan karbonasi. Ujian karbonasi kualitatif dan kuantitatif dijalankan untuk menentukan kadar karbonasi mortar RHB dan PKS. Penambahan bio-arang telah terbukti mempercepatkan proses karbonasi, seperti yang ditunjukkan dengan peningkatan kedalaman karbonasi dan tahap karbonasi. Mortar PKS mempunyai penyerapan CO₂ yang lebih tinggi berbanding mortar RHB. Mortar PKS yang tepu menunjukkan penyerapan CO₂ yang tertinggi sebanyak 24.8% (iaitu 248 gCO₂/kg mortar PKS), lebih tinggi daripada mortar PKS yang tidak tepu. Selain itu, mortar yang dikarbonasi menunjukkan kekuatan yang lebih tinggi berbanding mortar yang diawetkan dengan air, menyelesaikan isu kekuatan dengan penambahan bio-arang yang tinggi. Peningkatan kekuatan akibat pengawetan karbonasi berkisar antara 26.7 – 87.0%. Secara keseluruhannya, penggantian optimum PKS pada 30% mengikut isipadu menyumbang kepada penyerapan karbon yang lebih tinggi dan kekuatan yang lebih baik dalam mortar simen melalui pengawetan karbonasi. Laporan ini memberi penilaian kepada potensi bio-arang sebagai bahan tambahan dalam mortar simen. Bio-arang bukan sahaja mengurangkan kesan alam sekitar tetapi juga mempunyai kemampuan untuk menyerap lebih banyak karbon dalam infrastruktur awam.

Kata Kunci: Bio-arang, Penggantian isipadu tinggi; Pengawetan karbonasi; Kekuatan Mampatan; Bio-arang tepu.

ACKNOWLEDGEMENTS

I would like to extend my deepest gratitude to my supervisors, Dr. Onn Chiu Chuen, Prof. Ir. Dr. Mo Kim Hung and Associate Prof. Dr. Lee Hwei Voon, for their invaluable advice, continuous guidance and support throughout the course of my research and thesis writing. I truly appreciate their expertise and insights, which have played a pivotal role in shaping this work. Their support has not only facilitated my academic growth but has also been a source of motivation and inspiration.

I am also deeply thankful to my parents and family members for their endless love, encouragement, and understanding. They have been a constant source of strength and motivation for me. Their belief in me has been the foundation upon which I have built my academic journey.

A special and heartfelt thank you goes to my friends, whose guidance, assistance, and companionship have been indispensable throughout this process. Their help has been invaluable, and their support has been greatly appreciated. I am truly fortunate to have such amazing friends who have stood by me every step of the way. Besides, I would like to thank all the laboratory staff for their technical assistance.

I would like to acknowledge the support of the Ministry of Higher Education Malaysia under the Fundamental Research Grant Scheme (FRGS).

Last but not least, to all who have contributed in any way to the completion of this thesis, thank you for your support and encouragement. Your contributions have been truly valued and greatly appreciated.

TABLE OF CONTENTS

Abstract	iii
Abstrak	v
Acknowledgements	vii
Table of Contents	viii
List of Figures	xii
List of Tables.....	xv
List of Abbreviations.....	xvi
 CHAPTER 1: INTRODUCTION.....	1
1.1 Background.....	1
1.2 Problem Statement.....	4
1.3 Research Objectives.....	6
1.4 Research Scope	6
1.5 Research Significance.....	7
1.6 Thesis Organization.....	8
 CHAPTER 2: LITERATURE REVIEW.....	10
2.1 Introduction to Biochar.....	10
2.1.1 Market Analysis of Biochar	11
2.1.2 Properties and Applications of Biochar.....	12
2.1.3 Carbon Sequestration Potential of Biochar	15
2.1.4 Biochar Production Techniques and Parameters.....	19
2.1.5 Availability of Biochar in Malaysia	23
2.1.5.1 Rice Husk Biochar (RHB).....	23
2.1.5.2 Palm Kernel Shell Biochar (PKS).....	23

2.1.5.3	Coconut Husk Biochar (CHB)	24
2.1.5.4	Bamboo Biochar (BB).....	25
2.2	Utilization of Biochar in Cementitious Materials.....	25
2.2.1	Mechanical strength	26
2.2.2	Fluid Transport Properties.....	28
2.2.3	Chemical Stability	30
2.2.4	Thermal Conductivity.....	31
2.2.5	Flammability	32
2.3	Carbon Capture and Storage (CCS) in Cementitious Materials	32
2.3.1	Implementation of Carbon Capture and Storage (CCS) in the Industry ..	34
2.3.2	Accelerated Carbonation Curing	36
2.3.2.1	Pre-curing Condition	38
2.3.2.2	Carbonation Curing Condition	39
2.3.2.3	Post-curing Condition	41
2.3.2.4	Properties of Material in Influencing the Carbonation Rate	41
2.3.3	Carbonation Curing of Biochar-Added Cementitious Materials.....	43
2.4	Identification of Research Gap	47
2.5	Summary.....	48
CHAPTER 3: METHODOLOGY.....		50
3.1	Introduction.....	50
3.2	Preparation of Raw Materials	52
3.2.1	Sourcing of Binders	52
3.2.2	Characterization of Binders	56
3.2.2.1	X-ray Fluorescence (XRF)	56
3.2.2.2	Field Emission Scanning Electron Microscopy (FESEM).....	57
3.2.2.3	X-ray Diffraction (XRD).....	57

3.2.2.4	Proximate Analysis	57
3.2.2.5	Ultimate Analysis	58
3.2.2.6	Carbon Sequestration Potential (CSP)	58
3.2.2.7	Fourier-Transform Infrared Spectroscopy (FTIR)	60
3.2.2.8	Particle Size Distribution (PSD)	60
3.2.3	Fine Aggregates and Water	60
3.3	Saturation of Biochar with Carbon Dioxide (CO ₂).....	61
3.4	Mix Design	62
3.5	Mixing, Casting and Curing	65
3.5.1	Casting.....	65
3.5.2	Moist Curing.....	65
3.5.3	Carbonation Curing	65
3.6	Test Methods	66
3.6.1	Porosity.....	66
3.6.2	Carbonation Depth	67
3.6.3	Compressive Strength.....	68
3.6.4	Carbonation Degree.....	68
3.7	Microstructure Analysis.....	69
3.7.1	X-ray Diffraction (XRD) Analysis.....	69
3.7.2	Fourier-Transform Infrared Spectroscopy (FTIR) Analysis	70
3.7.3	Field Emission Scanning Electron Microscopy – Energy Dispersive X-ray (FESEM-EDS) Analysis.....	71
CHAPTER 4: RESULTS AND DISCUSSION		72
4.1	Characterization of Biochar	72
4.1.1	X-ray Fluorescence (XRF)	72
4.1.2	Field Emission Scanning Electron Microscopy (FESEM).....	73

4.1.3	X-ray Diffraction (XRD).....	74
4.1.4	Proximate Analysis.....	76
4.1.5	Ultimate Analysis	77
4.1.6	Carbon Sequestration Potential (CSP)	79
4.1.7	Fourier-Transform Infrared Spectroscopy (FTIR)	81
4.1.8	Particle Size Distribution (PSD).....	84
4.1.9	Saturation of Biochar with Carbon Dioxide (CO ₂)	85
4.2	Porosity of Biochar-Added Mortar	86
4.3	Carbonation Depth of Biochar-Added Mortar.....	91
4.4	Compressive Strength of Biochar-Added Mortar.....	97
4.5	Carbonation Degree of Biochar-Added Mortar.....	106
4.6	X-ray Diffraction (XRD) Analysis	114
4.7	Fourier-Transform Infrared Spectroscopy (FTIR) Analysis.....	117
4.8	Field Emission Scanning Electron Microscopy – Energy Dispersive X-ray (FESEM-EDS) Analysis	120
CHAPTER 5: CONCLUSION AND RECOMMENDATIONS		127
5.1	Conclusion	127
5.2	Recommendations.....	129
References		130
List of Publications and Papers Presented		142

LIST OF FIGURES

Figure 1.1: Main SDGs addressed in this study	3
Figure 2.1: Hardwood biochar	11
Figure 2.2: Extrapolated Global Biochar Market Size from 2023 to 2032 (Precedence Research, 2023).....	12
Figure 2.3: Various applications of biochar (Shafawi et al., 2021)	14
Figure 2.4: Possible mechanisms of CO ₂ adsorption on biochar (Shafawi et al., 2021)	16
Figure 2.5: Factors affecting biochar adsorption of CO ₂ (J. Liu et al., 2022).....	17
Figure 2.6: Conversion of biomass into biochar at different pyrolysis temperatures (A) Characteristics phases of biochar (B) Composition of biochar (Jung et al., 2019).....	21
Figure 2.7: Recycling of crude palm oil waste (Golden Agri-Resources, 2018).....	24
Figure 2.8: Compressive strength of wood biochar-added mortar (Navaratnam et al., 2021)	27
Figure 2.9: Thermal conductivity and biochar dosing correlation (Sikora et al., 2022).....	31
Figure 2.10: CCS technology in the industry (CarbonCure Technology, 2024)	35
Figure 2.11: Six types of carbonation curing methods (Ferrara et al., 2023)	37
Figure 2.12: Common procedures for the carbonation curing process (D. Zhang et al., 2017)	37
Figure 2.13: Preconditioning improves carbon uptake (El-Hassan et al., 2013)	39
Figure 2.14: Effect of w/b ratio on carbonation degree of cement paste (J. Wang et al., 2019)	42
Figure 3.1: Conceptual Framework of the research study	51
Figure 3.2: The production of RHB from rice husk waste at Sendi Enterprise	53
Figure 3.3: The biochar experimenters kit at MPOB, Kajang (Haryati et al., 2018).....	54
Figure 3.4: Locally obtained biochar (a) RHB (b) PKS (c) CHB (d) BB	55
Figure 3.6: Operating carbonation chamber at the set parameters	66

Figure 3.7: Color change of phenolphthalein solution.....	68
Figure 4.1: Surface morphology of (a) RHB; (b) PKS; (c) CHB; (d) BB at magnification 500x.....	73
Figure 4.2: XRD patterns of biochar (a) RHB (b)PKS (c) CHB (d) BB	75
Figure 4.3: The Van Krevelen diagram of biomass and its equivalent biochar	78
Figure 4.4: T ₅₀ values obtained from TGA graph	80
Figure 4.5: FTIR results for RHB	82
Figure 4.6: FTIR spectra for PKS	83
Figure 4.7: PSD of raw materials	84
Figure 4.8: FTIR results for both saturated and unsaturated RHB	85
Figure 4.9: Apparent porosity for XRHB-added cement mortar for both water and carbonation curing.....	87
Figure 4.10: Apparent porosity for XPKS-added cement mortar for both water and carbonation curing.....	89
Figure 4.11: Comparison of apparent porosity for RHB and PKS biochar	90
Figure 4.12: Carbonation depth of RHB-added mortars for 3d and 7d of carbonation curing.....	91
Figure 4.13: Carbonation depth of PKS-added mortars for 3d and 7d of carbonation curing	93
Figure 4.14: Comparison of carbonated area with RHB and PKS-added mortars using ImageJ analysis	97
Figure 4.15: Compressive strength of RHB-added mortar at 3d curing against control	98
Figure 4.16: Compressive strength of RHB-added mortar at 7d curing against control	99
Figure 4.17: Compressive strength of RHB-added mortar at 28d curing against control	100
Figure 4.18: Combined curing for XRHB-added mortar	101
Figure 4.19: Compressive strength for PKS-added mortar at 3d, 7d and 28d	103

Figure 4.20: Comparison of compressive strength for combined curing of PKS-added mortar	104
Figure 4.21: Comparison of saturated and unsaturated PKS-added mortar at (a) 7d and (b) 28d curing	105
Figure 4.22: Comparison of compressive strength of RHB and PKS-added mortars for (a) water curing and (b) carbonation curing	106
Figure 4.23: Comparison of TGA curves for water cured and carbonation cured control specimens at 7d	107
Figure 4.24: TGA curves for (a) RHB-added mortar and (b) PKS-added mortar at 7d carbonation curing.....	108
Figure 4.25: CO ₂ uptake of RHB and PKS-added mortar at 3d, 7d and 28d carbonation curing.....	109
Figure 4.26: CO ₂ uptake and calcium carbonate content of saturated and unsaturated PKS at 7d curing.....	111
Figure 4.27: Compressive strength versus CO ₂ uptake for (a) SPKS- added mortars (b) SRHB-added mortars after full 7d carbonation curing	113
Figure 4.28: XRD patterns of RHB-added mortar	115
Figure 4.29: XRD patterns for PKS-added mortar	116
Figure 4.30: FTIR spectra of RHB-added mortar	118
Figure 4.31: FTIR Spectra for PKS-added mortar	119
Figure 4.32: FESEM images of (a) RN10X-W28 (b) RN20X-W28 (c) RN30X-W28 (d) RN40X-W28 at 1000x magnification	121
Figure 4.33: (a) RN20X-W28 at magnification 1000x (b, c) RN20X-C28 (d) N0-C28 at magnification 10,000x.....	122
Figure 4.34: EDS elemental spectrum of FESEM spots in Figure 4.33 and 4.34.....	123
Figure 4.35: (a) N0-W3 (b) PN20X-W3 (c) N0-W28 (d) PN20X-W28 (e) PN30X-W28 (f) PN40X-W28 at magnification 1000x.....	124
Figure 4.36: PN20X-C28 at magnification 1000x	125
Figure 4.37: (a) PN10X-W28 (b) PN20X-W28 at magnification 1000x (c) N0-C28 (d) PN40X-C28 at magnification 10,000x.....	126

LIST OF TABLES

Table 2.1: Summary of surface modification and CO ₂ adsorption capacity of biochar of previous studies.....	18
Table 2.2: Comparison of different production techniques of biochar (Cha et al., 2016; Danesh et al., 2023; Uday et al., 2022)	20
Table 2.3: Summary and results of carbonate cured biochar-added cementitious materials	45
Table 3.1: Standard strength requirement based on ASTM C109M.....	52
Table 3.2: Methods for characterization of biochar according to their properties.....	56
Table 3.3: Particle size distribution of CEN reference sand	60
Table 3.4: Mix proportion of biochar-added mortar	63
Table 3.5: Mix proportion of biochar-added paste.....	64
Table 3.6: Different curing regimes for biochar-added cement mortar	64
Table 4.1: Chemical composition of OPC, RHB, CHB and BB through XRF.....	72
Table 4.2: Proximate analysis of biochar	76
Table 4.3: Physicochemical properties of biochar through ultimate analysis.....	77
Table 4.4: Assessment parameters for CSP calculation of the biochar.....	80
Table 4.5: FTIR spectra of RHB	82
Table 4.6: FTIR spectra wavelengths for PKS.....	83
Table 4.7: Carbonation depth results of RHB-added mortars using imageJ analysis.....	95
Table 4.8: Carbonation depth results of PKS-added mortars using imageJ analysis.....	96
Table 4.9: Summary of FTIR peaks and bands for biochar-added mortar.....	119

LIST OF ABBREVIATIONS

AFm	:	Aluminate Ferrite Monosulfate
AFt	:	Ettringite
BB	:	Bamboo Biochar
Ca/Si	:	Calcium-to-silicon ratio
CCS	:	Carbon Capture and Storage
CHB	:	Coconut Husk Biochar
CO ₂	:	Carbon Dioxide
C-S-H	:	Calcium Silicate Hydrate
CSP	:	Carbon Sequestration Potential
EDS	:	Energy-Dispersive X-Ray Spectroscopy
FESEM	:	Field Emission Scanning Electron Microscopy
FTIR	:	Fourier-Transform Infrared Spectroscopy
GHG	:	Greenhouse Gas
PKS	:	Palm Kernel Shell Biochar
PSD	:	Particle Size Distribution
RHB	:	Rice Husk Biochar
SPKS	:	Saturated Palm Kernel Shell Biochar
SRHB	:	Saturated Rice Husk Biochar
TGA	:	Thermogravimetric Analysis
w/b	:	Water-to-binder ratio
XPKS	:	Unsaturated Palm Kernel Shell Biochar
XRHB	:	Unsaturated Rice Husk Biochar
XRD	:	X-ray Diffraction
XRF	:	X-ray Fluorescence

CHAPTER 1: INTRODUCTION

1.1 Background

Global warming presents a major risk to numerous facets of life, such as the economy, the environment, and public health. Energy generation and manufacturing industries have substantially contributed to the rapid increase in greenhouse gas (GHG) emissions worldwide. The cement manufacturing is energy intensive and it releases a substantial amount of carbon dioxide (CO₂) into the atmosphere. This widespread emission of GHG from development and construction activities contributes to global crises, including pollution, climate change, resource depletion, and other environmental problems. In the year 2022 alone, more than 36.8 billion tonnes of CO₂ were released into the atmosphere, accelerating at an unprecedented rate of 2.2 ppm per annum, with the cement industry alone accounting for at least 7% of global CO₂ emissions (International Energy Agency, 2022; Kaliyavaradhan & Ling, 2017; Supriya et al., 2023).

The environmental consciousness in the construction industry, with a stronger focus on sustainability becomes more pronounced towards the end of the 20th century and into the early 21st century. During this period, many parties, including governments and regulatory bodies, started implementing stricter environmental regulations and policies aimed at reducing GHG emissions and promoting sustainable construction practices.

The Paris Agreement adopted in 2015 targets to combat climate change and accelerate actions needed for a sustainable, low-carbon future. This agreement seeks to keep the global average temperature rise well below 2°C above pre-industrial levels, with efforts to limit the increase to 1.5°C (UNFCCC, 2015). Since the adoption of the Paris Agreement, public awareness and corporate efforts have been intensified, with a strong commitment on achieving net-zero emissions by the second half of the century, ideally by 2050.

Abundant research had been carried out to investigate the feasibility of alternative supplementary cementitious materials. These substitute materials include limestone, recycled aggregate, natural pozzolans, silica fume, metakaolin, slag, fly ash, biochar, etc. to promote green concrete production while maintaining the performance of the concrete. These materials serve as partial replacements for cement or sand, thus reducing pollution and lessening reliance on non-renewable resources (Mehdizadeh et al., 2022; Ren et al., 2022).

Biochar is being studied for its potential as a supplementary cementitious material to promote waste reduction and sustainability. Biochar is a stable form of charcoal produced through the pyrolysis of agricultural waste. Biochar has excellent properties as a material, exhibiting high adsorption capability through its numerous pores, wide surface area and good stability, addressing multiple contemporary concerns in the industries (Barbhuiya et al., 2024). The applications of biochar included are livestock farming, agriculture, construction industries, soil remediation, decontamination, chemical recovery, carbon sequestering and wastewater treatment. Biochar exhibits its significant effect in the long-term approach in reducing CO₂ emission and sequestering of GHG.

Decarbonization of the concrete industry leading to carbon neutral concrete can also be done through the mineralization of activated minerals or industrial wastes to form carbonates. This process of capturing CO₂ and converting it into stable carbonate minerals complements the carbon capture and storage (CCS) technologies. In recent years, the carbonation of cement, supplementary cementitious materials, artificial aggregates and wastes have been explored and examined to embody a negative carbon footprint (Z. Liu & Meng, 2021; D. Zhang et al., 2017). Therefore, a study is to be conducted to research and enhance the CO₂ sequestration of biochar through concrete carbonation. The adoption of green technology not only enhances the characteristics of cement-based composites,

but also facilitates waste recycling and CO₂ utilization, with the aim of successfully achieving carbon negative concrete production.

The application of biochar into cementitious materials promotes the attainment of the Sustainable Development Goals (SDG). The SDG provides a global framework for guiding sustainable development practices in the construction sector. Figure 1.1 illustrates the SDGs related to the current research of integrating biochar into cementitious materials.



Figure 1.1: Main SDGs addressed in this study

Utilization of biochar from waste contributes to SDG 7 and SDG 12. The production of biochar promotes the use of biomass waste, which can be considered part of clean energy solutions, reducing reliance on non-renewable resources. The pyrolysis of biochar also produces syngas and biofuel, which can be used for heat and power generation. This process reduces waste generation, promotes recycling of materials, and adopts sustainable production processes. Integrating biochar into concrete can decrease the demand for Portland cement, which is energy-intensive to produce. According to the SDG progress report 2024, global CO₂ emissions per unit of GDP have decreased by 11.5% from 2015 to 2021, with the manufacturing sector achieving a 16% reduction (United Nation, 2023).

SDG 9 involves the development of resilient infrastructure, the promotion of sustainable industrialization, and innovation in construction practices. Incorporating biochar into mortar enhances the properties of construction materials, such as thermal insulation and strength. It is an innovation that encourages the adoption of new technologies and practices, producing sustainable building materials. SDG 11 relates to building sustainable cities and communities, including green building practices and sustainable urban planning. The incorporation of biochar in mortar reduces the carbon footprint of construction materials, resulting in lower environmental impacts.

Biochar has a unique ability to sequester carbon, which directly contributes to SDG 13 by enhancing the carbon sequestration ability of the construction materials. The use of biochar in mortar can significantly lower CO₂ emission compared to conventional Portland cement. By implementing biochar into cementitious material, the construction industry can mitigate climate change impacts. The environmental benefits of biochar also extend to SDG 15 by promoting sustainable land management and reducing the environmental impact of construction activities.

1.2 Problem Statement

The construction industry faces significant sustainability challenges due to its reliance on cement, which contributes substantially to CO₂ emissions and environmental degradation. As the demand for concrete continues to rise, there is an urgent need to find supplementary cementitious materials to reduce the usage of cement, even if only partially. Biochar presents a promising alternative due to its potential for carbon sequestration and its ability to enhance the properties of cementitious materials. However, the effectiveness of biochar as a supplementary cementitious material in reducing the carbon footprint of concrete and improving its performance remains relatively underexplored. The current emphasis of biochar research is primarily on soil application

due to its significant benefits in agriculture. The understanding of the distinct effects of biochar on concrete application is still rather limited. The effect of biochar added into cementitious materials is strongly dependent on the type and characteristic of the biochar. Different types of biochar with different content may affect the mortar properties differently. The interaction between biochar and cement composite needs to be thoroughly studied to comprehend its role in governing the mechanical strength of the cementitious material.

Biochar has been widely recognized for its environmental benefits, but most of the research focused on biochar produced from generic sources. This has left a significant gap in understanding the specific properties and potential advantages of biochar derived from local waste materials. The unique characteristics of local waste biochar may offer distinct benefits. This study aims to fill the gap by investigating the properties of biochar derived from local waste sources. By focusing on locally available materials, this research seeks to demonstrate the environmental advantages of using local waste biochar, particularly in enhancing carbon sequestration. The findings could provide valuable insights into how local waste can be transformed into a resource that contributes to both environmental sustainability and local economies.

Moreover, much of the research to date has focused on biochar applied at standard dosage levels of 0.5 – 5%, overlooking the potential outcomes of higher dosage levels on environmental and material performance. The impact of applying biochar in high dosages remains unexamined. This approach of high dosages of biochar aims to recycle more waste while enhancing the carbon capture efficiency of construction materials.

Furthermore, the assessment of the carbon sequestration potential of biochar-infused cement composites must be done. It is crucial to quantify the extent of carbon

sequestration improvement achieved by incorporating biochar into cementitious materials to evaluate its sustainability in reducing carbon emissions effectively.

Despite the increasing interest in using biochar as a partial replacement for conventional cement, uncertainties and unexplored possibilities limit its widespread application in the construction industry. Thus, this research seeks to address these gaps by investigating the effects of high dosage of local waste biochar in cement mortar, aiming to contribute to more sustainable practices in waste management and carbon sequestration.

1.3 Research Objectives

The primary aim of this research is to investigate the carbon capture ability in cementitious material with local waste biochar. In achieving this aim, the research objectives are constructed as follows:

- I. To determine the characteristics of the local waste biochar obtained.
- II. To investigate the compressive strength of high-volume biochar replacement in cement-based material.
- III. To assess the carbon sequestration performance of high-volume biochar replacement in cement-based material.

1.4 Research Scope

Comprehensive assessments were carried out to characterize biochar and the biochar-added mortar composites as an initial phase to develop eco-friendly concretes. The research begins with obtaining four kinds of biochar, which are rice husk biochar (RHB),

palm kernel shell biochar (PKS), coconut husk biochar (CHB) and bamboo biochar (BB). The characterization of the physical and chemical properties of biochar provide insights into its effects when being incorporated into cementitious materials. The scope was narrowed down to two types of biochar with the best carbon sequestration potential selected for further evaluation in cement composites.

The biochar was introduced into the cement admixtures by 10, 20, 30 and 40% replacement by volume. Accelerated carbonation curing was employed to improve the carbon uptake of the cement mortars. Tests involving comparing different curing conditions (water curing and carbonation curing) and assessing the properties of the biochar-added mortar were conducted. These test included the compressive strength test and the porosity test. The depth and extent of carbon uptake were quantified, and the impact of integrating saturated and unsaturated biochar was also investigated.

A series of microstructural tests were conducted to study the interaction of biochar with the cement matrix and to correlate these findings with the macroscopic performance of the composites. The microstructural tests included were X-Ray Diffraction (XRD), Fourier-Transform Infrared Spectroscopy (FTIR) and Field Emission Scanning Electron Microscopy mounted with Energy Dispersive X-Ray (FESEM-EDS). The porosity and the strength performance of the produced mortars were evaluated, with the overall carbon sequestration of the cement mortars assessed.

1.5 Research Significance

The incorporation of biochar into mortar holds significant research value, particularly in enhancing carbon sequestration in cementitious materials. Biochar can effectively trap and store CO₂, aiding the mineralization process within the mortar. Additionally, the

accelerated carbonation curing approach proves to be a viable method for carbon sequestration in cement, thereby reducing the carbon footprint of construction materials. This aligns with global efforts to combat climate change by utilizing materials that mitigate carbon emissions.

Furthermore, the use of biochar provides a solution for reducing agricultural waste, addressing disposal problems, and promoting waste management. By partially incorporating biochar into cement composites, cement usage is reduced, leading to lower CO₂ emissions. By exploring the potential of biochar-mortar composites, this research aims to contribute by maximizing waste valorization and carbon uptake, contributing to the development of green, environmentally friendly alternatives and promoting sustainable concrete production.

1.6 Thesis Organization

This thesis is divided into five chapters, consisting of introduction, literature review, methodology, results and discussion and conclusion and recommendations. The contents of each chapter are structured as follows:

Chapter 1 provides an overview of the background in the context of the research, outlining the problem statement, objectives, and the scope of the study. This chapter also emphasizes the research significance and presents an overview of the structure of the thesis, providing a roadmap for the subsequent chapters.

Chapter 2 presents a comprehensive review of the relevant literature, focusing on biochar and its applications in cementitious materials. The market dynamics of biochar, its properties, and its performance in cement-based materials were presented. In addition, this chapter also covers the CCS technique, including the mineralization mechanism,

accelerated carbonation curing conditions and its implementation in industries. The research gap from the review has also been highlighted in this section.

Chapter 3 outlines the research methodology used in the study. It details the preparation and characterization of raw materials, including Ordinary Portland Cement (OPC) and biochar, and describes the mix design, casting, and curing processes. Following on, the testing methods used to evaluate the properties of the concrete are explained. The testing methods employed are porosity, carbonation depth, compressive strength, carbonation degree and several microstructural analyses.

Chapter 4 presents the overall findings of the research. It covers the characterization of biochar and its effects on mortar properties, including porosity, carbonation depth, compressive, and carbonation degree. This chapter integrates the results with existing literature, highlighting the performance of biochar-added mortar and providing a detailed discussion on the observed trends, correlations, and significance of the results. The carbon sequestration ability of the biochar-added mortar is especially evaluated and discussed in this chapter.

Chapter 5 summarizes the key conclusions drawn from the research and provides recommendations for future work. It reflects the overall findings and suggests areas for further research and development.

CHAPTER 2: LITERATURE REVIEW

2.1 Introduction to Biochar

In an era where environmental sustainability and waste management have become critical global concerns, innovative solutions are needed to address these challenges. One of such solution is biochar, a carbon-rich material derived from organic biomass waste. Biochar is a form of charcoal produced through pyrolysis at temperatures ranging from 500 – 700°C in an oxygen-limited environment (Uday et al., 2022). Pyrolysis refers to the thermal decomposition of biomass at high temperatures, producing biochar and by-products of syngas and bio-oil. The resulting biochar is a stable, carbon-rich substance that can be used to enhance soil health and productivity. There is a wide variety of feedstock for producing biochar including wood, agricultural waste (straw, husk, and stalks from any kind of crops), forestry residues, livestock manures, food residues, and municipal waste. The supply for the feedstock of biochar is easily available and affordable and thus is considered as a renewable and sustainable source of energy.

The production of biochar offers an effective strategy for reducing organic waste. Agricultural activities often generate significant amount of biomass waste, posing challenges to waste management and disposal. These wastes are usually left to decompose in the land field or burned, resulting in significant pollution. Landfilling will lead to pollution in soil and groundwater by leachate and toxins. There is also the problem of limited available landfill space. Besides that, disposal through open burning releases pollutants into the air, contributing to air quality problems and health issues. Up till now, only a small amount of waste is utilized in a useful manner, such as converting it to biomass energy or through upcycling. Converting these wastes into biochar is considered a sustainable waste management by minimizing pollution and maximizing resource recovery. Figure 2.1 shows a biochar derived from hardwood.



Figure 2.1: Hardwood biochar (Foundation for Food & Agriculture Research, 2024)

2.1.1 Market Analysis of Biochar

Biochar is emerging as a valuable product in recent years due to the discovery of its high potential in various application. Conversion of waste biomass into biochar provides a solution for achieving long-term carbon sequestration and many other favourable impacts on the environment. The global biochar market is experiencing significant growth, driven by increasing awareness of its environmental benefits and its potential role in sustainable agriculture and waste management.

According to the Precedence Research report, the global biochar market was valued at USD 220.27 million in 2022 with an estimated growth at a compound annual growth rate of 11.14 % from 2022 to 2032 (Precedence Research, 2023). The report also revealed that biochar has gained significant attention globally within the past decade. The Asia Pacific region dominates the global market and China became the leading producers of biochar

accounting for highest production of biochar in the world. The Philippines, Vietnam, South Korea, Japan, Australia and Malaysia are currently developing the markets of biochar and are projected to experience an outstanding growth in product supply and demand in the coming years. Figure 2.2 shows the extrapolated global biochar market according from 2023 to 2032.

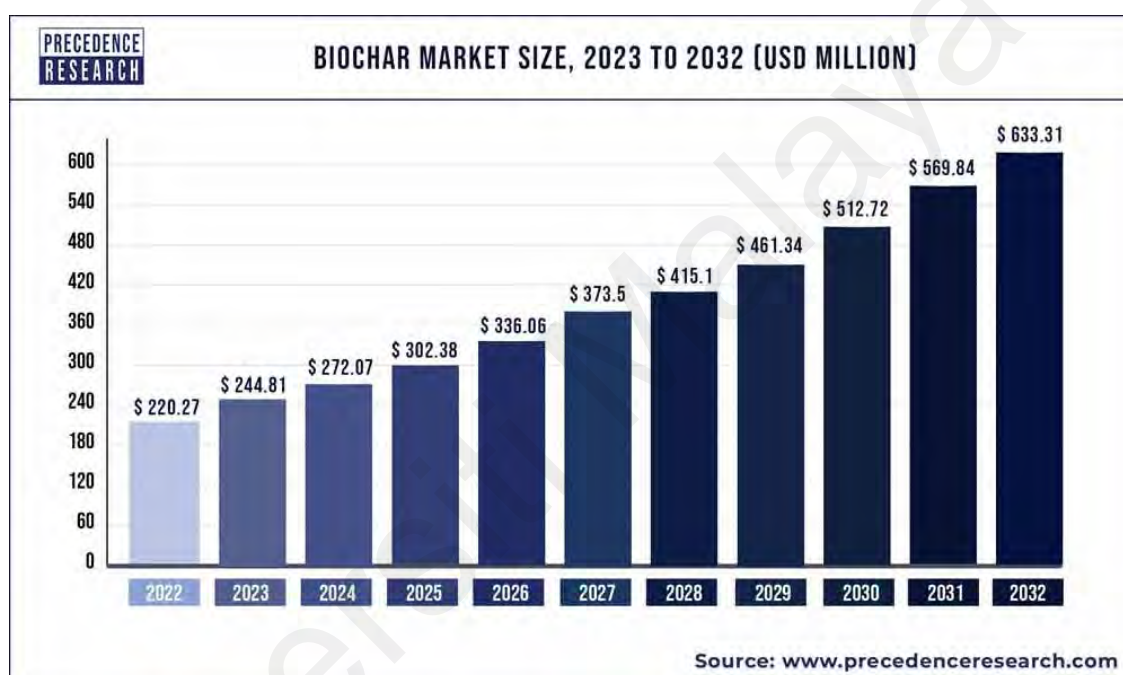


Figure 2.2: Extrapolated Global Biochar Market Size from 2023 to 2032
(Precedence Research, 2023)

2.1.2 Properties and Applications of Biochar

Biochar possesses many favorable characteristics, including porous structure, strong adsorption ability, high stability, environmentally friendliness, and low cost. These attributes grant it significant potential in many fields (Jagadeesh & Sundaram, 2023; Lu & Zong, 2018). The high porosity and affinity for non-polar compounds of biochar make it highly effective for adsorbing CO₂, rendering it a valuable tool for carbon sequestration.

The exceptional adsorption skills of biochar also capture contaminants and pollutants in purification and filtration system (Uday et al., 2022).

Biochar has become significantly developed and widely utilized in the agricultural sector for carbon sequestration and soil remediation (Shaaban et al., 2018). Due to its high stability and resistance to decomposition, biochar can persist in soil for an extended period of time, storing carbon and addressing climate change. This quality positions it as a reliable long-term solution for trapping GHG and reducing carbon emissions. When applied to soil, biochar effectively locks carbon away, preventing its release into the atmosphere as CO₂, thereby offsetting carbon emissions and reducing atmospheric CO₂ concentrations, which mitigates the greenhouse effect and global warming (Guo et al., 2022, Mulabagal et al., 2015).

Moreover, apart from its carbon storage benefits, biochar can enrich soil fertility, promote plant development, and increase crop yield. Its porous structure and high surface area enhance soil structure, promote aeration, and increase water retention capacity, thereby improving soil health (Gabhane et al., 2020; Khan et al., 2024; Yang et al., 2018). The porous network enables biochar to absorb and retain water, providing efficient capillary action, ensuring uniform distribution of water throughout the soil profile and accessibility to plant roots. Thus, biochar serves as a crucial tool for improving soil moisture levels, mitigating water stress, and enhancing crop yields in agricultural settings. Additionally, biochar acts as a reservoir for nutrients, preventing leaching and making essential nutrients more available to plants over time. Furthermore, biochar facilitates the growth of beneficial soil microorganisms, thereby enhancing nutrient cycling and promoting overall soil health, which leads to increased productivity of crops (Haider et al., 2022; Joseph et al., 2021).

The versatility of biochar extends beyond carbon sequestration and soil remediation, encompassing applications such as livestock farming, agriculture, construction industries, soil remediation, decontamination, biogas production, chemical recovery, carbon sequestering, anaerobic digestion, wastewater treatment, power industry, textiles, wellness (Cha et al., 2016; Danesh et al., 2023; Feliz Florian et al., 2024). Figure 2.3 shows other applications of biochar.



Figure 2.3: Various applications of biochar (Shafawi et al., 2021)

With its multifaceted advantages, biochar contributes to achieving sustainable development goals and resource conservation. The potential applications of biochar in various fields are currently being explored, with ongoing research aimed at maximizing

its potential and utilization across industries. Numerous studies are being conducted to improve biochar production methods and optimize its application practices. These efforts aim to unlock its full potential in addressing contemporary challenges, advancing sustainable development, and achieving carbon neutrality.

2.1.3 Carbon Sequestration Potential of Biochar

The introduction of biochar in soil reduces GHG emissions such as methane gas, nitrous oxides, and CO₂ into the atmosphere. Spokas et al. (2009) found that adding biochar to soil reduced the decomposition activity of microorganisms, which led to a decrease in CO₂ emissions by 2 – 60%. Other studies have found that biochar can reduce 870 kg of CO₂ equivalent per tonne of biomass feedstock, depending on the type and production parameters (Roberts et al., 2010). Wang et al. (2023) indicated that utilizing biochar across various sectors could reduce total GHG emissions by up to 2.56 billion tonnes of CO₂ equivalent annually, representing 5% of the worldwide GHG emissions.

While the primary role of biochar in carbon sequestration is through stabilization of carbon in its solid form, its adsorption properties can also contribute to the sequestration of CO₂. The specific surface area of biochar can range from 100 to 700 m²/g, depending on the feedstock and production conditions. This extensive surface area enhances its capacity to adsorb and fix carbon in its chemical structure, demonstrating affinity for non-polar molecules like CO₂. Biochar stores CO₂ through physical and chemical mechanisms, such as physisorption and chemisorption (Wang et al., 2023). Physisorption occurs on the micropores of the biochar through van der Waals force generated by intermolecular interactions. Biochar with higher specific surface area and microporous volume will promote higher CO₂ adsorption capacity. Chemisorption occurs through the

formation of weak bonds between the surface functional group and CO₂. Figure 2.4 shows the mechanisms of CO₂ adsorption on biochar.

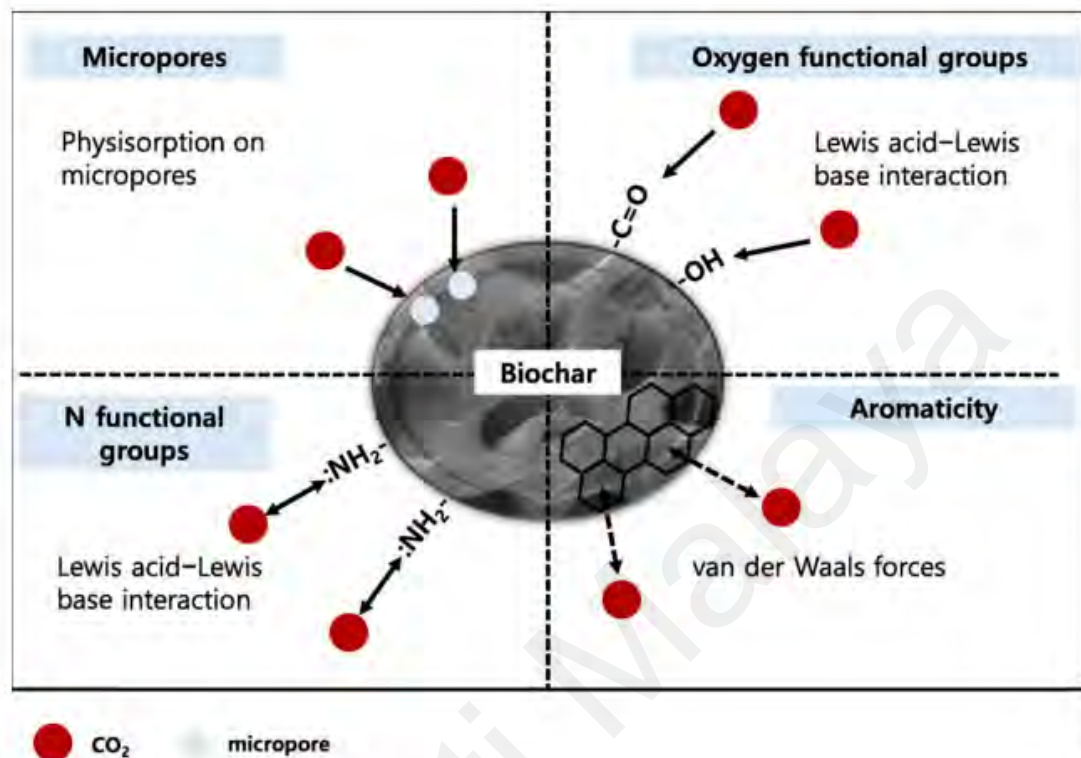


Figure 2.4: Possible mechanisms of CO₂ adsorption on biochar (Shafawi et al., 2021)

Physical and chemical modifications may be done to enhance the adsorption capacity of the biochar. Common physical modifications include thermal activation and grinding. Common chemical activation methods for enhancing CO₂ adsorption in biochar include amination, surface oxidation, and impregnation with metal oxides or alkali metals (Shafawi et al., 2021). Amination introduces amine groups that react with CO₂ to form carbamate complexes, thus improving CO₂ adsorption. Surface oxidation adds oxygen-containing functional groups, increasing active sites and enhancing surface acidity and polar characteristics. Metal oxide impregnation allows biochar to capture CO₂ through chemical adsorption and carbonate formation, utilize the high CO₂ affinity of metal oxides

(Q. Shi et al., 2021). Impregnation with alkali metals creates basic sites on the biochar surface, which interact strongly with CO₂, thereby enhancing chemisorption.

Modifications are done to enhance the affinity of biochar toward CO₂ by improving the specific surface area, pore structure and basic surface functional groups of the biochar. However, it is important to note that the adsorption capacity differs based on the type of biochar and the parameters of the production process. Figure 2.5 illustrates the various factors influencing the adsorption mechanism of CO₂ by biochar while Table 2.1 is a summary of previous studies on the surface modification and CO₂ adsorption capacity of biochar.

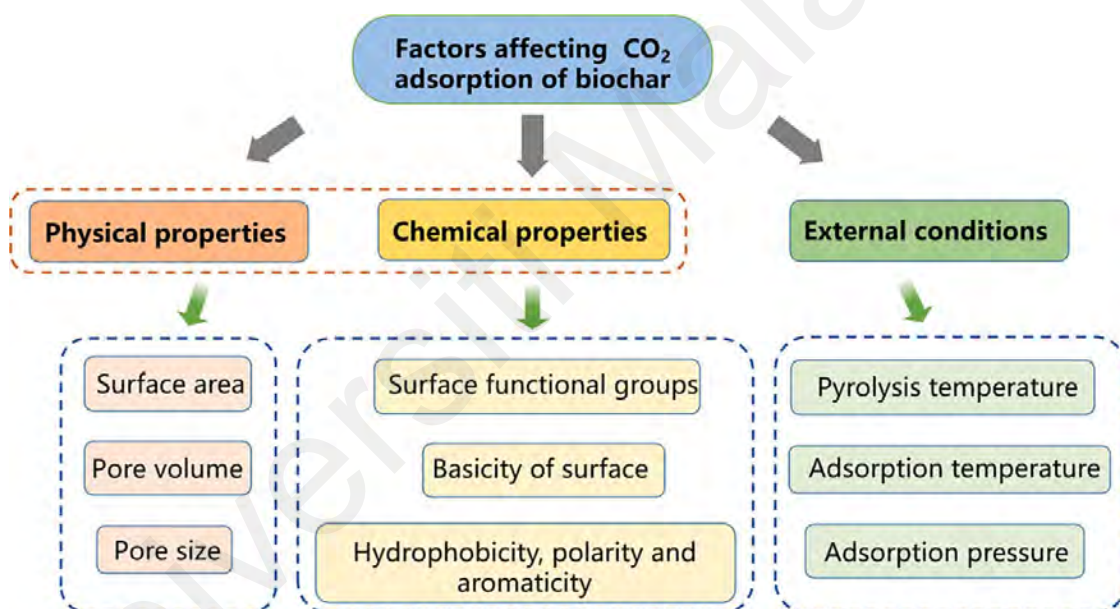


Figure 2.5: Factors affecting biochar adsorption of CO₂ (J. Liu et al., 2022)

Table 2.1: Summary of surface modification and CO₂ adsorption capacity of biochar of previous studies

Type of Biochar	Pyrolysis Temperature (°C)	Activation Method	Specific surface area (m ² /g)	Total pore volume (cm ³ /g)	Adsorption capacity (mmol/g)	References
Peanut hull	500	-	2.2	0.006	0.86	(Gupta, Kashani, et al., 2021)
Wood sawdust	400	-	126.9	0.104	1.30	(Gupta, 2021)
Pine sawdust	300	-	1.3	0.003	-	(J. Li et al., 2018)
Palm shell	500	-	389	-	0.46	(Promraksa & Rakmak, 2020)
Physical activation						
Vine shoot	600	CO ₂ at 800°C for 1h	767	0.37	1.58	(Manyà et al., 2018)
Olive mill	350	CO ₂ at 850°C for 1h	1135	0.48	2.95	(González & Manyà, 2020)
Wheat straw	500	CO ₂ at 800°C for 1h	514	-	2.44	(Manyà et al., 2020)
Chemical activation						
Palm shell	600	KOH, N ₂ at 850°C for 1h	1250	0.61	4.40	(Ello et al., 2013)
Chicken manure	700	HNO ₃ , NH ₃ at 450°C for 1h	302	0.22	10.15	(Nguyen & Lee, 2016)
Coconut shell	500	KOH, N ₂ at 600°C for 1h	718	0.28	4.23	(J. Yang et al., 2017)
Coffee ground	600	MgO, N ₂ at 600°C for 2h	9.8	-	1.57	(Y. Guo et al., 2020)

Biochar offers a durable and effective means of capturing and storing atmospheric carbon. By converting organic waste into a stable form of carbon, biochar helps mitigate climate change through long-term carbon sequestration. The effective carbon sequestration of biochar in soil underscores the potential for employing similar carbon capture techniques in cementitious materials, a focal point of this research. As biochar demonstrates its capability to lock away carbon in soil, it prompts further exploration into harnessing similar mechanisms within cementitious materials. This study seeks to contribute to the development of sustainable practices in construction with biochar, ultimately aiding in the global effort to combat climate change.

2.1.4 Biochar Production Techniques and Parameters

Biochar is commonly produced through thermochemical conversion of agricultural waste at temperatures of 500 – 700°C under limited oxygen supply. Thermal conversion of biomass breaks down the organic materials into biochar, bio-oil, and syngas. Biochar can be produced through various methods, each with its own advantages, disadvantages, and applications. Different process parameters yield different outcomes in biochar production. The process parameters will influence key characteristics of biochar, such as yield, elemental composition, morphology, surface functional groups, surface area, and stability. Common types of biochar production methods include pyrolysis, gasification, hydrothermal carbonization, and torrefaction. Table 2.2 summarizes the different types of thermochemical conversion of biochar with its parameters.

Table 2.2: Comparison of different production techniques of biochar (Cha et al., 2016; Danesh et al., 2023; Uday et al., 2022)

Production	Temperature (°C)	Residence time (min)	Major product	By-products	Biochar yield (%)
Slow Pyrolysis	300 – 700	> 60	Biochar	Bio-oil, syngas	30 – 55
Fast Pyrolysis	~500	0.02	Bio-oil	Biochar, syngas	10 – 26
Gasification	~800	0.2 – 0.4	Syn gas	Biochar, tar, oil	10 – 25
Torrefaction	200 – 300	10 – 60	Torrefied biomass	Water, volatile gas	70 – 80
Flash Carbonization	300 – 600	< 30	Biochar	Bio-oil, syngas	37
Hydrothermal carbonization	180 – 250	60 – 720	Hydrochar	Biocrude, gases	50 – 80

Pyrolysis is widely employed in the industry for biochar production. Pyrolysis can be carried out using different equipment such as batch, continuous, or fluidized bed reactors, and the process parameters can be adjusted to produce biochar with desired properties. Slow pyrolysis involves heating biomass at relatively low temperatures ranging from 300 – 700°C, with low heating rate 5 – 7°C/min for an extended period in the absence of oxygen (Feliz Florian et al., 2024). This method results in a higher yield of solid carbonaceous biochar, making it a preferred method for maximizing char production. Biochar emerges as a primary product, constituting around 30–55% of the total, alongside other outputs such as bio-oil (25 – 35%) and syngas (20 – 30%).

Fast pyrolysis is a rapid heating method that involves heating biomass to moderate temperatures of approximately 500°C with a heating rate more than 100°C/min for a very short duration in the absence of oxygen. This method results in a lower yield of biochar (10 – 20%) compared to slow pyrolysis, but a higher yield of bio-oil (75%), and ~13% of syngas. This method is favored when the objective is to produce bio-oil rather than

biochar. The produced biochar typically has moderate carbon content. Figure 2.6 illustrates the carbonization process of biochar during pyrolysis at different temperature ranges.

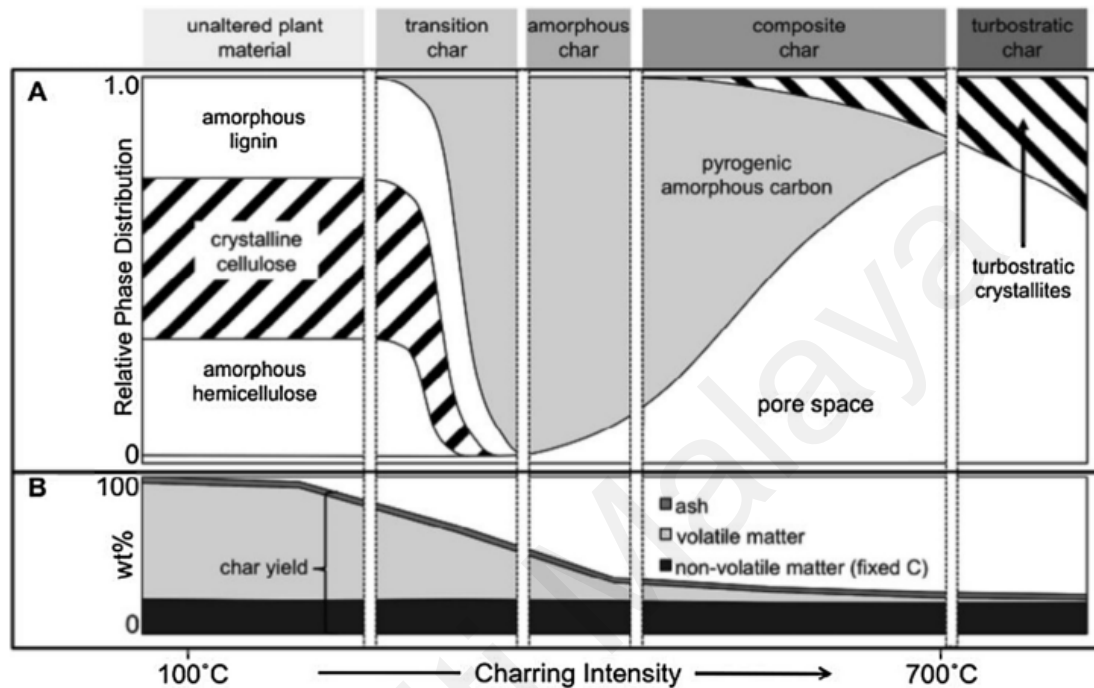


Figure 2.6: Conversion of biomass into biochar at different pyrolysis temperatures (A) Characteristics phases of biochar (B) Composition of biochar
(Jung et al., 2019)

Gasification is conducted at a higher temperature of around 800°C with a rapid heating rate and a residence time of 10 – 20 minutes. Gasification converts biomass into syngas (a mixture of hydrogen, carbon monoxide, and methane) in the presence of oxygen and steam. This process is designed to produce syngas as the major product (~85%), with biochar being a minor byproduct (5 – 10%) and 5% of tar. The biochar produced has a low carbon content due to the high degree of conversion of biomass into gaseous products.

Torrefaction is performed at lower temperatures (200 – 300°C) with a moderate residence time of 10 – 60 minutes. Biomass undergoes partial decomposition, resulting

in the removal of moisture and volatile organic compounds, leaving behind approximately 80% of torrefied biomass. Torrefaction improves the energy density and hydrophobicity of the biomass, making it more suitable to be used as a fuel in combustion applications (Cha et al., 2016).

Flash carbonization is a relatively recent method involving temperatures between 300 – 600°C and a very short residence time of less than 30 minutes. The heating rate is high, leading to the rapid production of biochar. This method yields a moderate amount of biochar ~37%. The fast nature of this process makes it suitable for quickly producing biochar and bio-oil. The carbon content of the biochar is variable depending on the process conditions.

Hydrothermal carbonization is a wet biomass conversion process that involves heating biomass in the presence of water at 180 – 250°C over a longer residence time ranging from 1 to 12h. This process produces 50 – 80% hydrochar, which is similar to biochar but contains more oxygen and moisture. Hydrochar can be further processed or dried to produce biochar. Hydrothermal carbonization also produces biocrude and gaseous byproducts, which can be further utilized for other purposes (Uday et al., 2022).

These biochar production methods each have unique characteristics and are chosen based on the desired end products and specific biomass feedstocks. Slow pyrolysis is optimal for maximizing biochar yield, fast pyrolysis for bio-oil, and gasification for syngas. Torrefaction improves biomass properties for energy applications, flash carbonization offers rapid biochar production, and hydrothermal carbonization is advantageous for processing wet biomass.

2.1.5 Availability of Biochar in Malaysia

Biochar is opted in this study as there are a broad variety of available biomass resources in Malaysia. The four kinds of biochar selected are RHB, PKS, CHB and BB.

2.1.5.1 Rice Husk Biochar (RHB)

The plantation of rice in Malaysia generates up to 770,000 tonnes of rice husk waste annually, which is usually discarded as waste after the rice milling process (Bao et al., 2023). A minority of the waste is utilized as animal feed and fertilizers, while most of it is left dumped in the field and eventually burned for disposal. This underscores the necessity of addressing the environmental and economic challenges related to rice waste. The Malaysian government plans to reduce rice husk waste by 50% by 2025 by promoting it as a renewable resource (SEDA Malaysia, 2021).

2.1.5.2 Palm Kernel Shell Biochar (PKS)

The production of palm oil is dominated by several key countries in the Southeast Asia with Indonesia being the largest producer followed by Malaysia with an output of 18.55 million tonnes of crude palm oil in 2023 (MPOB, 2024). After the extraction of crude palm oil, numerous residues are left behind, including oil palm trunks, oil palm fronds, empty fruit bunches, palm pressed fibres, palm shells, and palm oil mill effluent. About 75.61 million tonnes of solid bio-mass waste are generated annually in the palm oil industry in Malaysia (Dalton et al., 2017). These residues are largely underutilized, creating a significant disposal problem. Efforts have been made to address the potential for energy recovery in the palm oil industry. Palm shells, for example, are exported to countries like Japan for energy generation. Pyrolysis represents a better method for

valorizing these wastes. Figure 2.7 summarizes the recyclable waste for palm oil production.

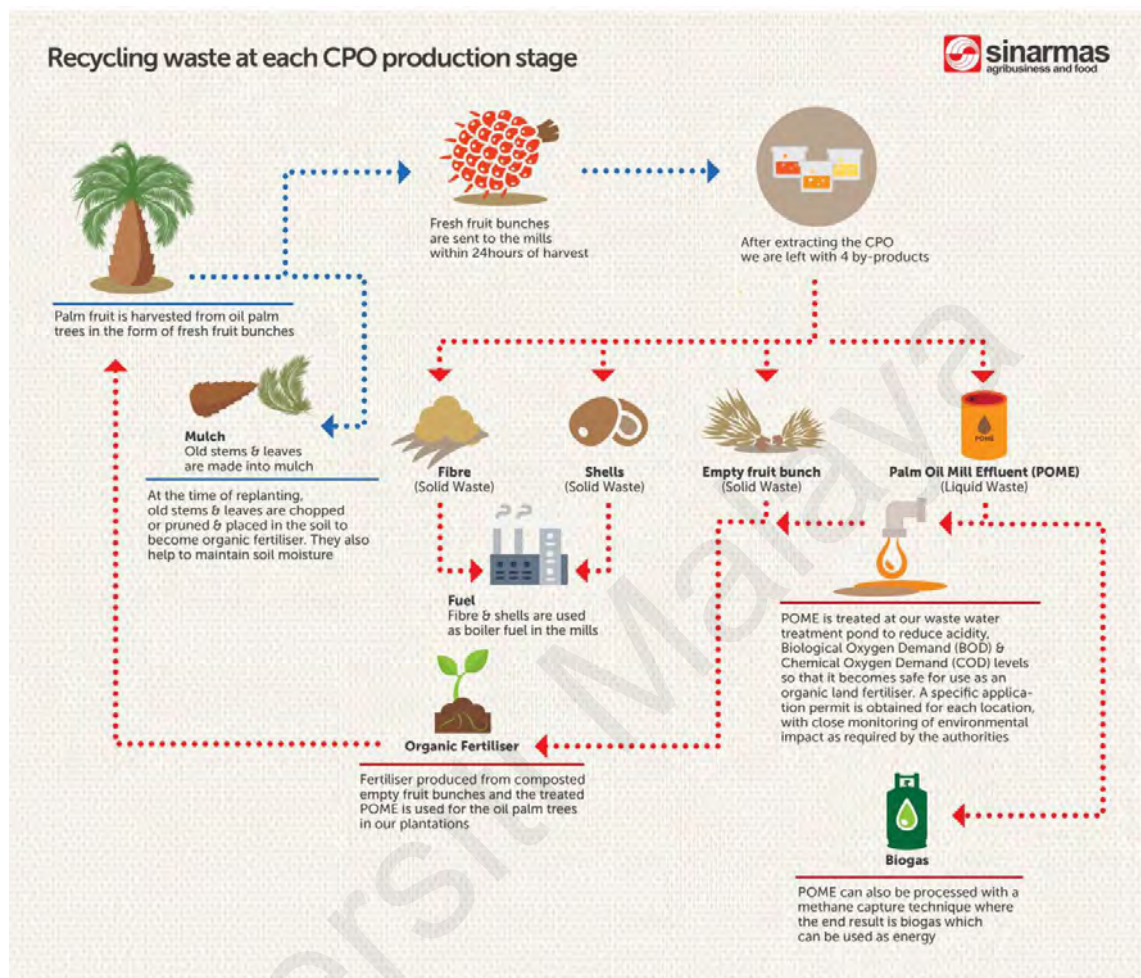


Figure 2.7: Recycling of crude palm oil waste (Golden Agri-Resources, 2018)

2.1.5.3 Coconut Husk Biochar (CHB)

The coconut is the fourth largest cultivation in Malaysia, after palm oil, rice and rubber. The coconuts are primarily used for their water, milk, and oil, which are essential ingredients in various food products and cosmetics. The coconut industry generates substantial waste, including husks, shells, and fronds, which are often disposed of through burning or landfilling. The coconut husk waste makes up to 6.7% of all agricultural waste generated in Malaysia, amounting to 80,000 tonnes per year (Bao et al., 2023). Some of the waste from coconut plantations is used to produce activated carbon for water

purification, air filtration, and industrial decontamination processes. Activated carbon can effectively remove impurities, odors, and contaminants. Additionally, it is utilized in various applications such as gold recovery, gas purification, and the production of pharmaceuticals.

2.1.5.4 Bamboo Biochar (BB)

Bamboo plantations are becoming increasingly prominent in Malaysia due to their potential in boosting the local economy and reducing environmental impact. Bamboo, known for its rapid growth and versatility, is used in a wide range of applications, including construction, furniture, paper, and textiles. The cultivation of bamboo helps in soil conservation, carbon sequestration, and providing livelihoods to local communities. However, BB is harder to obtain compared to other types of biochar due to the varied and prioritized uses of bamboo. Additionally, producing high quality BB involves precise pyrolysis techniques and careful management of bamboo resources, which can further complicate its availability. However, bamboo biochar offers valuable benefits, including high carbon content and soil enhancement properties.

An important point to consider is that different types of feedstocks, each with its own properties and composition, can significantly influence the final characteristics of the produced biochar.

2.2 Utilization of Biochar in Cementitious Materials

Recent research demonstrates biochar as an admixture of cementitious material improved various properties. Studies on humidity control, hygrothermal, performance in elevated temperature, durability, mechanical strength, permeability,

hydration kinetics, nano-modification, and economic viability are ongoing, with a significant increase in publications especially from 2019 onwards (Beskopylny et al., 2022; Navaratnam et al., 2021; Park et al., 2021). Biochar also exhibits low thermal conductivity, low flammability, and good chemical stability in cementitious material (Akinyemi & Adesina, 2020; Bolan et al., 2022; Boumaaza et al., 2023; Gupta et al., 2020; Gupta & Kua, 2017).

2.2.1 Mechanical strength

The porous structure of biochar provides high surface area and good adsorption capacity, generating good interaction with cementitious matrix. The use of biochar in cementitious mixtures has been shown to be beneficial leading to an improvement of the physical and mechanical properties of the material (Aman et al., 2022). Sikora et al. (2022) reported that at optimum of 2% of biochar replacement, the compressive strength improves by 3 – 4%. Gupta et al. (2021) reported that the addition of 2% to 3% biochar led to a noticeably higher strength at 7 days and 28 days. Muthukrishnan et al. (2019) findings show that low replacement of RHB can improve the compressive strength by 17%. The presence of small amount of biochar improves cement hydration, producing a dense structure and higher mortar strength (J. Liu et al., 2022). The optimum amount of biochar as a cement replacement is concluded from various studies and is reported to range between 0.08% and 5% (Agarwal et al., 2023; Bolan et al., 2022; Boumaaza et al., 2023; Chen & Gao, 2019; Navaratnam et al., 2021; Praneeth et al., 2020; Sikora et al., 2022). This wide range reflects variations in findings across different research efforts, were dependent on many factors including the type of biochar used, its production conditions, and the specific properties of the concrete composite being evaluated. These studies collectively indicate that within this range, biochar can enhance certain properties

of concrete composites, including strength, durability, and environmental performance. Any higher dosage of biochar may only reduce the strength of the cement mortar due to high porosity. Figure 2.8 depicts the highest strength obtained at optimum 5% replacement of biochar by weight.

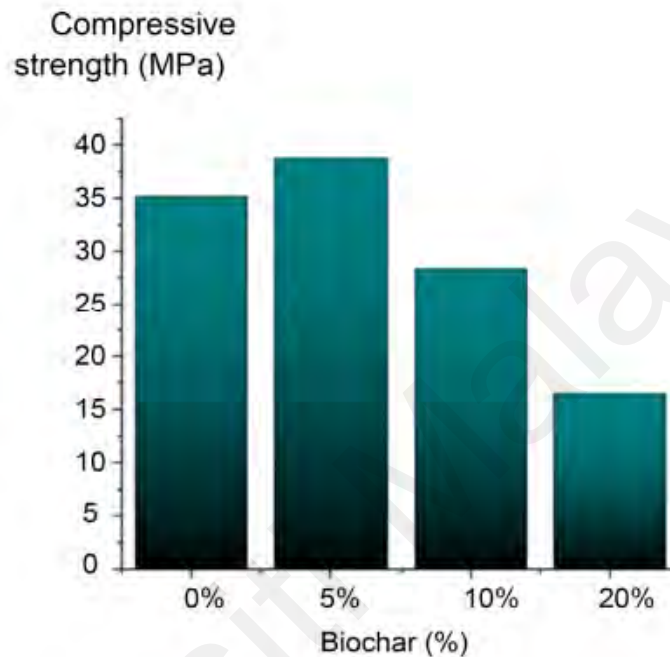


Figure 2.8: Compressive strength of wood biochar-added mortar (Navaratnam et al., 2021)

The addition of biochar generally has a smaller impact on tensile strength compared to compressive strength. It may cause a reduction in tensile strength due to the formation of weak zones within the tensile plane (Senadheera et al., 2023). The incorporation of biochar leads to microcracks at the interface between the biochar particle and the cement matrix, resulting in detachment and reduced bond strength. Excessive biochar may lead to aggregation and local weak zones, further reducing tensile strength.

The incorporation of biochar also has little impact on flexural strength. The flexural strength generally decreases with higher biochar content due to the introduction of pores and weak zones in the cement matrix (Liu et al., 2022). Gupta, et al. (2020) reported that

the optimal flexural strength increase in cement paste was achieved with a 0.5% woody biochar admixture, while higher biochar content resulted in a reduction of flexural strength. Muthukrishnan et al. (2019) found that flexural strength decreased by 16–27% after replacing rice husk ash and biochar with 20% cement, the porosity in the biochar weakens the tensile plane of the mortar and promotes crack formation and propagation.

2.2.2 Fluid Transport Properties

The fluid transport properties of biochar-added mortar are critical to its durability, as they influence the permeability, sorptivity, and diffusivity of the composite. The incorporation of biochar, either as a cement replacement or additive, has attracted significant attention due to its potential to enhance these properties through its unique physical and chemical characteristics. The pore structure of the biochar refines the pore network in the cement matrix, effectively reducing capillary pores that are primary conduits for fluid transport. This refinement decreases permeability and sorptivity, especially when biochar is added in optimal dosages. However, excessive biochar content can increase water absorption due to its high internal porosity, which may lead to elevated sorptivity if not properly managed.

Water absorption and sorptivity are critical indicators of concrete durability, reflecting its microstructure and resistance to aggressive environments. Sirico et al. (2020) reported that the inclusion of 5% biochar significantly reduces the initial rate of water absorption by 18%, lowering the sorptivity rate to 0.0101 mm/ \sqrt{s} . This improvement is attributed to the densification effect of biochar particles, which fill fine capillary pores and retain mixing water, releasing it during curing to enhance hydration and reduce porosity. The effect of biochar on secondary sorptivity is less pronounced, with longer test periods showing a diminished impact. Total water absorption also decreased by 3.64% in the

biochar-added mix compared to the reference, further supporting the enhanced microstructure and improved durability due to the densification effect. Additionally, the addition of biochar can reduce the rate of capillary water absorption, which is crucial for concrete durability in wet environments. Optimized biochar content enhances resistance to sorption by refining pore connectivity. Furthermore, pre-treatment methods such as surface activation or saturation can mitigate biochar's natural water absorption tendency, improving its overall performance.

Similar findings reported that the inclusion of biochar in concrete formulations under normal curing conditions leads to enhanced water tightness by reducing capillary absorption and penetration depth (Gupta et al., 2020). A 2% biochar dosage reduced sorptivity by 43.5% and water penetration depth by 45%, demonstrating improved water tightness. These improvements are driven by the densification effect of biochar particles, which refine the pore structure and contribute to better hydration. The addition of biochar densify the concrete matrix, fill pores, minimize capillary networks, and support hydration through the gradual release of absorbed water during curing. The optimal dosage range of 1% to 2% ensures an effective balance between improved permeability and preserving workability, ultimately enhancing concrete durability and reducing its vulnerability to water ingress especially in tropical regions with high humidity and warm climates.

Several factors influence the fluid transport properties of biochar-modified concrete. Biochar content plays a crucial role, with studies indicating that replacement levels of 5–10% biochar consistently yield the most significant improvements in fluid transport properties. However, higher dosages may negatively impact performance, possibly due to increased internal porosity. The biochar properties, including the feedstock used, pyrolysis temperature, and any pre-treatment methods, also significantly affect biochar's

ability to modify fluid transport behavior. These factors influence the pore structure and overall effectiveness of biochar as a densifier and internal curing agent. Additionally, mix design is a key consideration, as the water-to-cement ratio and the admixtures used in the mix determine how biochar interacts with the cementitious system. Optimizing these variables ensures the desired improvements in permeability and sorptivity.

The inclusion of biochar in cement composites offers a promising approach to enhancing fluid transport properties, contributing to improved durability and sustainability. However, achieving these benefits requires careful optimization of biochar content, treatment, and mix design. Further studies focusing on field applications and long-term performance are recommended to validate laboratory findings and address practical implementation challenges.

2.2.3 Chemical Stability

Biochar has good chemical stability. Chemical interactions involving chloride, or carbonation caused cement matrix degradation over time. Biochar has excellent chemical stability because of the fixed carbon and its chemical composition having oxide groups. The high production temperature increased the content of carbon and the surface area of the biochar. When surface area increased, the reactive zones of oxygen and hydrogen decreased, making biochar stable and will not react to produce harmful substances when incorporated into cementitious material (Akinyemi & Adesina, 2020).

Gupta et al. (2021) did a series of experiments to study the resistance of biochar-added mortars to chloride and sulfate attacks. Cement composite with 1% wood waste biochar by weight maintain 8 – 11% more strength after 120d of exposure to a chloride-rich (NaCl) environment compared to regular cement. Moreover, biochar addition notably reduces the overall absorption of chloride, which contributes to the improved durability

of the composite. In the case of sulfate exposure after 120d, composites with 2% wood waste biochar and RHB have 14 – 17% higher compressive strength than that of control samples. The addition of biochar minimizes strength loss due to sulfate attack in cement composites. Therefore, the addition of biochar to cement enhances its resistance to chloride and sulfate attacks, leading to improved durability and structural integrity of the cementitious composite.

2.2.4 Thermal Conductivity

The thermal conductivity of the biochar concrete is approximately 60% lower than that of the normal concrete composite. Sikora et al. (2022) also reported similar trend of thermal conductivity of biochar concrete as shown in Figure 2.9.

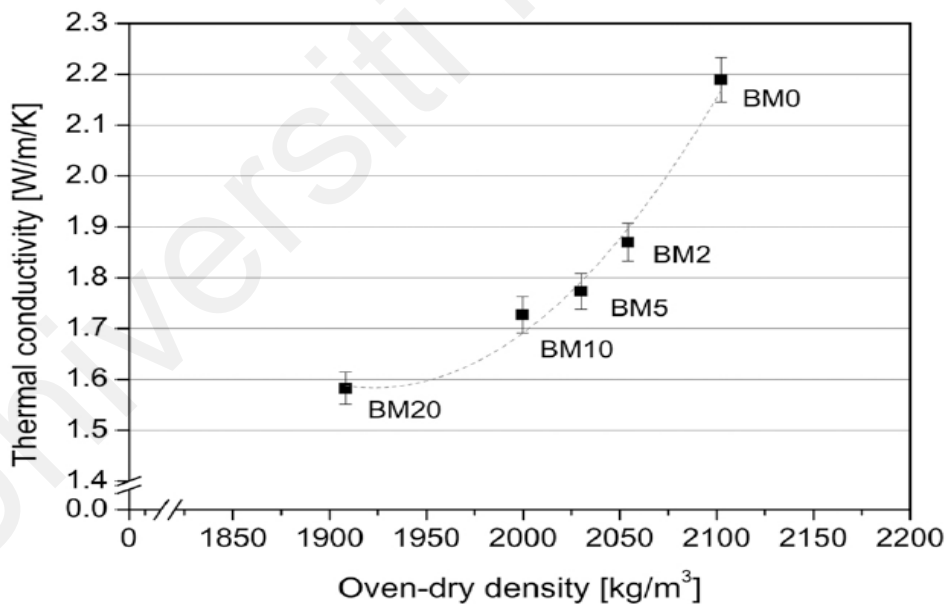


Figure 2.9: Thermal conductivity and biochar dosing correlation (Sikora et al., 2022)

Incorporating small amount of biochar, around 1 – 2% into cement admixture can effectively reduce thermal conductivity. This reduction occurs due to the presence of a

wide range of pores on the surface of the biochar and high carbon content, which act as insulating barriers within the cement matrix. The pores of biochar break the thermal bridging in the biochar concrete, thus improving its thermal insulation. By limiting the transfer of heat through the material, biochar helps to improve the thermal efficiency of the resulting cement composite, making it ideal for thermal insulation purposes in buildings.

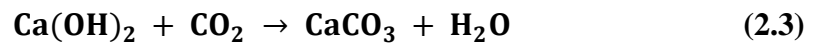
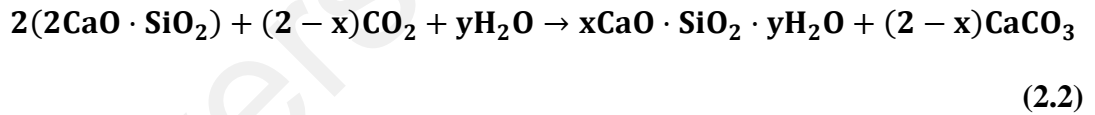
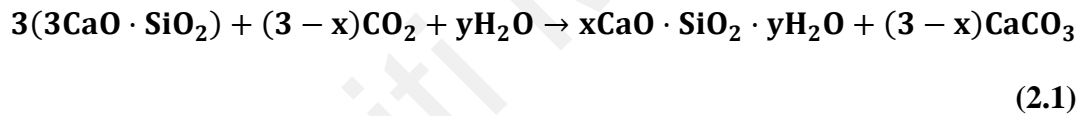
2.2.5 Flammability

Biochar is considered as a thermally stable material, with low flammability. This low flammability arises from its high carbon content, which makes it less prone to combustion compared to many other materials. The carbonaceous border of the biochar in concrete delays the passage of the oxygen and fuel required for combustion to occur, preventing the spread of fire. Sikora et al. (2022) reported that below 300°C, there is little changes in the mechanical strength of the biochar cement mortar. In comparison to its respective feedstock and other conventional materials, biochar demonstrated lower peak heat release rate, time to ignition, total heat release, and total carbon monoxide generated, as shown by flammability studies of Gong et al. (2014). Consequently, biochar is considered to have low flammability, making it a potentially valuable material for applications where fire safety is a priority, such as in construction materials.

2.3 Carbon Capture and Storage (CCS) in Cementitious Materials

CCS involves a series of technologies designed to capture CO₂ emissions from industrial activities and power generation, transport them, and securely store them underground in geological formations, ensuring long-term isolation from the atmosphere.

CCS aids in reducing GHG in the atmosphere and lowering the carbon footprints of the manufacturing industries. Traditionally, CCS involves pumping and securing supercritical CO₂ into deep geological formations and using it for enhanced oil recovery (Pavlova et al., 2022). Technologies have advanced and evolved into many other types of carbon sequestration. Carbon sequestration in cement materials occurs when unreacted cement and hydrated products (mainly portlandite) react with CO₂ to form a stable calcium carbonate compound. Carbonation provides a natural way to sequester CO₂, helping to reduce the carbon footprint of concrete structures and contributing to environmental sustainability. The carbonation reactions are as below (D. Zhang et al., 2017):



Equation 2.1 describes the carbonation of alite into calcium carbonate, equation 2.2 shows the carbonation of belite into calcium carbonate and equation 2.3 depicts the carbonation of portlandite into calcium carbonate. Natural carbonation typically occurs when atmospheric CO₂ penetrates the concrete surface and forms calcium carbonate. This is a long process and may take many years for atmospheric CO₂ to diffuse into the pores of the concrete. Carbonation is directly related to the hardening, durability, and

deterioration of cementitious materials, influencing the overall performance of concrete structures (Z. Liu & Meng, 2021). The formation of calcium carbonates within the concrete pores can enhance the strength and density of concrete, making it more durable and resistant to wear and tear. Carbonation also reduces the permeability of concrete by filling the pores with calcium carbonate. This makes the concrete less susceptible to the ingress of harmful substances, such as water, chloride ions, and other aggressive chemicals. Additionally, the reaction products of carbonation can improve the surface hardness of concrete, making it more resistant to abrasion and wear. One of the disadvantages of carbonation is the risk of reinforcement corrosion. Carbonation may lead to corrosion of steel, which potentially compromises the structural integrity over time. Carbonation can also cause shrinkage and microcracking in concrete, providing pathways for the ingress of water and other deleterious substances (Šavija & Luković, 2016). Thus, it is crucial to balance these factors and improve the design and maintenance of the concrete structures, to ensure their durability and performance over time.

2.3.1 Implementation of Carbon Capture and Storage (CCS) in the Industry

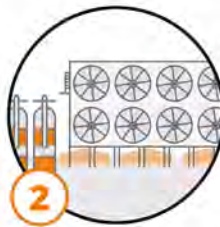
CCS in concrete can be implemented by injecting CO₂ either during the mixing process or during the curing process. Several companies in the market are actively engaged in advancing carbon capture technologies for concrete production, for example, Blue Planet Ltd., CarbonBuilt, Carbicrete, Aramco, and Fortera. CarbonCure Technologies Inc. is one of the leading companies in the field of carbon capture and utilization for concrete production. CarbonCure has developed an innovative technology to inject captured CO₂ into fresh concrete mix during the production process. Calcium carbonate is formed and the CO₂ used in this reaction is permanently sequestered within the concrete. Concrete produced with CarbonCure technology has improved compressive strength, it provides a practical solution for reducing the carbon footprint of concrete without compromising on quality. CarbonCure reported to have saved a total of 504,924.2 tonnes of CO₂ emissions

(CarbonCure Technology, 2024). Figure 2.10 gives a clear picture of the CCS in the industry.

CarbonCure: From Carbon to Concrete



CarbonCure is installed at an existing concrete plant in one visit, once a CO₂ tank has been installed.



Carbon dioxide (CO₂) gas is primarily sourced as a by-product from industrial processes.



The purified CO₂ gas is delivered in pressurized vessels by commercial gas suppliers.



CarbonCure's proprietary delivery system, contained in the Valve Box, precisely injects the CO₂ into the concrete mix.



CarbonCure's Control Box is wired to the Valve Box and integrated with the batch computer; so adding CO₂ is just like adding an admixture.



Once injected, CO₂ reacts with cement to form a nano-sized mineral that becomes permanently embedded in concrete.

Figure 2.10: CCS technology in the industry (CarbonCure Technology, 2024)

Another CCS technology for concrete is through carbonation curing. This method accelerates the carbonation process, leading to notable improvements in the strength and durability of the concrete. Instead of traditional water curing, pre-cast concrete products can undergo carbonation curing. Examples of pre-cast products that benefit from this technique include panels, masonry units, blocks, bricks, pavers, slabs and tiles. Carbonation curing is applicable to prefabricated units and non-steel reinforced

cementitious materials. This technology is utilized by various companies in the industry, such as Solidia Technologies, Cemex and Holcim. These companies and technologies represent a growing trend towards sustainable concrete production through the utilization of captured CO₂. Each offers unique methods and applications, contributing to the broader goal of reducing the carbon footprint of the construction industry.

2.3.2 Accelerated Carbonation Curing

Carbonation efficiency in cementitious composites can be increased through accelerated carbonation, potentially offsetting substantial emissions from cement manufacturing (J. Liu et al., 2022). The accelerated carbonation curing enhances the natural process of carbonation in concrete, which typically develops gradually over time. It is typically performed in an expedited controlled environment with higher CO₂ concentrations and shorter curing times. The cementitious material absorbs CO₂ during carbonation and permanently immobilize the CO₂ by forming carbonation products, which improves the mechanical properties of the concrete, with higher early strength and strong surface hardness and enhances durability (Kaliyavaradhan & Ling, 2017). Figure 2.11 summarizes the methods for implementing CO₂ mineralization or carbonation curing on materials.

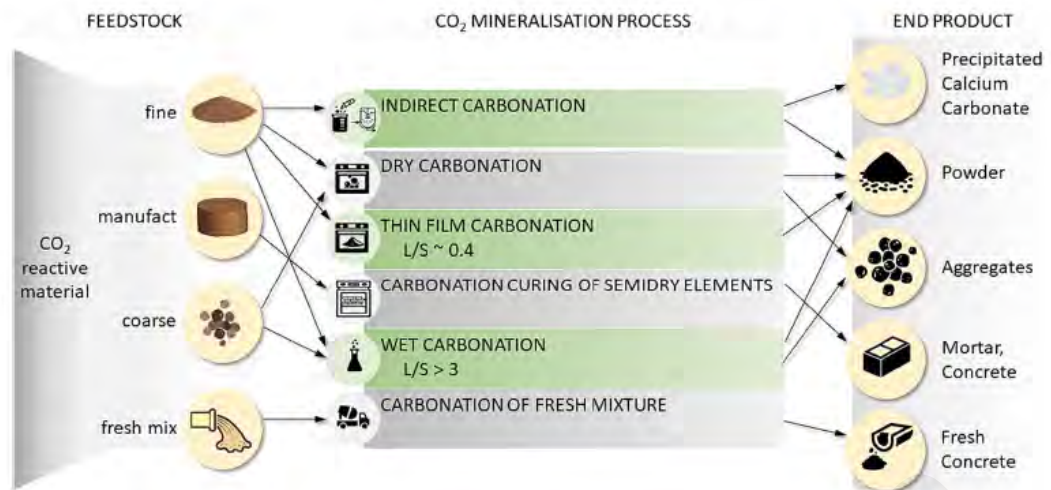


Figure 2.11: Six types of carbonation curing methods (Ferrara et al., 2023)

When undertaking carbonation curing, many considerations and factors must be considered, as each parameter determines the effectiveness and efficiency of the carbonation process. Variation in these parameters can lead to different physical, chemical, and mechanical properties in the cured specimens. Figure 2.12 summarizes the procedures of carbonation curing, with pre-curing followed by carbonation curing and post-curing.

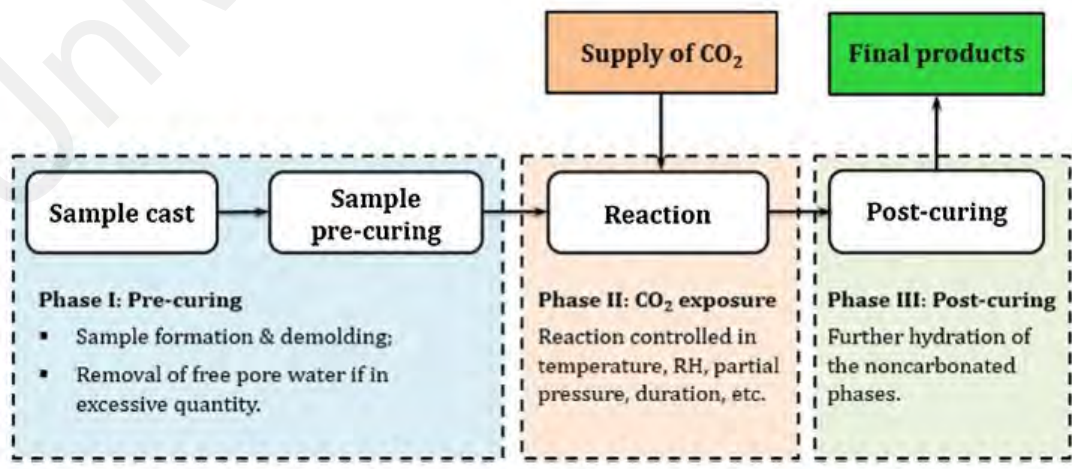


Figure 2.12: Common procedures for the carbonation curing process (D. Zhang et al., 2017)

2.3.2.1 Pre-curing Condition

Pre-curing refers to the controlled removal of water from concrete specimens before carbonation to enhance CO₂ diffusion during carbonation curing. An optimal water content is crucial as excessive water inhibits CO₂ diffusion while water depletion halts the carbonation reaction. Pre-curing is essential to ensure proper and optimal moisture content within the specimens to maximize the CO₂ diffusion for effective carbonation. The duration and temperature of pre-curing is usually adjusted to reduce 30-40% of water from the specimens. The value may also vary depending on the water/binder ratio of the mixtures. Shi et al. (2014) discovered that for mixtures with a w/b of 0.5, the value could be approximately a 4.5% water loss, while for mixtures with a w/b of 0.34, approximately 30% water loss could result in the highest carbonation degree and strength gain. This discrepancy is because mixtures with higher w/b ratios require less water loss to achieve optimal moisture content. Mixtures with higher w/b ratios demand less water loss to create sufficient channels for CO₂ diffusion, whereas those with lower w/b ratios require more water loss to achieve the same channel space. Figure 2.13 portrays the role of preconditioning in affecting the CO₂ uptake.

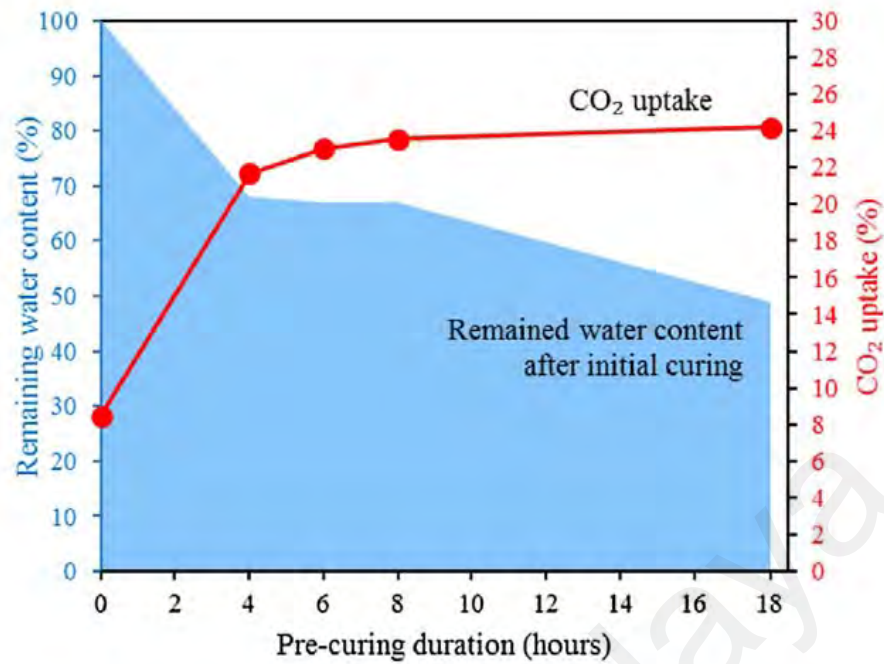


Figure 2.13: Preconditioning improves carbon uptake (El-Hassan et al., 2013)

2.3.2.2 Carbonation Curing Condition

During carbonation curing, factors to be put into considerations include pressure, concentration of CO₂, relative humidity and temperature (Z. Liu & Meng, 2021). Pressure and CO₂ concentration are the most influential factors governing carbonation efficiency. A higher CO₂ concentration of 20% promotes crystallization of calcium carbonate and carbonation depth. Increasing CO₂ concentration significantly enhances the carbonation degree, with studies showing an exponential increase in carbonation degree when increasing CO₂ concentration from 1% to 20%. Li and Ling (2020) demonstrated that after just 2h of concentrated carbonation with 20% CO₂, cement paste samples exhibited compressive strength four times higher than air-cured control samples. Other groups also done concentration of 5-100% studying the carbonation rate (Agarwal et al., 2023; Chen & Gao, 2019; Šavija & Luković, 2016).

Pressurized carbonation has been shown to enhance CO₂ diffusivity and increase carbonation efficiency in previous studies (Ahmad et al., 2017; Tang et al., 2021). For instance, samples carbonated under 0.1 MPa CO₂ for 4h exhibited compressive strengths twice the pressure of control samples after one day (El-Hassan et al., 2013). Optimal pressure of 0.2 MPa have been found to promote carbonation more efficiently (Zhan et al., 2016; D. Zhang & Shao, 2016). Despite its effectiveness, pressurized CO₂ curing is energy-intensive in practical application.

Relative humidity (RH) in the curing chamber affects the carbonation efficiency of samples by influencing CO₂ diffusion and providing water for reaction. Experimental models have demonstrated that carbonation efficiency is favoured at an RH of 50%-70%, as excessively high RH can hinder CO₂ diffusion due to the lower diffusion coefficient in water compared to air. Lower or higher RH can decrease the carbonation degree, although the variation is relatively low. Therefore, RH within an ambient range is usually adopted in the carbonation procedure.

Ambient temperature, typically 20-25°C, is commonly used for early-age carbonation of cementitious materials. However, temperature can affect carbonation efficiency in various ways. High temperatures can reduce CO₂ dissolution in liquid water and accelerate water evaporation. It also promotes the migration of ions in the pore solution and CO₂ diffusivity. Thus, it has both positive and negative effects. Zhan et al. (2016) found increasing temperature to 80°C does not affect the carbonation degree of concrete blocks while Wang et al. (2019) reported that a high temperature (around 80–100 °C) curing method can significantly improve the carbonation degree of high early strength cement paste. However, to compensate for evaporation at high temperatures, water supply is necessary. When high temperature is use, a high RH is also needed to prevent water evaporation in elevated temperature (D. Zhang et al., 2017).

2.3.2.3 Post-curing Condition

In some cases, postconditioning after carbonation is done to compensate water for continuation of hydration reaction after carbonation. Water removal from preconditioning to a certain extent hinders hydration, thus water curing is needed to allow hydration to enhance additional strength gains. After carbonation, there may be some unreacted cement remain which need water for further hydration, as carbonation degree are typically below 50% (Šavija & Luković, 2016). The unreacted cement can experience approximately 20% and 10% additional hydration reactions, underscoring the advantages of this phase. Moreover, research has observed that alite can undergo hydration and generate calcium monocarboaluminate hydrate in the presence of calcium carbonate (D. Zhang et al., 2018). El-Hassan et al. (2013) demonstrated that the reduction in hydration caused by water loss during pre-curing negatively impacted long-term strength. Nevertheless, by providing adequate water for hydration, the 28 days compressive strength could match that of the reference samples. Balancing early carbonation with subsequent hydration is vital for maximizing strength development. The role of internal concrete structure and external curing conditions during the carbonation stage is significant.

2.3.2.4 Properties of Material in Influencing the Carbonation Rate

Other factors influencing the carbonation rate are internal factors, such as the properties of the cement-based material. Such factors include parameters like water/binder (w/b) ratio and porosity of the composite structures. The porosity of the cement composite will directly impact the CO₂ diffusivity, which is closely linked to the w/b ratio of the cement mixture. High porosity demonstrates effective CO₂ diffusion

during carbonation. Consequently, blocks and masonry with more porous structures are preferred for commercial carbonation curing applications. The open pore structure of pervious concrete facilitates CO₂ sequestration, leading to deeper and more homogeneous carbonation and improved mechanical properties. A higher w/b ratio increases porosity, facilitating CO₂ diffusion and improve carbonation degree, but it also simultaneously decreases the compressive strength before carbonation. Interestingly, while higher w/b ratios typically decrease strength in normal hydrated cement-based composites, in carbonation curing, increased porosity can lead to greater strength gains during carbonation. This implies that a relatively higher w/b ratio may be favorable for mixtures in carbonation curing. Figure 2.14 depicts that higher w/b ratio improves carbonation degree.

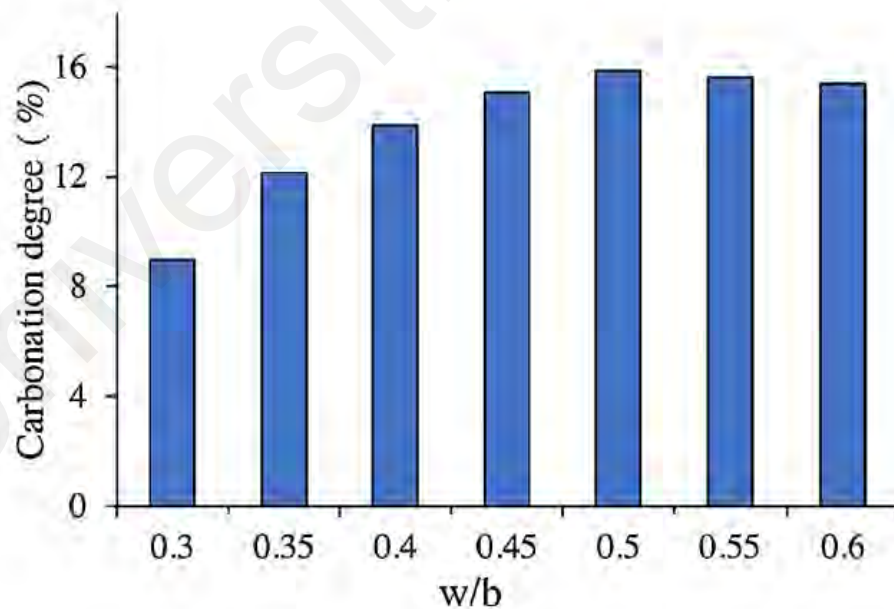


Figure 2.14: Effect of w/b ratio on carbonation degree of cement paste (J. Wang et al., 2019)

Another factor affecting the CO₂ uptake will be the specimen size. Thinner specimens show higher CO₂ uptake due to greater penetration. Surface areas exhibit higher carbonation degrees than internal sections due to initially dense surface microstructures. However, high carbonation degrees may lead to pH reduction below 8.3, potentially causing carbonation corrosion and increased susceptibility to weathering. As a summary, accelerated carbonation curing is influenced by many parameters. By optimizing the CO₂ concentration, pressure, temperature, humidity, w/b ratio, and mix design, it is possible to achieve significant improvements in concrete strength, durability, and sustainability.

2.3.3 Carbonation Curing of Biochar-Added Cementitious Materials

Cementitious material absorbs CO₂ during carbonation and permanently immobilize the CO₂ by forming carbonation products. The inclusion of biochar enhances carbonation through its ability to absorb CO₂. Furthermore, the high surface area of biochar strengthens the internal pore network of the cement matrix, enhancing CO₂ diffusion rate and providing more sites for carbonation reactions. The pores of the biochar can serve as nucleation sites for both hydration and carbonation products, accelerating the rate and deepening the degree of carbonation. The practice of carbonation curing on biochar-added cementitious material is a relatively new and recent development in the field of sustainable construction materials, emerging since the year 2020. Praneeth et al. (2020) confirmed the positive effect of corn stover biochar on the carbon sequestration performance of fly ash–cement mixtures. Gupta et al. (2021) reported that adding 3 wt.% of peanut hull biochar may improve carbon uptake by 5–7% while Chen et al. (2022) found out that 5 wt.% of corn straw biochar increase uptake by 1.14%. Yang and Wang (2021) also observed an increase in carbonation product as the biochar content is

increased. A summary of the previous studies conducted on the carbonated curing of biochar added-cement mortar is listed in Table 2.3.

Gupta (2021) did a thorough study on biochar-added mortars and evaluated the influence on the GHG emission. They found out that both unsaturated and saturated biochar-added mortars had lower net global warming potential and reduced CO₂ emission levels as compared to the control mortar. Saturating biochar with CO₂ before adding into cement admixture allows extra CO₂ adsorption of 7 mmol/g which is translated to a reduction of 300kg CO₂/tonne of dry feedstock (Wei et al., 2012).

Table 2.3: Summary and results of carbonate cured biochar-added cementitious materials

Mix composition (wt%)	Types	w/b ratio	CO ₂ concentration (%)	Duration	RH (%)	Temperature (°C)	Methods	CO ₂ uptake (%)	Reference
OPC Rice husk: 3, 5, 10	Paste	0.5	10	7d, 28d	75	23	TGA	7d: 5.2–10.2 28d: 6.1–11.3	(Agarwal et al., 2023)
OPC Fly ash: 20, 40, 50 Corn stover: 2, 4, 6, 8	Paste	0.53	100	2h	-	-	Mass change	23.96	(Praneeth et al., 2020)
OPC Silica fume: 8 Corn stover: 2.5	Paste	0.4	2	28d	65	30	Mass change	17.83	(Gupta, 2021)
OPC Biochar: 2, 5	Paste, Mortar	0.5	5	3d, 7d, 28d	60	23	TGA	Calcium carbonate content 72.2g/g	(X. Yang & Wang, 2021)
OPC Fly ash: 10 Biochar: 1	Mortar	0.485	12	7d	65±3	23±5	TGA	3.84–7.39	(Mishra et al., 2023)
OPC Corn straw: 5	mortar	0.4	20	3d, 28d	70	20	TGA	10.25–10.85	(Chen et al., 2022)

Table 2.3: Continued

Mix composition (wt%)	Types	w/b ratio	CO ₂ concentration (%)	Duration	RH (%)	Temperature (°C)	Methods	CO ₂ uptake (%)	Reference
OPC									
Fly ash: 10, 25, 40	Mortar	0.5	12	7d, 28d	65 ± 3%	23 ± 5	TGA	7d: 7–16 28d: 15–23	(Mishra et al., 2023)
Biochar: 2.5, 5									
OPC	Mortar	0.4	0.5	48h	-	-	TGA	2.94	(Kua & Tan, 2023)
Wood assortment: 0.05									
OPC	Mortar	0.3	100	24h	-	-	Mass change	-	(L. Wang et al., 2020)
Sawdust: 0.1, 1.0, 2.5									
OPC									
Fly ash: 20	Mortar	0.5	1	7d, 28d	55	23	Mass change	18.07	(Gupta, Kashani, et al., 2021)
Peanut hull: 1, 3									

2.4 Identification of Research Gap

While biochar offers numerous improvements in physical and mechanical properties, the outcomes are highly dependent upon the type of biochar used. There is an abundance of literature on biochar derived from wood sawdust (Gupta, 2021; Gupta et al., 2018; Gupta et al., 2020), and wood chips (Gupta et al., 2022; Maljaee et al., 2021; Restuccia et al., 2020) due to its widespread availability worldwide. Numerous studies have also explored the potential of biochar-concrete produced from sources such as corn stover and corn straw (Chen et al., 2022; Praneeth et al., 2020), peanut hull (Gupta & Kashani, 2021; Haris Javed et al., 2022), bagasse (Zeidabadi et al., 2018) and many others.

However, research on the selected RHB, CHB, PKS, and BB is relatively limited, despite the fact that neighbouring countries around Malaysia are among the largest producers of these materials. Specifically, China is the largest producer of rice and bamboo, Indonesia leads in coconut and palm oil production, and the Philippines is also a major coconut producer. Although studies on these biochar do exist (Beskopylny et al., 2022; Flórez et al., 2019; Gupta, Krishnan, et al., 2020; W. Liu et al., 2022), they are relatively fewer compared to the scale of production in these countries.

Despite the growing interest in biochar-cement composites, there remains a significant gap in research focusing on local materials and conditions. The selected four types of biochar are all available in Malaysia. This study focuses on evaluating the carbon sequestration performance of locally obtained biochar in cementitious materials, with the additional aim of reducing local agricultural waste.

Additionally, another critical area where research is lacking is the use of larger volumes of biochar as a replacement in cement composites. While many studies have explored the incorporation of small quantities of biochar, the effects of replacing a substantial portion of cement with biochar have not been investigated. Research should

focus on understanding the impacts of high-volume biochar replacement on the mechanical properties. Thus, this study aims to incorporate a substantial amount of biochar into cementitious composites and investigate its interaction, performance, and potential for enhancing carbon sequestration. Addressing these gaps can enhance the understanding and practical application of biochar in cement composites, leading to more sustainable and locally relevant solutions in the construction industry.

2.5 Summary

Chapter 2 provides a comprehensive review of biochar and its relevance to cementitious materials, with revisions addressing key aspects highlighted in the comments. The chapter begins with an introduction to biochar, including market analysis, physical and chemical properties, and its diverse industrial applications. The carbon sequestration potential of biochar is detailed in Section 2.1.3, emphasizing its role in mitigating climate change by capturing and storing carbon.

Section 2.1.4 has been expanded to include detailed insights into biochar production techniques, such as pyrolysis, and the parameters influencing its quality, including porosity, surface area, and chemical composition. Section 2.1.5 discusses the availability of biochar in Malaysia, focusing on local production capabilities and distribution.

In the context of cementitious materials, Section 2.2 reviews the performance of biochar-modified composites, with an enhanced discussion on the suitability of biochar as a cement replacement material. Key aspects, including its environmental benefits, pozzolanic reactivity, and its effects on concrete properties such as compressive strength, durability, thermal conductivity, and fluid transport, are presented. Challenges, such as biochar's water demand and variability in properties, are also addressed.

Section 2.3 explores broader CCS techniques in concrete, focusing on accelerated carbonation curing and the potential integration of biochar into these processes. Section 2.4 identifies research gaps from the literature, offering directions for future studies.

Overall, Chapter 2 provides a detailed and updated overview of current research, applications, and technological advancements related to biochar and CCS in the concrete industry, aligning with the comments to enhance the discussion of production, properties, and applications of biochar.

Universiti Malaysia

CHAPTER 3: METHODOLOGY

3.1 Introduction

This chapter provides an overview of the research methodology employed in the study. The basic premise is to identify and select the biochar with the best ability to sequester carbon, which will be applied to boost the carbon uptake ability of cement mortar. The conceptual framework of the research is structured based on the research objectives. The first step is to obtain and characterize different types of biochar, followed by saturation of biochar with CO₂, incorporating biochar into cement mortar, and performing microstructure analysis for quantification of the carbon uptake.

Section 3.2 describes the sourcing and preparation of raw material and its characterization methods. Section 3.3 provides the saturation process of biochar powder with CO₂. In section 3.4, the mix design of the mortar and paste are provided followed by the casting and curing process of the biochar-added mortar. Section 3.5 describes the mixing, casting and curing processes for the cement mortars. Subsection 3.6 provides information on the test methods for porosity, compressive strength, carbonation depth, and carbonation degree. The final subsection details the specific procedures and technique used for microstructural analysis. Figure 3.1 displays the overall approach of the study.

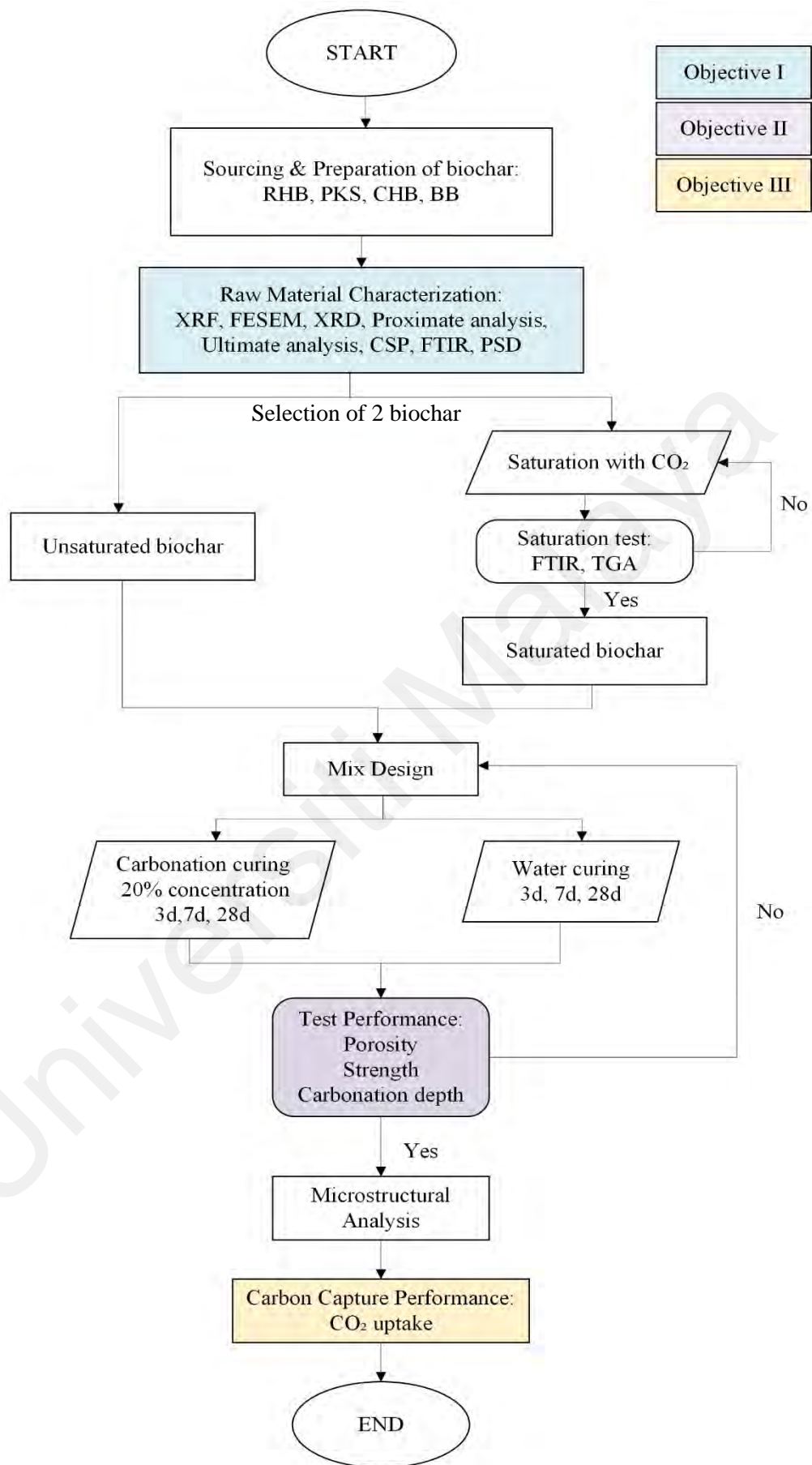


Figure 3.1: Conceptual framework of the research study

3.2 Preparation of Raw Materials

3.2.1 Sourcing of Binders

The binders used in this research project were Ordinary Portland cement (OPC) and four different kinds of biochar, namely RHB, PKS, CHB and BB. Ordinary Portland cement manufactured by YTL Cement, Malaysia complying with both ASTM (Type I) and EN (42.5N) standards, with a specific gravity of 3.15 and a Blaine's specific surface area of 372 m²/kg, was utilized. Table 3.1 shows standard strength requirement of cement type I according to the ASTM standard.

Table 3.1: Standard strength requirement based on ASTM C109M

Compressive strength (MPa)	Cement Type I
1 day	...
3 day	12.0
7 day	19.0
28 day	...

RHB was acquired from Sendi Enterprise Sdn. Bhd., Tanjung Karang, Selangor, Malaysia. Rice husk waste from the paddy field was burned and carbonized at thermal condition of 800°C in a short duration of approximately 8 – 10 seconds to produce RHB. A water sprinkler system was activated to cool down the RHB, preventing it from turning into ash. The RHB was then packed into polypropylene woven bags of 10kg each and then further transported to buyers. The market for RHB was usually used in soil conditioning and to boost plantation by farmers. Figure 3.2 shows the granary and production of RHB from rice husk waste.



Figure 3.2: The production of RHB from rice husk waste at Sendi Enterprise

PKS was obtained from the Malaysia Palm Oil Board (MPOB) located at Kajang, Selangor, Malaysia. The palm kernel shell waste was converted into PKS at pilot scale using a pyrolysis machine as shown in Figure 3.3. The palm kernel shell biomass waste was air-dried, and then further oven dried to a moisture content of <10%. The dried biomass waste was fed into the hopper and pyrolyzed at 600°C for 30 minutes. The controlled pyrolysis of palm kernel shell produced PKS and bio-oil as a side product.



Figure 3.3: The biochar experimenters kit at MPOB, Kajang (Haryati et al., 2018)

CHB was sourced from Pakar Management Technology Sdn. Bhd. located at Kajang, Selangor. The coconut husk was collected from various sources and air-dried. CHB was obtained through carbonization at 450 – 550°C using a closed kiln at low concentration of oxygen. The CHB was then cooled naturally, the impurities were screened off and further packed to be exported. CHB demand was high for its usage as biofuel and especially as activated carbon.

BB was obtained from Golden Toad Bamboo Industry situated at Tambunan, Sabah. The BB was 100% made from bamboo plants and has a high carbon content. BB was produced through pyrolysis, the carbonization process under temperature of 400°C up to 1000°C for 8h. BB had more carbon at the same pyrolysis temperature compared to other biochar. BB was primarily used in soil, as a deodorizer, and as activated carbon. Figure 3.4 shows the four types of biochar obtained.



Figure 3.4: Locally obtained biochar (a) RHB (b) PKS (c) CHB (d) BB

The physical appearance of the biochar reflects the source material and its production process. The RHB obtained have shapes of the rice husk, which was fibrous and elongated, having sizes of approximately 1 cm. The RHB was very brittle and can be crushed easily. The RHB was oven-dried and crushed by using ball mill for 0.5 hour and sieve passed 75 μm . The RHB obtained had a bulk density of 105 kg/m^3 . The PKS obtained have irregular shapes and sizes ranging from 0.5 – 2.5 cm in diameter. It is hard and chunky, having a more solid appearance as compared to the other types of biochar. The PKS had a BET surface area of more than 250 m^2/g and a bulk density of 490 kg/m^3 . The PKS was crushed using a ball mill for 24h and sieve passed 75 μm .

The CHB obtained was granular and flaky, composing of small fragments and particles. The particle size ranges from fine powder up to larger flakes of few millimetres.

The CHB were also brittle in nature, it was ball milled for 0.5 hour and further sieved passed 75 μm . The obtained CHB had a bulk density of 399 kg/m^3 . The BB obtained is in a fine and homogeneous powdered form. It has a bulk density of 241 kg/m^3 . The BB was ground for 20 minutes and sieved passed 75 μm . All the biochar samples were ensured to have similar particle sizes to ensure homogeneity for further characterization.

3.2.2 Characterization of Binders

The physicochemical properties of the biochar were studied through a series of techniques as listed in Table 3.2.

Table 3.2: Methods for characterization of biochar according to their properties

No	Analysis Method	Abbreviation	Purpose
1	X-Ray Fluorescence	XRF	Determination of chemical composition.
2	Field Emission Scanning Electron Microscopy	FESEM	Observation of morphology.
3	X-Ray Diffraction	XRD	Assessment of crystallinity.
4	Proximate analysis	-	Determination of moisture content, volatile matter, fixed carbon, and ash content.
5	Ultimate analysis	-	Determination of carbon (C), hydrogen (H), nitrogen (N), sulphur (S) and oxygen (O) contents.
6	Carbon Sequestration Potential	CSP	Determination of biochar with the best carbon uptake.
7	Fourier-Transform Infrared Spectroscopy	FTIR	Determination of functional groups.
8	Particle Size Distribution	PSD	Determination of particle sizes.

3.2.2.1 X-ray Fluorescence (XRF)

The oxide composition of the binders was obtained through Supermini 200 XRF Spectrometer with X-ray 50kV and 200W Pd-anode.

3.2.2.2 Field Emission Scanning Electron Microscopy (FESEM)

The surface morphology and porous structure of the biochar was observed using FESEM (Zeiss Gemini Auriga).

3.2.2.3 X-ray Diffraction (XRD)

The mineralogy and crystallinity of the biochar was studied through Rigaku MiniFlex 600. X-rays were generated at 40kV and 15mA and scanning was conducted over a 2θ range of $5 - 70^\circ$ using Cu-K α radiation with a step width of 0.02° and speed $6^\circ/\text{min}$.

3.2.2.4 Proximate Analysis

The proximate analysis is a fundamental technique used to evaluate the composition of organic materials, providing the basic characterization information about biochar. This analytical method provides valuable insights into the qualitative and quantitative distribution of moisture content, volatile matter, fixed carbon, and ash content in the given sample. The proximate analysis was obtained through TGA conforming to ASTM D2974. The rate of mass change according to temperature was used to study the thermal degradation and combustion behaviour of the biochar. The biochar samples were tested at heating rate of $10^\circ\text{C}/\text{min}$ and continuous nitrogen gas flow of $50 \text{ ml}/\text{min}$ from room temperature to 105°C and held for 10 minutes to remove moisture. The samples were further heated to 900°C and held for 15 minutes to remove all volatile components. The residue left in the samples were considered as the fixed carbon content of the samples. The ash content was obtained by combusting the biochar sample at 750°C and held for

30 minutes. The mass loss at each stage was recorded as the moisture content, volatile matter, fixed carbon and ash content of the biochar.

3.2.2.5 Ultimate Analysis

The ultimate analysis is used to determine the elemental composition of the biochar. The key elements analyzed were carbon (C), hydrogen (H), nitrogen (N), sulphur (S) and oxygen (O). The analysis was obtained using LECO TruSpec Micro CHNS Analyzer. The molar ratio of H/C and O/C were important indicators to estimate the stability and degree of carbonization. Lower ratios of H/C and O/C were preferred indicating higher degree of carbonization and high stability. H/C ratio lower than 0.2 was characterized as being hardly degradable in the environment, having a half-life of more than 1000 years while ratio higher than 0.7 will have a half-life of more than 100 years. The calculations of H/C and O/C molar ratios were shown as equation 3.1 and 3.2 as follows:

$$H/C \text{ ratio} = \frac{\text{mass}_H(\%)}{\text{mass}_C(\%)} \times \frac{\text{molar mass}_C (g/mol)}{\text{molar mass}_H (g/mol)} \quad (3.1)$$

$$O/C \text{ ratio} = \frac{\text{mass}_O(\%)}{\text{mass}_C(\%)} \times \frac{\text{molar mass}_C (g/mol)}{\text{molar mass}_O (g/mol)} \quad (3.2)$$

3.2.2.6 Carbon Sequestration Potential (CSP)

The CSP of each biochar was assessed through TGA. (Saleem et al., 2022). The CSP calculation of the biochar was presented in equation 3.3:

$$CSP (\%) = \frac{Y \times C_{\text{biochar}} \times R_{50}}{C_{\text{raw}}} \quad (3.3)$$

Where,

Y is the yield of the biochar (%), C_{biochar} is the carbon content in the biochar, R_{50} is the recalcitrance index, and C_{raw} is the carbon content of the feedstock.

The recalcitrance of biochar indicated its stability toward thermal, physical, and chemical degradation. The value of R_{50} was calculated using equation 3.4 (Harvey et al., 2012):

$$R_{50} = \frac{T_{50}}{T_{50, \text{Gr}}} \quad (3.4)$$

Where,

T_{50} is the temperature at which 50% of the biochar sample was thermally oxidized, $T_{50, \text{Gr}}$ is the T_{50} of graphite = 886°C (Harvey et al., 2012).

The moisture correction for TGA data was done through equation 3.5 (M. Ahmad et al., 2019):

$$W_c = 100 + 100 \times \frac{W_{\text{UC}} - W_{200, \text{UC}}}{W_{200, \text{UC}} - W_{\text{cut, UC}}} \quad (3.5)$$

Where,

W_c and W_{UC} are the corrected and uncorrected weight losses in the initial sample, respectively, $W_{200, \text{UC}}$ is the weight loss at 200°C, and $W_{\text{cut, UC}}$ is the temperature at which no further weight loss was observed.

The CSP (%) of each biochar was calculated and compared. Only the first two types of biochar with the highest CSP will be selected for further characterization and casting into cement mortar.

3.2.2.7 Fourier-Transform Infrared Spectroscopy (FTIR)

The functional group of the selected biochar was determined using FTIR-Spectrum 400. The test was performed with wavelength in the range of $400 - 4000\text{cm}^{-1}$ and spectral resolution of 4cm^{-1} . Pellets were made with a hydraulic press by mixing 1 mg of each dried paste specimen with 400 mg of potassium bromide (KBr) and then subjected to FTIR analysis.

3.2.2.8 Particle Size Distribution (PSD)

The particle size analysis of the OPC and the selected biochar was obtained using Malvern instruments Mastersizer 2000. The understanding and the controlling of the PSD of the material is critical to optimize the performance of the concrete composites. The PSD of the materials will directly affect the workability and eventually the strength and durability of the cement mortar.

3.2.3 Fine Aggregates and Water

CEN graded standard sand (with specific gravity of 2.65) conforming to the international standard EN196-1 was utilized. The grain sizes of the sand ranges between 0.08 and 2.00 mm. The grain size distribution of the sand is listed in Table 3.3. The maximum moisture content is 0.2%. The sand was portioned in bags of $1,350 (\pm 5)$ g. Tap water was used in this research.

Table 3.3: Particle size distribution of CEN reference sand

Square mesh size (mm)	2,00	1,60	1,00	0,50	0,16	0,08
Cumulative sieve residue (%)	0	7 ± 5	33 ± 5	67 ± 5	87 ± 5	99 ± 1

3.3 Saturation of Biochar with Carbon Dioxide (CO₂)

Some biochar was saturated with CO₂ prior to its incorporation into the cement. The purpose of this treatment was to enhance the carbon sequestration capacity of the biochar, thereby reducing the cement's overall carbon footprint. This process effectively locks CO₂ within the biochar structure, facilitating long-term carbon storage. Additionally, CO₂ saturation pre-fills the pores of the biochar with gas, influencing its interactions with water and cement during mixing. This, in turn, affects the compressive strength and durability of the resulting composite material. The study aimed to evaluate whether saturating biochar with CO₂ beforehand would improve the biochar-mortar performance more effectively compared to conventional carbonation curing.

The biochar was saturated with CO₂ by exposing it to a 100% CO₂ concentration for 4 hours. The adsorption capacity of the biochar was calculated through mass loss by thermogravimetric analysis (TGA) test at 500 – 600°C. The complete desorption of CO₂ from biochar occurs at 600°C (Gupta, 2021). The adsorption capacity was calculated according to equation 3.6:

$$\text{Adsorption (mmol/g)} = \frac{(m_x - m_s)}{m_i \times mm_{CO_2}} \quad (3.6)$$

Where,

m_x is the mass of the unsaturated biochar, m_s is the mass of the saturated biochar at temperature 500°C and 600°C respectively, m_i is the initial mass of the biochar and mm_{CO_2} is the molar mass of CO₂. A FTIR test was also conducted to analyze the changes in the physicochemical properties of the biochar after saturating it with CO₂. A comparison is made with the unsaturated biochar to study the CO₂ adsorption mechanism.

3.4 Mix Design

RHB and PKS were selected for use in the cement mortar due to their superior CSP compared to CHB and BB. The higher CSP of RHB and PKS enhances their capacity for CO₂ uptake, which is expected to improve the performance of the biochar-cement mortar. This higher CO₂ uptake can contribute to increased carbon storage within the material and potentially improve the strength and durability of the resulting composite. As a result, RHB and PKS were prioritized over CHB and BB for this study. A total of eighteen mortar mixes were designed to incorporate RHB and PKS each into cement mortar at high volume cement replacement of 10%, 20%, 30% and 40%. The mixing w/b ratio was set as 0.6 as higher w/b ratio produce porous mortars that were more suitable for CO₂ uptake (Z. Liu & Meng, 2021). RHB absorbs water about 110.05% of its dry weight due to its high-water retention capacity, which reduces the workability and may affect the early hydration of the cement matrix. PKS on the other hand absorbs water at 70.11% of its weight. As a result, to make up for the water loss due to absorption, additional water was added to attain similar flowability of about 220 ± 10 mm. It was also notable that the introduction of biochar into the cement mortar reduces the fresh density. Table 3.4 gives the mix design of the biochar-added mortar with the nomenclature. Cement pastes were further cast for microstructural characterization. The pastes were cast to achieve standard consistency and the ratio of water is listed in Table 3.5 while Table 3.6 summarized the curing regimes.

Table 3.4: Mix proportion of biochar-added mortar

Nomenclature	Cement (kg/m ³)	XRHB (kg/m ³)	SRHB (kg/m ³)	XPKS (kg/m ³)	SPKS (kg/m ³)	Water (kg/m ³)	Additional water (kg/m ³)	Sand (kg/m ³)
M0*	500	-	-	-	-	300	-	1434.4
RM10X	450	31.9	-	-	-	270	35.1	1434.4
RM20X	400	63.9	-	-	-	240	70.3	1434.4
RM30X	350	95.8	-	-	-	210	105.4	1434.4
RM40X	300	127.8	-	-	-	180	140.6	1434.4
RM10S	450	-	31.9	-	-	270	35.1	1434.4
RM20S	400	-	63.9	-	-	240	70.3	1434.4
RM30S	350	-	95.8	-	-	210	105.4	1434.4
RM40S	300	-	127.8	-	-	180	140.6	1434.4
PM10X	450	-	-	26.2	-	305	18.3	1434.4
PM20X	400	-	-	52.4	-	310	36.7	1434.4
PM30X	350	-	-	78.6	-	315	55.0	1434.4
PM40X	300	-	-	104.7	-	320	73.3	1434.4
PM10S	450	-	-	-	26.2	288	18.3	1434.4
PM20S	400	-	-	-	52.4	277	36.7	1434.4
PM30S	350	-	-	-	78.6	265	55.0	1434.4
PM40S	300	-	-	-	104.7	253	73.3	1434.4

* R = RHB; M = mortar; P = PKS; X = unsaturated; S = saturated.

Table 3.5: Mix proportion of biochar-added paste

Nomenclature	Cement (g)	RHB (g)	PKS (g)	w/b ratio
N0*	333.3	-	-	0.31
RN10X	300.0	21.3	-	0.36
RN20X	266.7	42.5	-	0.41
RN30X	233.3	63.7	-	0.48
RN40X	200.0	84.9	-	0.55
PN10X	298.1	-	17.4	0.35
PN20X	265.0	-	34.7	0.40
PN30X	231.9	-	52.1	0.46
PN40X	198.8	-	69.4	0.50

*N = paste

Table 3.6: Different curing regimes for biochar-added cement mortar

Nomenclature	Curing regime (curing period)	
	Carbonation curing (d)	Water curing (d)
C3	3	-
C7	7	-
C28	28	-
W3	-	3
W7	-	7
W28	-	28
C3W4	3	4
C3W25	3	25
C7W21	7	21

*Full nomenclature of the samples is denoted as follows:

- RM10S-W3: 10% SRHB-added mortar undergoing full 3 days water curing.
- RM20X-C3W4: 20% XRHB-added mortar undergoing 3 days carbonation curing and 4d water curing.
- PM30S-C28: 30% SPKS-added mortar undergoing full 28 days carbonation curing.
- PN40X-C28: 40% XPKS-added paste undergoing full 28 days carbonation curing.

3.5 Mixing, Casting and Curing

3.5.1 Casting

To produce mortar, cement and biochar were prepared and introduced into the mixing bowl. Water was added and mixed at low speed (140 ± 5 rpm) for 60 seconds. Sand was then added slowly into the mixture over a 30 second period and mixed at medium speed (285 ± 10 rpm) for another 60 seconds. The flowability was measured in accordance with ASTM C1437 and the entire mixture was remixed for 15 seconds. The fresh mortar was cast into 50 x 50 x 50 mm molds and further tamped for compaction and removal of air bubbles. After casting, specimens were covered with a perspex and left hardened for 24 hours. The mortar cubes were then demolded and subjected to curing until test day. Additionally, cement pastes with biochar subjected to full 28 days water curing and 28 days carbonation curing were used for further microstructural tests, namely XRD, FTIR and FESEM-EDS.

3.5.2 Moist Curing

The specimens were subjected to water curing until the testing age (3 days, 7 days and 28 days). For combined curing, the mortar was first subjected to carbonation curing and then followed by subsequent water curing until standard testing day as specified in Table 3.6.

3.5.3 Carbonation Curing

The specimens for carbonation curing were pre-conditioned in oven at 80°C for 2 hours. Pre-conditioning for a short period of time can improve the carbonation reaction (D. Zhang et al., 2017). The carbonation curing parameter was set with RH of $80 \pm 10\%$, a curing temperature of $20 \pm 3^\circ\text{C}$, CO₂ concentration of 20% and atmospheric pressure. The carbonation chamber used is shown in Figure 3.6.



Figure 3.5: Operating carbonation chamber at the set parameters

3.6 Test Methods

3.6.1 Porosity

The porosity of the produced specimens was evaluated based on the water absorption test according to ASTM C642. Unsaturated biochar was used for this test. Mortar cubes were subjected to water curing and carbonation curing for 28 days. The samples were then dried at 100°C for 2 days, cooled and the mass was recorded as (A). The samples were immersed in water for another 2 days to obtain the saturated mass after immersion (B). After that, the samples were placed in water bath and boiled for 5 hours and then allowed to cool for at least 14 hours. The surface-dried mass was obtained as (C). The value of apparent mass was obtained by suspending the samples by wire in water (D).

By using the values for mass determined, the average values of for three samples of mortar for water absorption and volume of pore permeable space were calculated through equation 3.7 and 3.8:

$$\text{Water absorption, \%} = \frac{B-A}{A} \times 100 \quad (3.7)$$

$$\text{Volume of permeable pore space (voids), \%} = \frac{C-A}{C-D} \times 100 \quad (3.8)$$

3.6.2 Carbonation Depth

The carbonation depth of the specimens was tested with a phenolphthalein indicator. The carbonation depth of the specimens was tested with a phenolphthalein indicator. The carbonated mortar cubes at 3 days and 7 days were dried, cut in half, and the cross-section area was sprayed with phenolphthalein solution to observe the carbonation depth. The nature of the test was based on the change in the pH system, resulting in different colors of the phenolphthalein solution. The uncarbonated areas exhibited a bright pink color (pH < 12), while the semi-carbonated areas were light pink, and the fully carbonated areas of the mortar turned colorless (pH < 9). Figure 3.7 shows the color change of the phenolphthalein indicator due to carbonation.

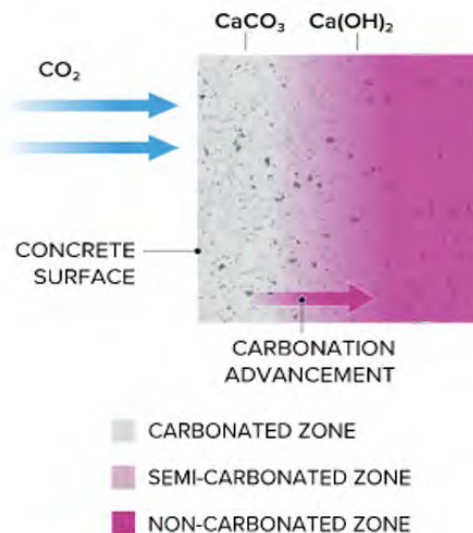


Figure 3.6: Color change of phenolphthalein solution

Digital images of the phenolphthalein treated specimens were captured using high-resolution imaging equipment. These images were transferred to ImageJ software for analysis. ImageJ was calibrated to ensure accurate measurement of pixel dimensions, and tools within the software were employed to analyze and quantify the areas corresponding to different colors of the phenolphthalein indicator. This approach facilitated precise measurement and comparison of carbonated and uncarbonated areas across the mortar specimens, providing valuable insights to the depth of the carbonation reaction.

3.6.3 Compressive Strength

The compressive strength of mortar specimens for water curing and carbonation curing were tested according to ASTM C109 for 3 days, 7 days and 28 days with universal testing machine and loading rate of 1.35kN/s. The average reading for compressive strength was taken based on three specimens.

3.6.4 Carbonation Degree

The carbonation degree and quantification of carbonation products were done through TGA according to ASTM C1872 and C1910. Mortar samples carbonation cured 3 days, 7 days, and 28 days were crushed and sieved to 150 μ m size. A mass of 40 mg of the samples were tested with the thermal analyzer NETZSCH STA 449F3 Jupiter at heating rate of 10°C/min and continuous nitrogen gas flow of 50 ml/min, heating from temperature 30 – 900°C. There were three main decomposition peaks obtained from DTG curves. The peak of weight loss occurred at 50 – 180°C was due to the dehydration of

ettringite (AFt) and aluminate ferrite monosulfate (AFm) (Vogler et al., 2022). Dehydration of calcium silicate hydrate (C-S-H) gels occurred over a continuous and broad temperature range, typically from 100 – 550°C. The third decomposition step was observed between 400 – 550°C due to dissociation of portlandite product and the last decomposition step was in the range of 550 – 950°C, showing the development of calcium carbonate in the RHB-added mortar. The amount of calcium carbonate formed through carbonation can be calculated from mass loss between 550 – 950°C (Kaliyavaradhan et al., 2020; Pham et al., 2024; X. Yang & Wang, 2021). Equation 3.9 shows the calculation steps for the calcium carbonate content while equation 3.10 and 3.11 calculates the CO₂ uptake for the biochar-added cement mortar:

$$\text{CaCO}_3 \text{ content (g/g)} = \frac{m_{550} - m_{950}}{m_{105}} \times \frac{100}{44} \times 100 \quad (3.9)$$

$$\text{CO}_2 \text{ carbonated (wt\%)} = \frac{m_{550} - m_{950}}{m_{105}} \times 100\% \quad (3.10)$$

$$\text{CO}_2 \text{ uptake (\%)} = \frac{\text{CO}_2 \text{ carbonated (wt\%)} - \text{CO}_2 \text{ initial (wt\%)}}{100 - \text{CO}_2 \text{ carbonated (wt\%)}} \times 100\% \quad (3.11)$$

3.7 Microstructure Analysis

3.7.1 X-ray Diffraction (XRD) Analysis

XRD is a pivotal technique for identifying and characterizing the crystalline phases in materials, including mortars, to assess their mineralogical composition and structural evolution. Using the Rigaku MiniFlex 600 diffractometer, the analysis was conducted with high precision, operating at 40 kV and 15 mA. Scans were performed over a 2θ range of 5°–70° using Cu-Kα radiation, with a step width of 0.02° and a scanning speed of 6°/min. This configuration ensured the accurate identification of crystalline structures.

The influences of biochar addition and different curing regimes on the microstructure and mineralogical properties of mortars were identified and analyzed. The components of the mortar were detected within their relevant 2θ ranges. The phases commonly observed in mortars included alite, belite, portlandite, calcium carbonate, and its polymorphs. Changes in the intensities and sharpness of peaks due to the addition of biochar and variations in curing regimes provided valuable insights for the detailed study and strength analysis of mortars.

3.7.2 Fourier-Transform Infrared Spectroscopy (FTIR) Analysis

Fourier Transform Infrared (FTIR) spectroscopy was a valuable technique for identifying the functional groups and chemical bonds present in materials, offering insights into their molecular structure. In the context of biochar-added mortars, FTIR analysis was particularly useful for understanding the functional groups and chemical interactions between biochar and cement hydration and carbonation products. The FTIR spectra were obtained using an FTIR-Spectrum 400. The test was performed over a wavelength range of $400\text{--}4000\text{ cm}^{-1}$ with a spectral resolution of 4 cm^{-1} . Specimens were prepared as pellets by mixing 1 mg of each dried paste sample with 400 mg of potassium bromide (KBr) and compressing the mixture using a hydraulic press before subjecting it to FTIR analysis. This method ensured accurate detection of chemical bonds and interactions within the material. Changes in the functional groups and the peak intensities under varying curing conditions provided critical insights into the interaction mechanisms between biochar and the cementitious phases. These insights were essential for optimizing the performance, durability, and sustainability of biochar-added mortars in construction applications.

3.7.3 Field Emission Scanning Electron Microscopy – Energy Dispersive X-ray (FESEM-EDS) Analysis

Cement pastes with varying levels of biochar replacement were prepared and cured under two distinct conditions: water curing and carbonation curing, both for a duration of 28 days. After curing, the hardened paste samples were broken into small pieces, ensuring at least one flat surface to facilitate accurate imaging and analysis. These prepared pieces were then subjected to detailed morphological and elemental analysis using a Field Emission Scanning Electron Microscope (FESEM), specifically the Zeiss Gemini Auriga model, equipped with Energy Dispersive Spectroscopy (EDS) using the EDAX AMETEK Apollo X system. The FESEM was operated at an accelerating voltage of 15 kV to achieve high-resolution imaging and reliable elemental detection.

The FESEM analysis will provide insights into the morphology of the biochar-modified mortars, including their porous structure, hydration products, and carbonation products. Porous structures were analyzed to evaluate changes in pore distribution and connectivity due to biochar inclusion and different curing regimes. The EDS system, mounted on the FESEM, enabled the elemental characterization of the cement matrix and biochar particles. It provided detailed information on the distribution of key elements such as calcium (Ca), silicon (Si), carbon (C), and oxygen (O), as well as any minor elements introduced by the biochar.

This combined morphological and elemental analysis using FESEM and EDS provided a comprehensive view of the interaction mechanisms between biochar, hydration products, and carbonation products, contributing to the optimization of biochar-added mortars for enhanced performance and sustainability.

CHAPTER 4: RESULTS AND DISCUSSION

4.1 Characterization of Biochar

4.1.1 X-ray Fluorescence (XRF)

The oxide composition of OPC and the four kinds of biochar is listed in Table 4.1.

Table 4.1: Chemical composition of OPC, RHB, CHB and BB through XRF

Oxide	OPC	RHB	PKS	CHB	BB
CaO	*74.71	2.41	74.38	9.30	17.38
SiO ₂	12.04	80.71	4.46	17.90	13.92
Fe ₂ O ₃	5.64	0.62	13.40	40.55	3.30
Al ₂ O ₃	1.84	-	-	2.41	-
MgO	0.37	-	-	-	-
K ₂ O	0.70	7.61	2.80	15.02	41.17
P ₂ O ₅	0.51	6.58	3.76	6.91	9.91
SO ₃	3.72	0.66	0.57	2.13	4.95
ZnO	0.06	0.20	0.19	2.75	0.54
MnO	-	-	-	0.62	5.53

*Values highlighted in blue indicate the major component of the biochar.

A high amount of SiO₂ component was observed in RHB where it meets the applicable requirements of class type F according to ASTM-C618, which can potentially exhibit pozzolanic properties. PKS had a higher CaO content similar to OPC. PKS was useful in processes like soil stabilization and metallurgical applications. CHB had the highest Fe₂O₃ content, ideal for applications like contaminant removal. BB contained the most K₂O, beneficial for agricultural use as it enhanced plant growth and resistance. Potassium and phosphorus components were usually used in agriculture as fertilizer. From the chemical composition shown in Table 4.1, it can be deduced that RHB and PKS, which had higher levels of calcium and silica, will contribute slightly better to strength compared to CHB and BB, which had higher levels of iron oxide and potassium oxide.

4.1.2 Field Emission Scanning Electron Microscopy (FESEM)

The surface morphology of the four different types of biochar can be observed through FESEM as shown in Figure 4.1.

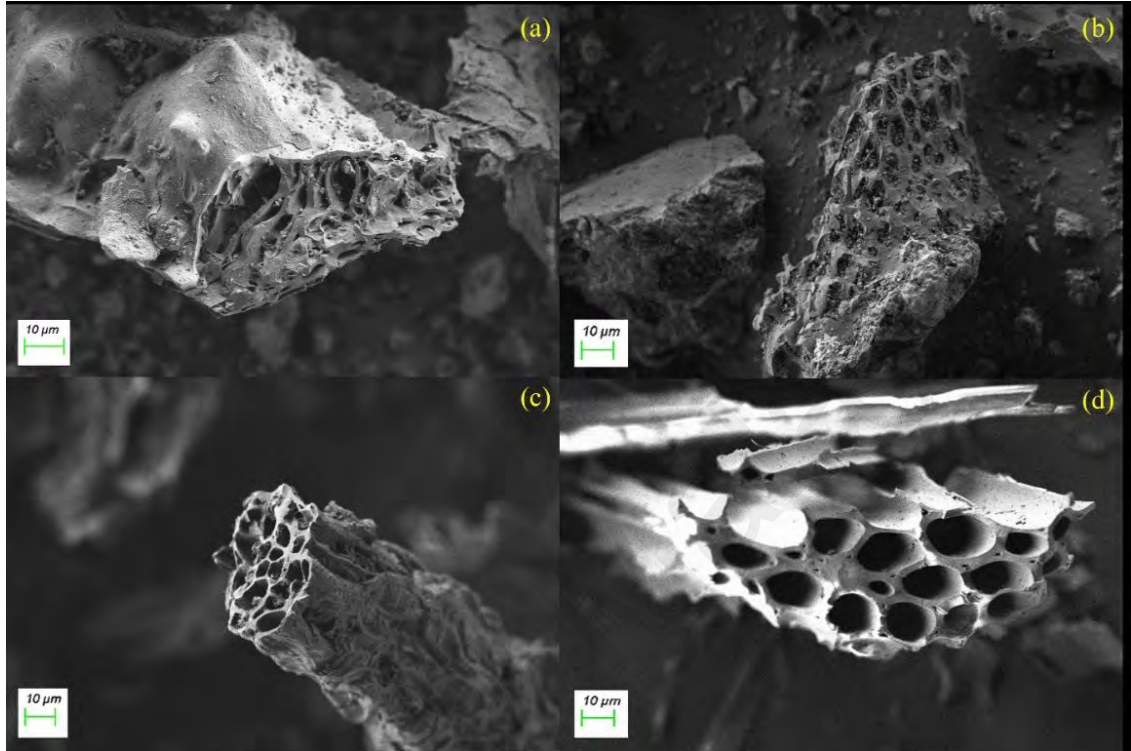


Figure 4.1: Surface morphology of (a) RHB; (b) PKS; (c) CHB; (d) BB at magnification 500x

Each type of biochar has a honeycomb-like porous structure that was high in surface area formed during pyrolysis. At high temperature, the cellulose and hemicellulose components of the plant biomass decompose, forming volatile compounds. As the volatile compounds released, pores and voids were left in the structure. The remaining solids undergo carbonization, transforming into a stable form of carbon and the pore structure becomes pronounced. The macropores ($>50\text{nm}$) were easily observed through FESEM and was responsible for the water retention or holding capacity of the biochar. The macropores will absorb and retain some part of the water during casting. At small amount of biochar replacement in the cement mortar, the smaller water retention capacity can

promote internal curing and nucleation of hydrate products in the pores (Muzyka et al., 2023). On the other hand, higher amount of biochar replacement may lead to high water retention which reduces workability of the mortar mix. There were smaller pores at the size of $< 2\text{nm}$, which were called micropores, these were the primary sites for CO_2 adsorption and storage (C. Zhang et al., 2023). CHB and BB were more fibrous and were seen to have elongated shape. RHB, CHB and BB have brittle structure, while PKS structure was compact and solid.

4.1.3 X-ray Diffraction (XRD)

Figure 4.2 shows the XRD patterns for biochar. All four types of biochar were seen to have a broad peak around $20 - 30^\circ$ indicating the amorphous structure of the biochar. The decomposition of the organic compounds in the biochar such as lignin, cellulose, and hemicellulose produce disorderly stacked graphite crystals and carbon rings.

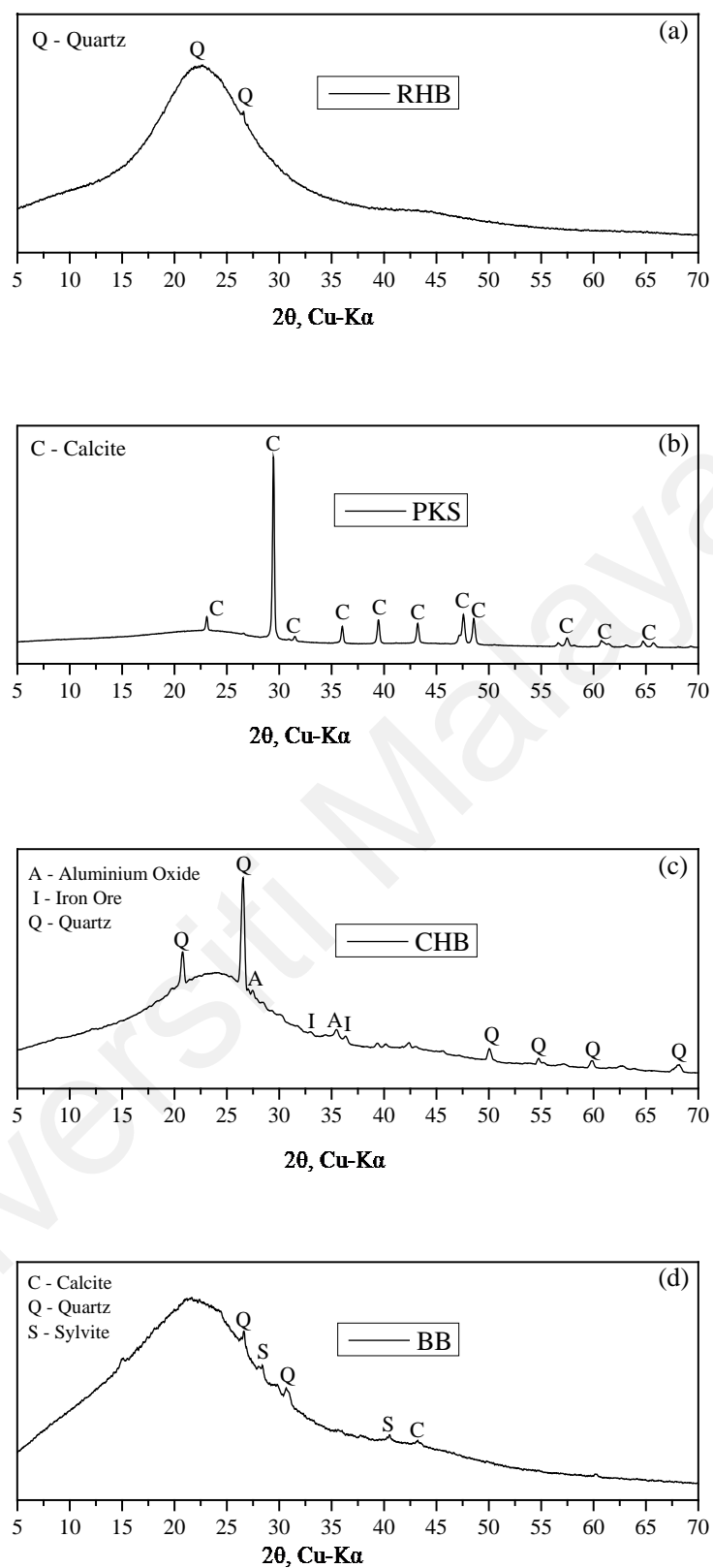


Figure 4.2: XRD patterns of biochar (a) RHB (b)PKS (c) CHB (d) BB

Mineralogy of RHB showed a broad peak at 22.6°, referring to an amorphous phase of SiO₂. This also showed that RHB has the potential of pozzolanic reaction, which may improve strength at a later age. The other three types of biochar PKS, CHB and BB were a mixture of amorphous and crystalline phases. PKS has sharper and stronger peaks of calcites at 23.06°, 29.44°, 31.50°, 36.06°, 39.48°, 43.25°, 47.55° and 48.57°. These distinctive peaks indicated that PKS has developed a more crystalline structure during pyrolysis. The peaks in CHB were attributed to the presence of silicate minerals, iron ore, and quartz. XRD peaks for BB at 28.36° and 40.57° indicate a crystalline phase for sylvite with the chemical formula KCl, a small amount of quartz and calcite at 26.52° and 43.34° respectively (Sahoo et al., 2021).

4.1.4 Proximate Analysis

The proximate and ultimate analysis provides the quality and the basic characterization information about the biochar. Table 4.2 shows the proximate analysis of biochar.

Table 4.2: Proximate analysis of biochar

	Moisture (%)	Volatile Matter (%)	Fixed Carbon (%)	Ash (%)
RHB	8.23	25.78	42.19	23.80
PKS	3.44	66.25	23.80	6.52
CHB	5.47	78.35	12.38	3.80
BB	6.68	30.68	57.35	5.30

Based on Table 4.2, all the biochar has low moisture content of less than 10%. The ash content indicated the presence of minerals and other inorganic substances in the samples. The ash content is high in RHB with 23.80% due to its high silica content. The ash content for the other biochar ranges from 3.80 – 6.52%. CHB exhibits the highest amount of volatile matter, followed by BB, RHB and PKS. The volatile matter indicates

the proportion of organic compounds that can be released as vapors when the biochar was heated and decomposed. It was usually comprised of water, hydrocarbons, organic acids, hydrogen, CO₂ and carbon monoxide. High volatile matter content suggests easier ignition and rapid energy release, while low volatile matter content indicates greater stability. PKS has the highest fixed carbon of 66.25%, followed by BB of 57.35%, RHB of 42.19% and CHB of 12.38%. Fixed carbon is the key parameter to evaluate the fuel value and combustion characteristics of the biochar. Higher fixed carbon indicates that the biochar has higher energy content, slower combustion, higher combustion temperatures, and greater stability for long-term applications. The good stability may suggest higher potential for carbon sequestration.

4.1.5 Ultimate Analysis

Table 4.3 shows the ultimate analysis for four types of biochar.

Table 4.3: Physicochemical properties of biochar through ultimate analysis

	C (%)	H (%)	N (%)	S (%)	O* (%)	H/C	O/C
RHB	33.40	0.50	9.20	1.80	55.10	0.18	1.24
PKS	61.59	3.31	0.70	2.16	32.24	0.64	0.39
CHB	57.11	1.81	0.80	0.23	40.05	0.38	0.53
BB	67.74	3.32	0.03	2.34	26.57	0.58	0.29

*O content is calculated by percentage difference.

Biochar had a high C content, and lower H, N and S contents. The C and H contents were generally higher in woody biomass, such as PKS, CHB and BB, compared to herbaceous biomass like RHB. Woody biomass had a higher lignin content, while herbaceous biomass contains more cellulose and hemicellulose. These differences affect the properties of the resulting biochar. The C content in the ultimate analysis is different from the fixed carbon content in proximate analysis. The C content in Table 4.3 referred to the total amount of C present in the material, including both fixed carbon and volatile

carbon. The fixed carbon content in Table 4.2 referred to the solid carbon residue that remained after all volatile matter was removed. The C content was used to evaluate the carbon sequestration potential of the biochar. BB had the highest C content of 67.74%, followed by PKS of 61.59%, CHB of 57.11% and RHB of 33.40%. Figure 4.3 shows a Van Krevelen diagram constructed for a better presentation of the H/C and O/C atomic ratio of biomass and its equivalent biochar.

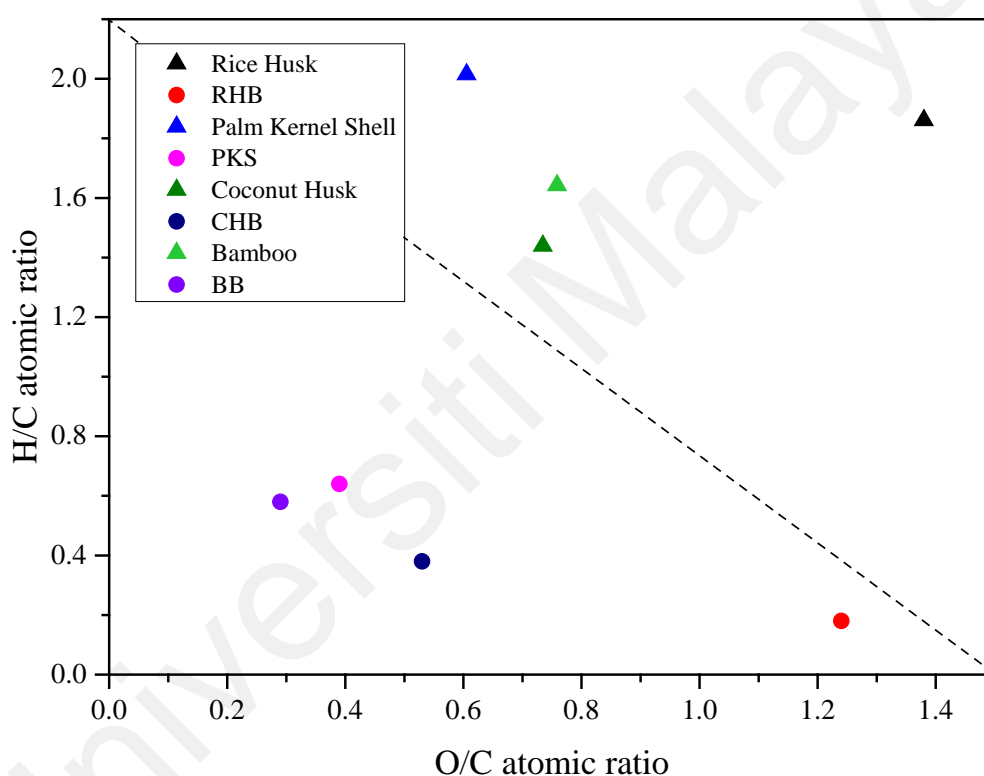


Figure 4.3: The Van Krevelen diagram of biomass and its equivalent biochar

Biomass with higher H/C and O/C atomic ratio, were situated on the upper right side of the Van Krevelen diagram while biochar with lower ratios is situated at the bottom left corner. During pyrolysis, the biomass undergoes thermal decomposition, causing a reduction of the H and O contents. As the volatile compounds released, the proportion of

carbon in the remaining solid mass increased, thus biochar had higher C content. Low H/C ratio indicated less H content relative to high C content, implying stabilization while low O/C ratio indicated carbonization and charring. All four of the biochar have low H/C molar ratio ranged from 0.18 to 0.64, thus all the biochar were considered stable for long term carbon storage. PKS, CHB and BB had relatively low O/C ratio, implying an increase in aromatization or coalification degree that was favourable for carbon sequestration. However, the O/C molar ratio for RHB of 1.24 was quite high, shown in Figure 4.3 indicating that the RHB had low aromaticity and maturity (Haryati et al., 2018). This was due to the short duration of pyrolysis that is less than 10 seconds during production at the factory. Either increasing the pyrolysis temperature or duration may aid in complete carbonization of the RHB and improve its properties.

4.1.6 Carbon Sequestration Potential (CSP)

The CSP of the four biochar was calculated and compared. Two of the biochar with the highest CSP were selected for the rest of the research. Figure 4.4 shows the parameters obtained from the corrected TGA graph while Table 4.4 summarized the calculated values of the CSP of the biochar.

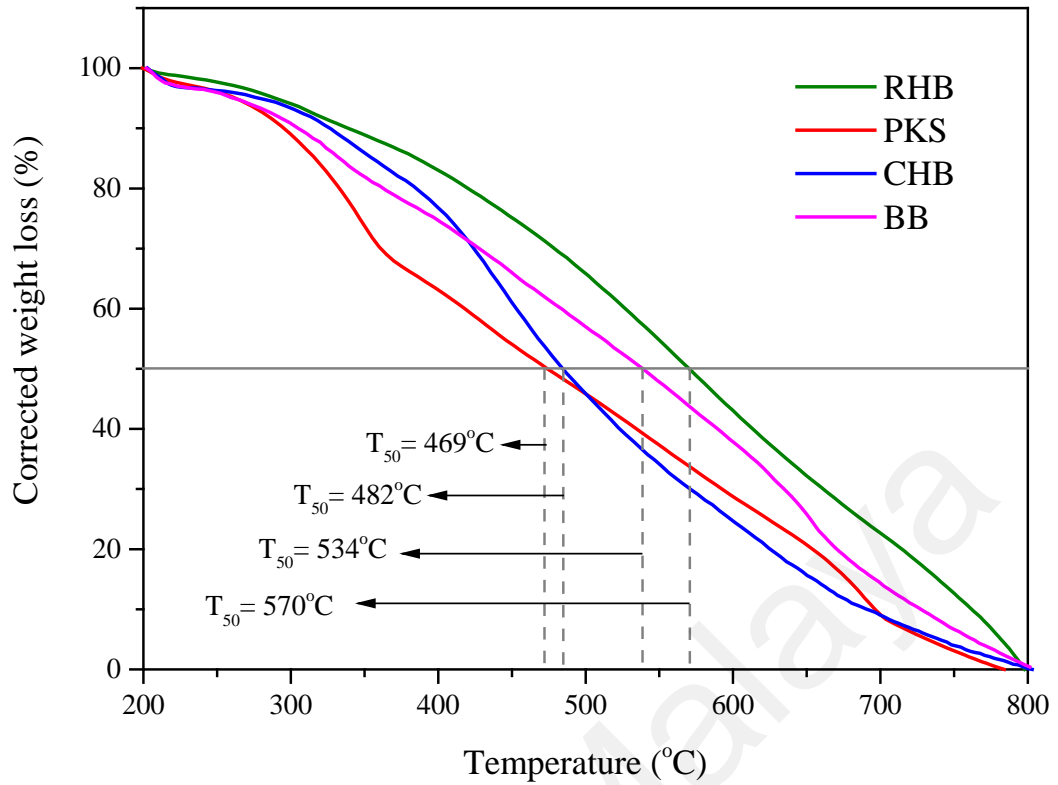


Figure 4.4: T₅₀ values obtained from TGA graph

Table 4.4: Assessment parameters for CSP calculation of the biochar

Parameters	RHB	PKS	CHB	BB
T _{50, Gr} (°C)	886	886	886	886
T ₅₀ (°C)	570	469	482	534
R ₅₀	0.64	0.53	0.54	0.60
Y (%)	42.80	43.40	36.90	30.30
C _{biochar} (%)	33.40	61.59	57.11	67.70
C _{raw} (%)	34.38	48.91	48.26	51.45
CSP (%)	26.75	28.93	23.76	24.03

The calculated CSP values were as follows: PKS led with 28.93%, followed by RHB with 26.75%, BB with 24.03%, and CHB with 23.76%. Consequently, RHB and PKS, with the higher CSP, were selected for further casting into cement mortar to study their CSP in cement. These two types of biochar were also much more readily available in

Malaysia compared to the latter. Further characterization will only be conducted for the selected biochar, RHB and PKS.

4.1.7 Fourier-Transform Infrared Spectroscopy (FTIR)

FTIR results in Figure 4.5 show the organic compound of RHB and the FTIR spectra of RHB is summarized in Table 4.5. The broad band absorption at 3392 cm^{-1} indicates O-H (hydroxyl) group with hydrogen bonding. Besides that, stretching at 2924 cm^{-1} and bending at 560 cm^{-1} was commonly related to C-H bond in alkanes or alkyl group (Sackey et al., 2021). The stretching vibration at 1606 cm^{-1} shows the aromatic compound of C=C functional group of lignin. The band at 1099 cm^{-1} was typically associated with stretching vibrations of siloxane bonds and C-O in alcohol groups of hemicellulose while the bending vibration at 801 cm^{-1} indicates the characteristic peak for Si-C bond in the RHB (Hidayat et al., 2023).

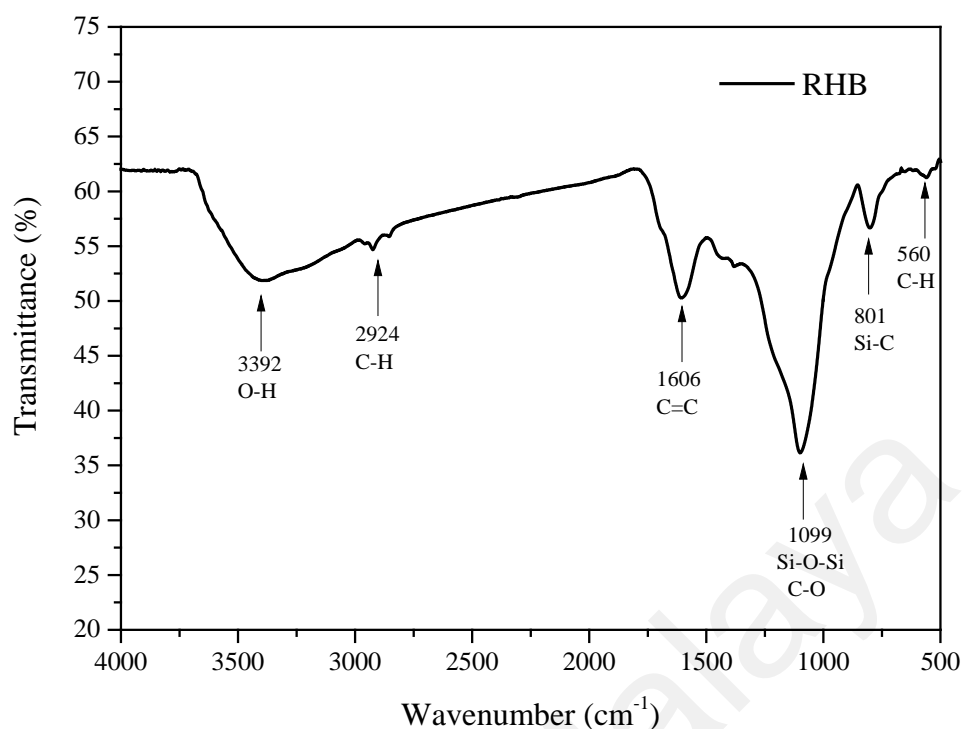


Figure 4.5: FTIR results for RHB

Table 4.5: FTIR spectra of RHB

Functional group	Frequency (cm ⁻¹)	Wavenumber (cm ⁻¹)	Description
-OH water	3100-3700	3392	hydroxyl stretch - strong
-CH alkane	2840-2950	2924	C-H stretch - weak
C=C alkene	1600-1680	1606	C=C aromatic - weak
Siloxane Bonds (Si-O-Si) and C-O stretch	1000-1200	1099	Presence of SiO ₂ content
silicon-carbon (Si-C) bonds	800-900	801	Presence of SiO ₂ content
-CH alkyl	~500	560	O-H stretch

Figure 4.6 portrays FTIR results for PKS whole the FTIR spectra of PKS is summarized in Table 4.6. The bands in the region 2500 to 3500 cm⁻¹ were barely visible due to degradation of the cellulosic and ligneous components during pyrolysis. There is a broad absorption stretch at 3215 cm⁻¹ showing the O-H group, an aliphatic band of C-

Hemicellulose at 2923 cm^{-1} and a carboxylic stretching of O-H at 2514 cm^{-1} (Kong et al., 2019). The band at 1797 cm^{-1} indicates a carbonyl C=O stretching. A very strong and intense aromatic C=C stretch at 1422 cm^{-1} and aromatic bending of =C-H between $675\text{--}1000\text{ cm}^{-1}$ indicates that the PKS was pyrolyzed well with high aromaticity (Hidayu et al., 2019; Ma et al., 2015).

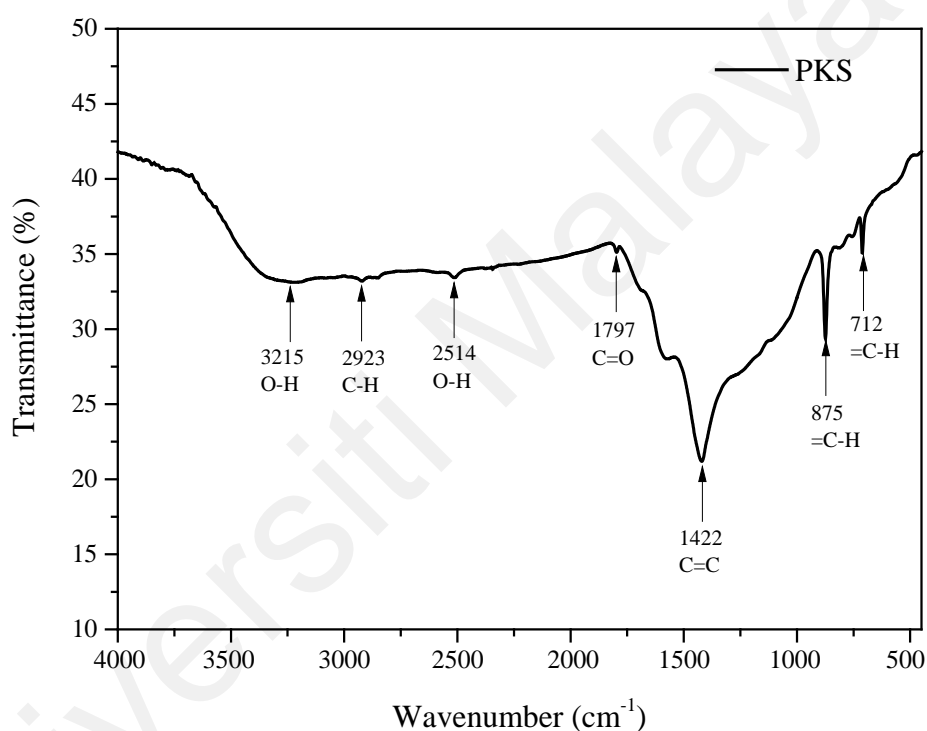


Figure 4.6: FTIR spectra for PKS

Table 4.6: FTIR spectra wavelengths for PKS

Functional Group	Frequency (cm ⁻¹)	Wavenumber (cm ⁻¹)	Description
-OH alcohol	3200-3600	3215	A broad stretch of R-OH group
-CH alkane	2850-3000	2923	C-H stretching of alkane
-OH Carboxylic acid	2500-3300	2514	Stretching of O-H in carboxylic acid
C=O Carbonyl	1670-1820	1797	Carbonyl stretching C=O

C=C alkene	1400-1600	1422	Aromatic ring stretching of C=C
=CH alkene	675-1000	875, 712	Aromatic bending of =C-H

4.1.8 Particle Size Distribution (PSD)

The PSD of OPC, ground RHB and PKS is presented in Figure 4.7. The D_{50} for cement, RHB and PKS were $20.51\mu\text{m}$, $23.77\mu\text{m}$ and $12.87\mu\text{m}$ respectively. RHB had slightly larger PSD with OPC while PKS had the smallest PSD. Generally, PSD equivalent to or smaller than that of OPC will be preferred to ensure the material achieved better packing density and higher surface area for hydration, which ultimately impacted the strength of the mortar.

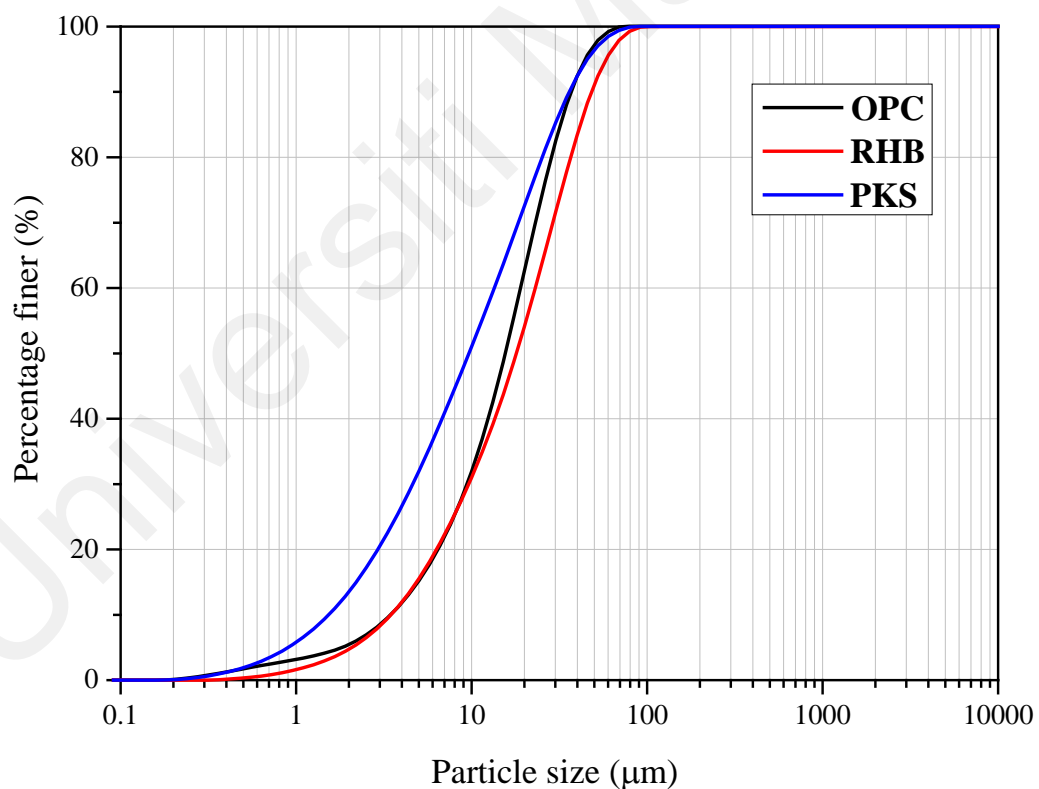


Figure 4.7: PSD of raw materials

The specific surface area of the material was also obtained from the same laser diffraction method of Mastersizer 2000. PKS had the highest specific surface area of 1.25 m²/g, followed by OPC and RHB of 0.815 m²/g and 0.598 m²/g respectively.

4.1.9 Saturation of Biochar with Carbon Dioxide (CO₂)

The adsorption capacity of RHB and PKS was calculated to be 1.83 mmol/g and 1.92 mmol/g through mass loss by TGA test at 500 – 600°C, for the complete desorption of CO₂ from biochar is at 600°C (Gupta, 2021). XRHB refers to unsaturated biochar while SRHB refers to biochar saturated with CO₂. Figure 4.8 compares the difference of saturated and unsaturated RHB.

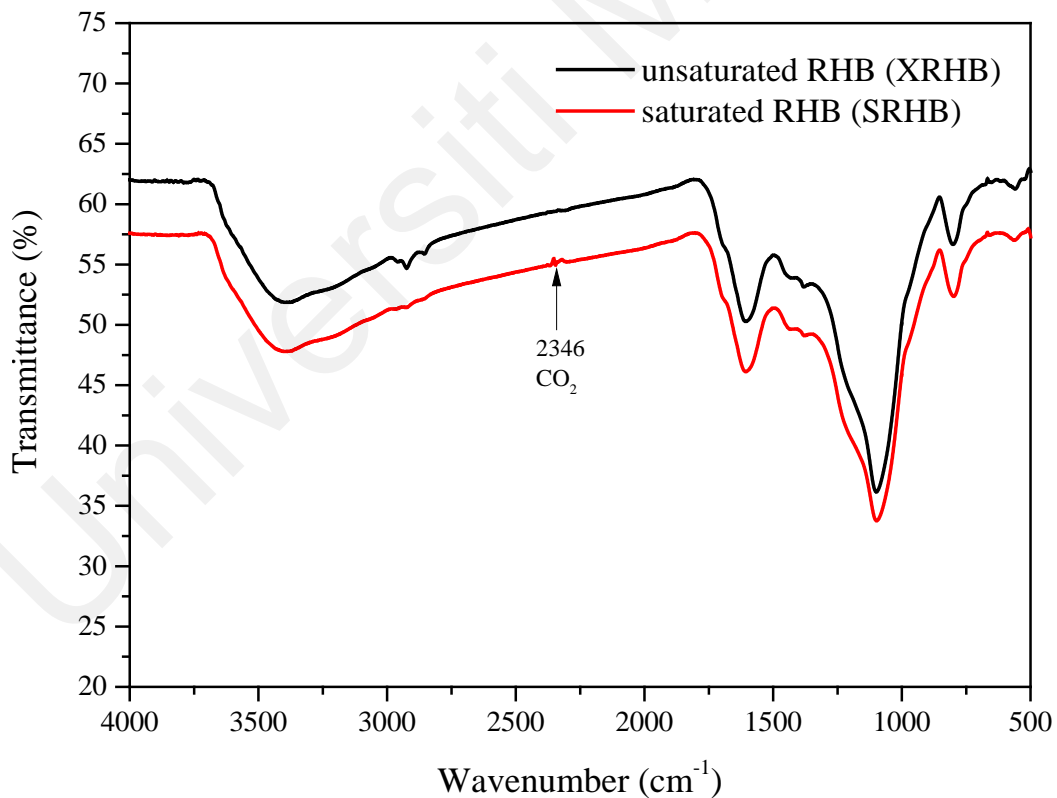


Figure 4.8: FTIR results for both saturated and unsaturated RHB

From the FTIR spectrum, both have similar functional groups, indicating that there were no chemical alterations due to the adsorption of CO₂. The only difference is the slight vibration band at 2346 cm⁻¹ indicating the presence of atmospheric CO₂ in the SRHB sample. Comparative analysis of other properties also show similarity in both the physical and chemical aspects (Gupta et al., 2018). Thus, the mechanism of CO₂ uptake mainly entails the physical adsorption of CO₂ in the micropores of biochar, without modifying its properties.

4.2 Porosity of Biochar-Added Mortar

The water absorption test is usually used to express the porosity of the mixes. Water absorption value was calculated by measuring the mass of water absorbed by the mortar specimens, which was highly dependent on the pore volume. The volume of permeable pore space (apparent porosity) of the cement mortar was directly related to the water absorption value. Since both the water absorption and apparent porosity have similar trends, thus only the apparent porosity will be discussed. Figure 4.9 shows the apparent porosity of the RHB-added mortar cubes.

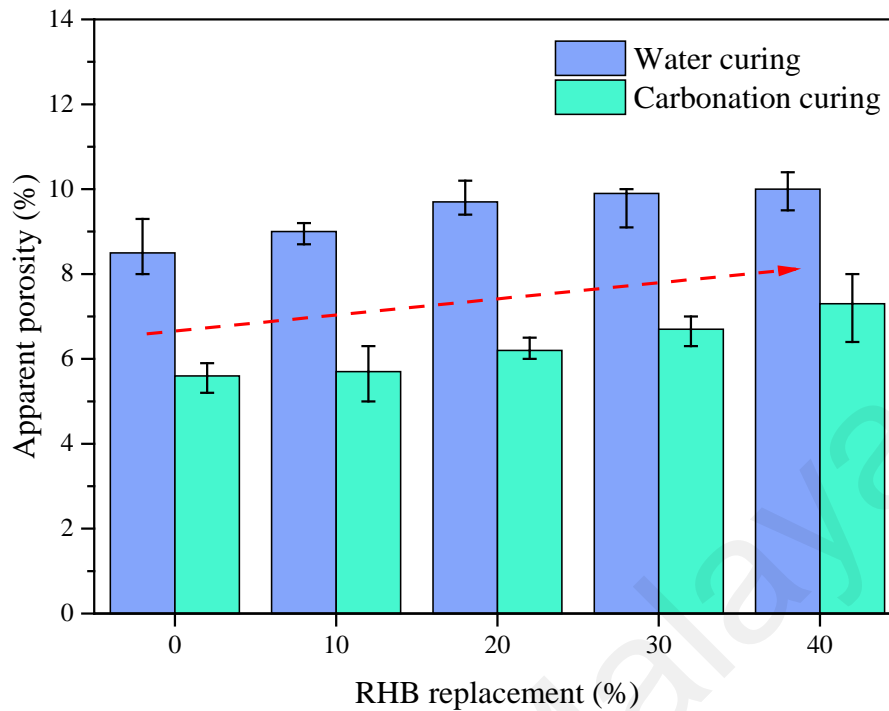


Figure 4.9: Apparent porosity for XRHB-added cement mortar for both water and carbonation curing

The permeability of cement mortar was closely related to its porosity, which influenced the diffusivity of CO_2 into the mortar. The apparent porosity had an increasing pattern as the dosage of RHB increased; this was due to the presence of mesopores and macropores in the mortar. The substitution of RHB into cement mortar formed a porous microstructure, making it easier for water to enter the mortar matrix. Besides that, higher w/b ratio, or excess water during mixing may cause formation of capillary pores and air voids, which compromised the strength of mortar. At lower dosage, the RHB cement matrix is denser. At higher dosage, RHB introduced many pores in the mortar, which resulted in higher water absorption, interrupting hydration and reducing strength growth.

As the RHB-added mortars became more porous, it became more favorable for carbon uptake. Thus, higher porosity of the RHB-added mortar was preferred for better

carbonation at a later stage. For carbonation cured mortars, the porosity results had similar pattern of increment to that of water curing. However, the values were much lower compared to water curing due to the formation of carbonate products which causes the cement pores to be filled up and densified with carbonate products. Gupta et al., 2021) conducted water capillary absorption test and the results obtained were consistent where water absorption reduces after carbonation due to the deposition of calcium carbonates in macropores of the mortar cubes. Thus, the carbonated mortars have denser structure and lower permeability which indicate higher compressive strength.

Figure 4.10 shows the results for PKS-added mortar. Generally, the addition of biochar will result in an increase in the porosity of the cement matrix. The high surface area and porous structure of the biochar introduced additional pore spaces within the structure and enhanced the overall porosity of the cement matrix, allowing for greater permeability and diffusivity. The PKS-added mortar had a slightly different trend than the RHB-added mortar.

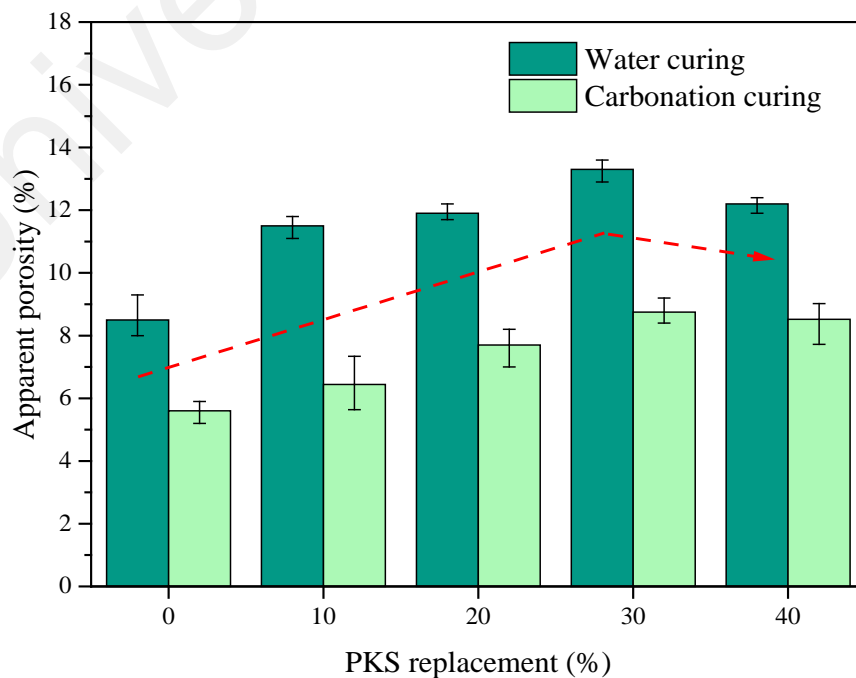


Figure 4.10: Apparent porosity for XPKS-added cement mortar for both water and carbonation curing

Maximum apparent porosity was observed at 30% PKS replacement, while 40% resulted in decreased porosity. This suggests that additional biochar did not contribute as effectively to further increasing porosity beyond the optimal replacement level. Additionally, aggregation or packing effects were noted at higher levels of biochar replacement, where the biochar particles filled up available space rather than creating additional pore spaces. The PKS replacement at 30% by volume was expected to achieve the highest carbon uptake due to its high permeability. After carbonation, the pattern for the apparent porosity was similar, much lower than the water cured specimens due to the densification of calcium carbonate in the cement matrix, reducing permeability.

Figure 4.11 compares the apparent porosity for both the RHB and PKS-added cement mortar.

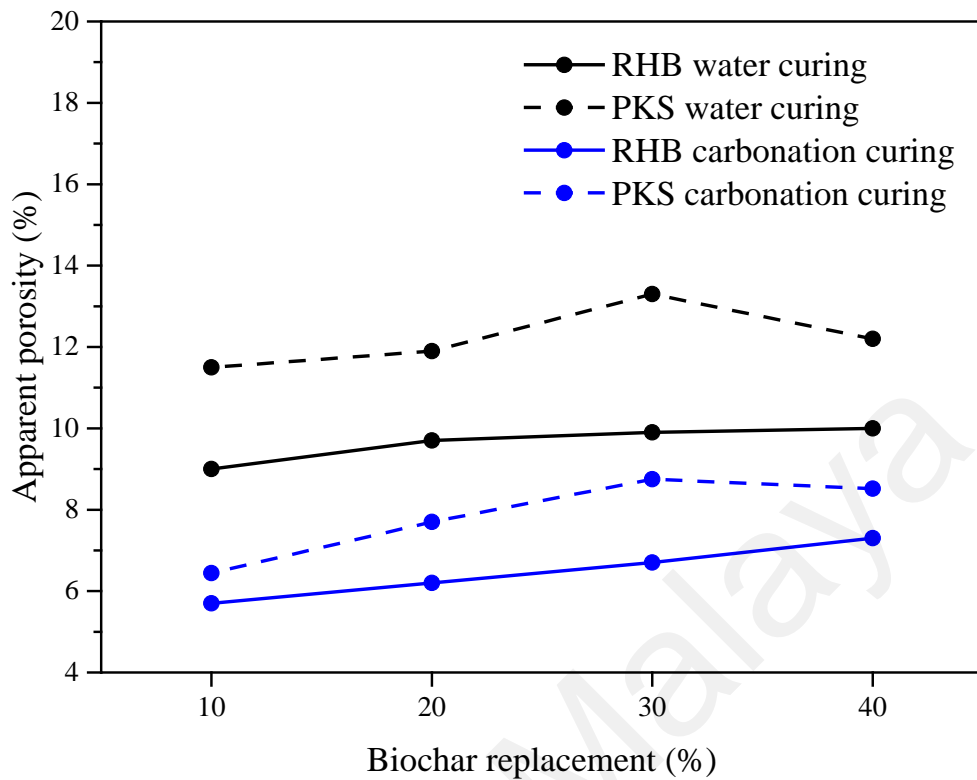


Figure 4.11: Comparison of apparent porosity for RHB and PKS biochar

Figure 4.11 clearly illustrates that the apparent porosity of PKS-added mortars was higher than that of RHB. The trends were similar for both water cured and carbonated specimens. The differences in apparent porosity between PKS and RHB highlight the significant role of the physical properties of the biochar in influencing the porosity of cementitious materials. It may be deduced that PKS possessed a more porous structure, with a greater number of mesopores and macropores compared to RHB. This structural characteristic allowed PKS to introduce more void spaces into the cement matrix, thereby increasing the apparent porosity of the specimens. Higher apparent porosity, as observed with PKS, enhanced the permeability and diffusivity of CO_2 within the mortar, which was crucial for the application of carbon sequestration in construction materials.

4.3 Carbonation Depth of Biochar-Added Mortar

An evident test for assessing the improvement in carbonation depth was the phenolphthalein test. This test allowed for the easy observation of qualitative carbonation rate and depth. The uncarbonated areas exhibited a bright pink color ($\text{pH} > 12$), while the semi-carbonated areas were light pink, and the fully carbonated areas of the mortar turned colorless ($\text{pH} < 9$). Figure 4.12 portrays the carbonation depth of RHB-added mortars observed through phenolphthalein solution.

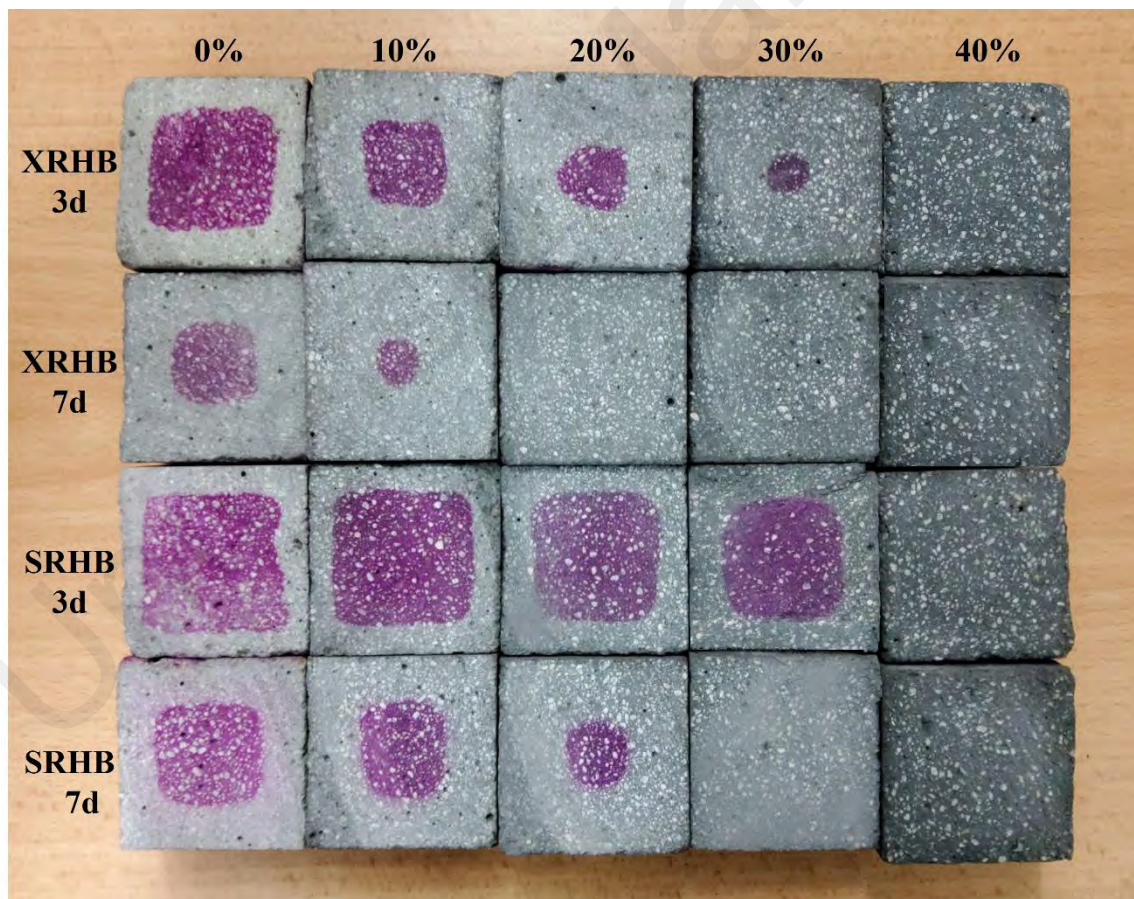


Figure 4.12: Carbonation depth of RHB-added mortars for 3d and 7d of carbonation curing

The carbonation reaction in cement mortar caused a drop in the pH level thus exhibiting different color gradient. Carbonation began from the surface of the mortar and slowly worked its way to the center of the cubes; thus, the colorless surface begins from the outer layer. As more calcium carbonates are formed on the surface of the mortar, it is difficult for CO₂ to penetrate to the interior of the mortar. Based on Figure 4.12, for both XRHB after 3 days and 7 days carbonation, the pink area was shown to decrease from 0% to 30%, proving that the addition of XRHB improved the CO₂ uptake and carbonation. The replacement of 40% did not show any pink color, possibly because of the significant amount of XRHB replacing cement, which diluted the alkalinity of the mortar, resulting in a more neutral pH. At 7 days carbonation for both 20% and 30% replacement, the specimens were colorless, indicating complete carbonation. Thus, specimens with carbonation beyond 7 days will not be conducted for this test. Similar patterns were observed for SRHB-added mortars, but at a lower carbonation rate. This could be attributed to adding water to SRHB during mixing, which may cause dilution or the formation of carbonic acid. These factors reduce both the carbonation rate and the compressive strength of the mortar simultaneously. Figure 4.13 shows the comparison of carbonation depth in PKS-added mortar specimens over time.

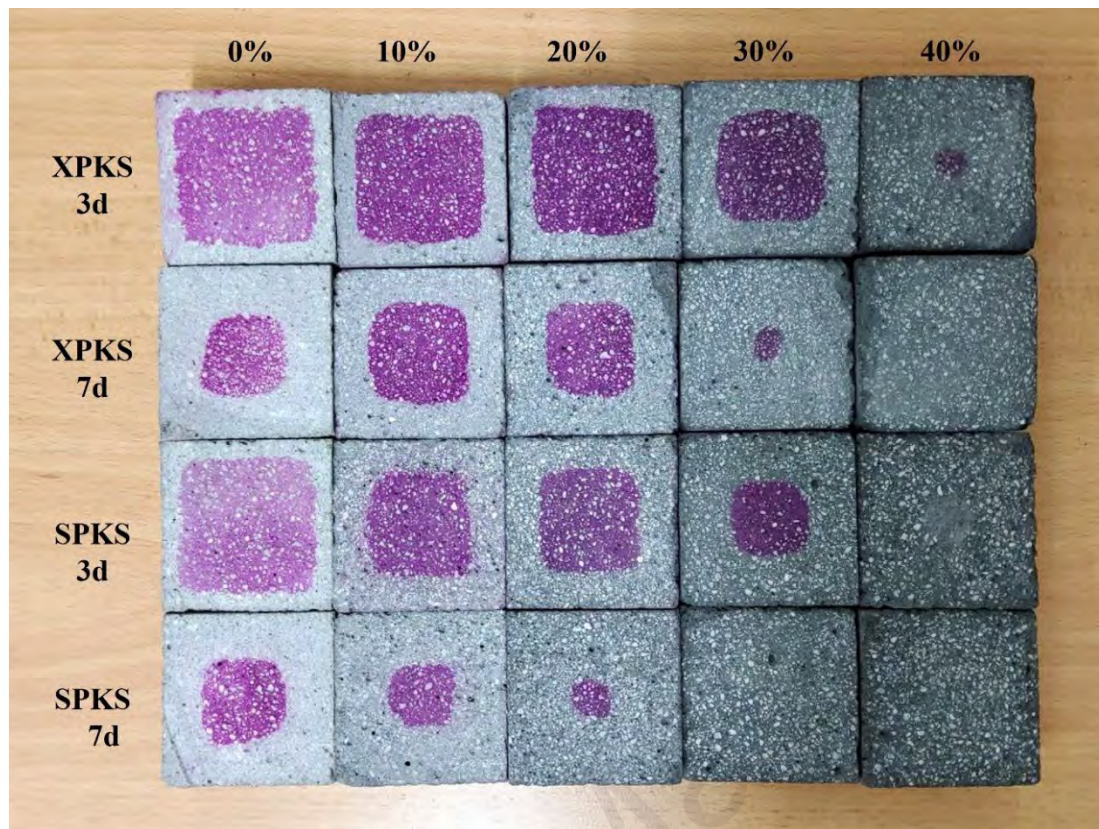


Figure 4.13: Carbonation depth of PKS-added mortars for 3d and 7d of carbonation curing

Overall, the addition of PKS represents a significant enhancement in carbonation depth within cementitious materials. The porous structure of the PKS allowed a deeper penetration of CO_2 into the cement mortar during the carbonation process. This enables CO_2 to reach the deeper layers of the cement matrix, thereby increasing the overall depth of carbonation. 7 days of curing further improved the carbonation reaction in the cement matrix, converting portlandite into carbonates and causing the change in pH level. 40% for XPKS replacement achieved complete carbonation from the surface to the core, exhibited by the colorless phase. It was observed that SPKS had better carbonation depth than XPKS. The CO_2 adsorbed within the pores of PKS enhanced the carbonation depth by supplying CO_2 from within the cement mortar. The combination of external and

internal supply of CO₂ catalyzed the carbonation kinetics, achieving deeper and more uniform carbonation throughout the cementitious material.

The images of the carbonation depth were analyzed using ImageJ software. Table 4.7 and 4.8 show the analysis results, with the calculated carbonated area in % and m² unit as well as the average length in cm of the carbonated part from the surface to the uncarbonated part of the biochar-added cement mortar. Figure 4.14 presents the comparison of the carbonated area of the SRHB and SPKS-added cement mortar. It is observed that the carbonated area of SPKS is higher than SRHB at 3 days and 7 days of carbonation. These results corresponded to the apparent porosity test, indicating that the addition of PKS produced cement mortars that were more porous than RHB and facilitated better carbonation.

Table 4.7: Carbonation depth results of RHB-added mortars using ImageJ analysis

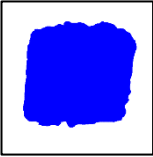
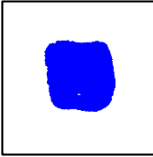
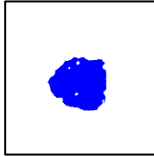
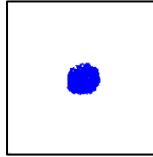



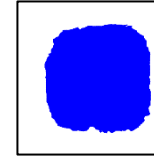

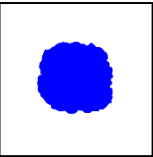
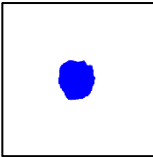


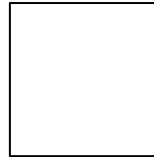
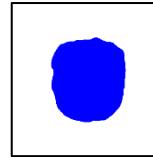
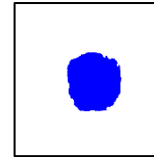
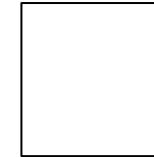
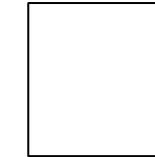




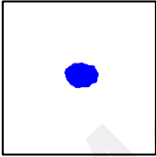


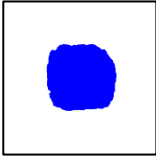
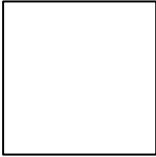
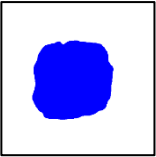



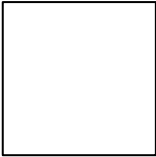
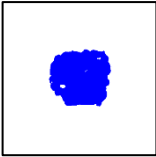
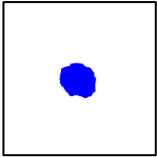
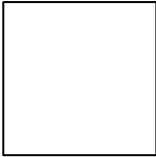
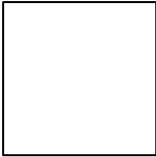
Curing duration	Control	XRHB 10%	XRHB 20%	XRHB 30%	XRHB 40%	SRHB 10%	SRHB 20%	SRHB 30%	SRHB 40%
3d									
Area (m ² /%)	0.009 m ² /	0.012 m ² /	0.013 m ² /	0.014 m ² /	0.015 m ² /	0.008 m ² /	0.009 m ² /	0.009 m ² /	.015 m ² /
/ Length	55.9 % /	80.7 % /	89.0 % /	96.1 % /	100.0 % /	50.3 % /	56.7 % /	61.9 % /	100.0 % /
(cm)	0.88 cm	1.51 cm	1.73 cm	2.00 cm	2.50 cm	0.71 cm	0.85 cm	0.92 cm	2.50 cm
7d									
Area (m ² /%)	0.012 m ² /	0.014 m ² /	0.015 m ² /	0.015 m ² /	0.015 m ² /	0.012 m ² /	0.013 m ² /	0.015 m ² /	0.015 m ² /
/ Length	82.7 % /	95.3 % /	100.0 % /	100.0 % /	100.0 % /	80.4 % /	89.6 % /	100.0 % /	100.0 % /
(cm)	1.38 cm	1.94 cm	2.50 cm	2.50 cm	2.50 cm	1.28 cm	1.73 cm	2.50 cm	2.50 cm

Table 4.8: Carbonation depth results of PKS-added mortars using ImageJ analysis

Curing duration	Control	XPKS 10%	XPKS 20%	XPKS 30%	XPKS 40%	SPKS 10%	SPKS 20%	SPKS 30%	SPKS 40%
3d									
Area (m ² /%)	0.006 m ² /	0.007 m ² /	0.007 m ² /	0.009 m ² /	0.015 m ² /	0.009 m ² /	0.010 m ² /	0.012 m ² /	0.015 m ² /
/ Length	40.0 % /	46.2 % /	49.5 % /	63.0 % /	97.6 % /	63.1 % /	67.2 % /	83.1 % /	100.0 % /
(cm)	0.55 cm	0.68 cm	0.68 cm	0.84 cm	1.93 cm	0.94 cm	1.04 cm	1.43 cm	2.50 cm
7d									
Area (m ² /%)	0.012 m ² /	0.009 m ² /	0.011 m ² /	0.015 m ² /	0.015 m ² /	0.013 m ² /	0.014 m ² /	0.015 m ² /	0.015 m ² /
/ Length	79.4 % /	60.8 % /	74.0 % /	97.1 % /	100.0 % /	87.2 % /	96.0 % /	100.0 % /	100.0 % /
(cm)	1.35 cm	1.01 cm	1.17 cm	2.07 cm	2.50 cm	1.49 cm	1.89 cm	2.50 cm	2.50 cm

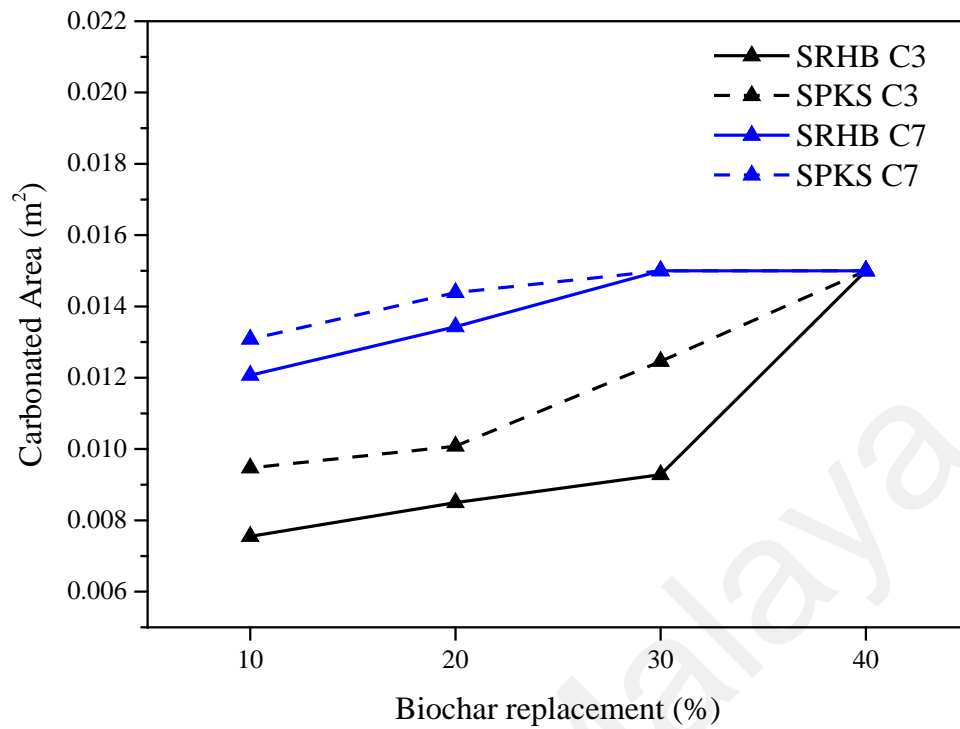


Figure 4.14: Comparison of carbonated area with RHB and PKS-added mortars using ImageJ analysis

4.4 Compressive Strength of Biochar-Added Mortar

Figure 4.15 depicts the compressive strength for both XRHB and SRHB under water curing, carbonation curing and combined curing at 3 days. In general, the addition of RHB produces porous mortar with lower strength. Strength reduced as more RHB was being replaced. This phenomenon was observed at every dosage and all curing stages.

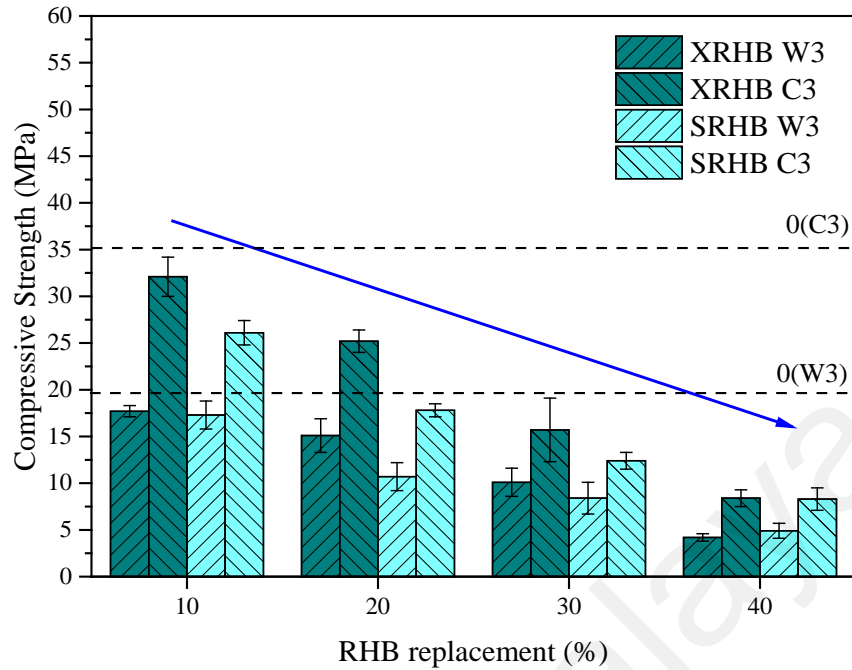


Figure 4.15: Compressive strength of RHB-added mortar at 3d curing against control

The reduction in strength is mainly due to dilution effect and high porosity of mortar matrix. The high replacement of RHB resulted in a decreased amount of cement and subsequently reducing the formation of hydration products like C-S-H, which contributes to strength. Mortar with high porosity was favoured for higher carbon sequestration during the carbonation curing. Another main reason for the reduction in strength is due to the excessive absorption of the additional water by the mix instead of being absorbed by the biochar (Lin et al., 2023).

Figure 4.16 presents the compressive strength results for 7 days curing. Accelerated carbonation curing enhanced the compressive strength for all samples at 7 days. From Figure 4.16 of carbonation 7 days, the compressive strength of M0-C7 showed an improvement of 48% as compared to M0-W7. Carbonation cured mortar for 7 days (M0-

C7) showed higher early age strength, reaching 111% of standard 28 days strength of the water cured mortar (M0-W28) of 42.4 MPa. During carbonation, the unhydrated cement and portlandite reacted with CO_2 to form calcium carbonate. The matrix pores and voids were precipitated with calcium carbonate crystals, causing the densification of the cement matrix, adding strength to the mortar. The findings were aligned with the porosity test presented earlier where carbonation cured specimens had higher compressive strength. The improvement of strength due to carbonation curing had similar trend for both 3 days and 7 days curing. Carbonation curing improved strength and addressed the issue of low strength of RHB-added mortar due to the porous structure.

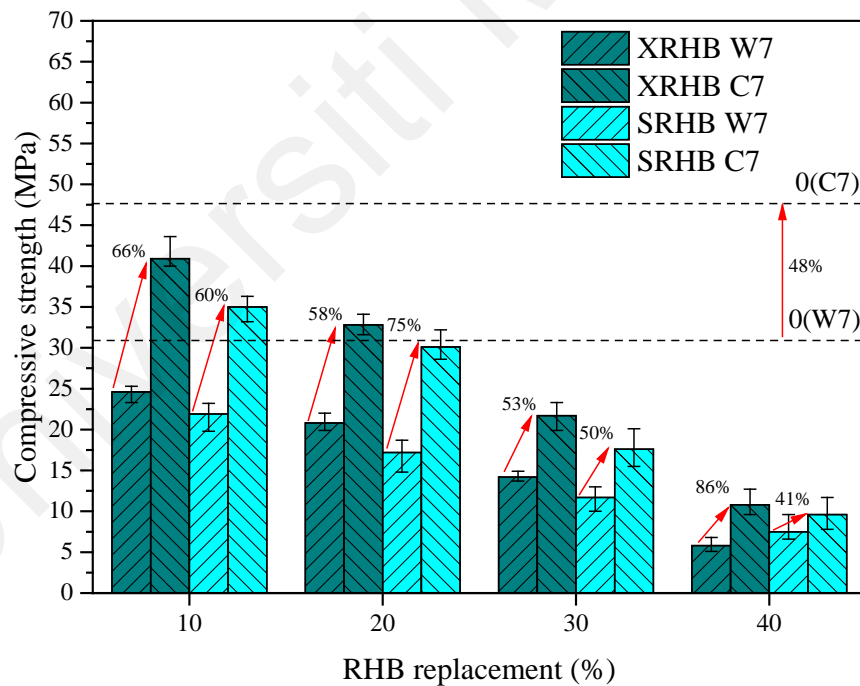


Figure 4.16: Compressive strength of RHB-added mortar at 7d curing against control

Furthermore, the presence of additional water in the pores of the mortar activated the unreacted cement particles to form C-S-H, thus hydration and carbonation occurred simultaneously, contributing to the binding of the particles and improvement of overall strength of the mortar. The formation of calcium carbonate developed a dense matrix at the surface of the mortar, making it harder for CO₂ to penetrate the mortar. These barriers will restrict CO₂ from entering the mortar and limit the movement within the mortar. It can be deduced that the rate of carbonation will reduce as carbonation duration becomes longer. Figure 4.17 depicts the strength result for 28 days curing.

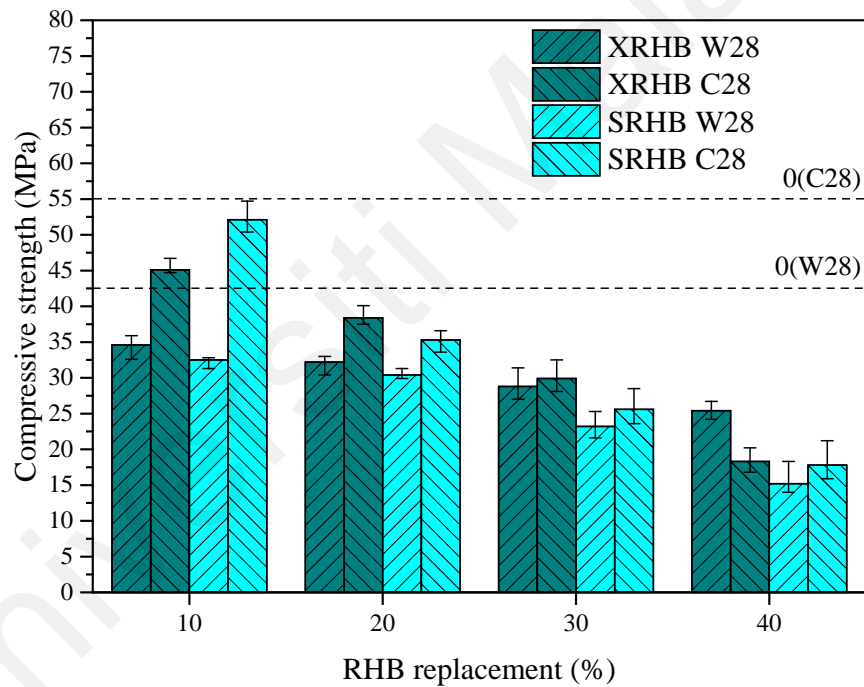


Figure 4.17: Compressive strength of RHB-added mortar at 28d curing against control

According to the 28 days strength results, the improvement in strength due to carbonation is much lesser compared to early days strength. Praneeth et al. (2020) confirmed the improvement of early day strength through carbonation. At higher RHB

replacement, the amount of cement and hydrates to react with CO₂ is lesser thus the strength is low. Hydration then becomes the major reaction thus water cured specimens have higher strength at 40% of RHB replacement by volume.

Combined curing was employed to provide and compensate water supply for further hydration after the carbonation curing. Figure 4.18 presents the results for the strength of combined curing.

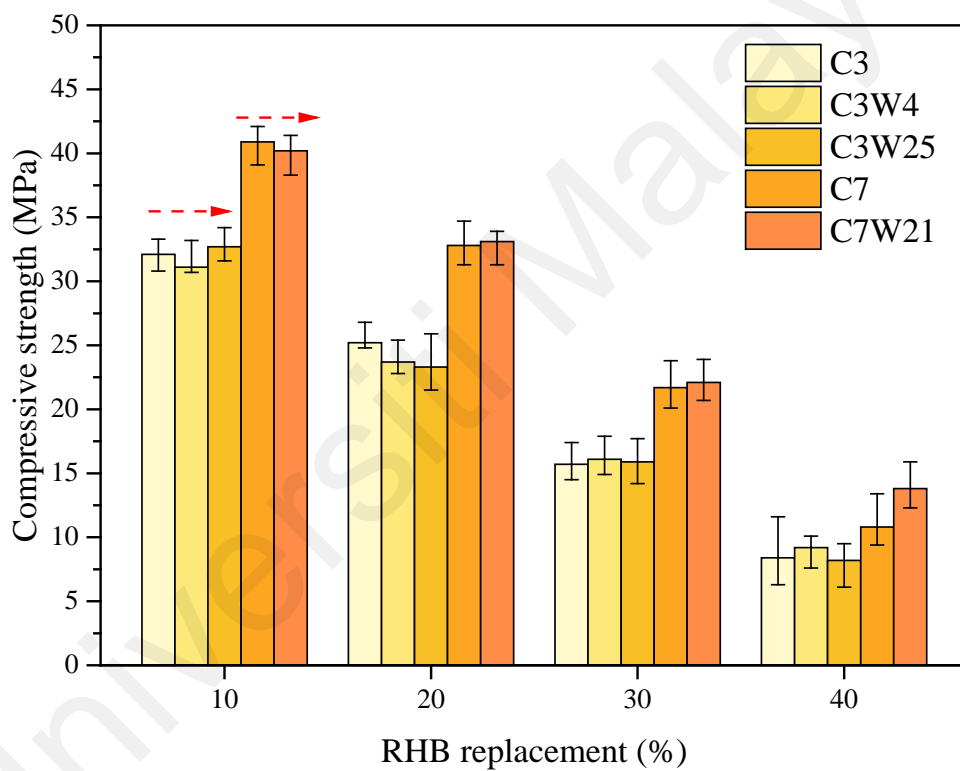


Figure 4.18: Combined curing for XRHB-added mortar

Based on Figure 4.18, the results had shown that C3W4 and C3W25 were comparable to C3. The trend was similar for all dosages and types of biochar whether it was XRHB or SRHB. The 3 days carbonation curing filled up the surface and pores of the mortar, leaving no room for water penetration and hydration into the mortar. The same goes for

C7 and C7W21, the strength of combine curing showed no improvement of strength as compared to sole carbonation curing.

Based on Figures 4.15 - 4.17, comparison of XRHB and SRHB was made for all results, the compressive strength for SRHB was generally lower than that of XRHB, which was counterintuitive. SRHB was expected to have higher strength as the CO_2 from the pores of RHB would be released and improved carbonation from within the mortar. The most likely reason was that the adsorbed CO_2 in RHB pores dissolved in water during mixing, generating carbonic acid. This resulted in an increased acidity within the cement matrix, which potentially reduced the overall strength by disrupting cement hydration. The acid reacted with the calcium component in cement, leading to degradation of cement structure over time. As a result, the mortar became weaker. Gupta et al. (2018) found that saturated biochar reduces compressive strength by 15% in mortar cured in water. They concluded that CO_2 trapped in the biochar pores causes expansive carbonation, leading to air voids and micro-cracks, weakening the bonds between biochar and cement, thereby decreasing strength. Wang et al. (2020) also confirmed that unsaturated biochar-added mortar exhibited higher strength. Thus, saturating biochar powder leads to detrimental effect on strength while carbonating mortar specimens improves the compressive strength.

Figure 4.19 shows the compressive strength results for PKS-added mortar. Similar to RHB-added mortar, strength reduced as more biochar was added into the mortar, this was mainly due to increased porosity.

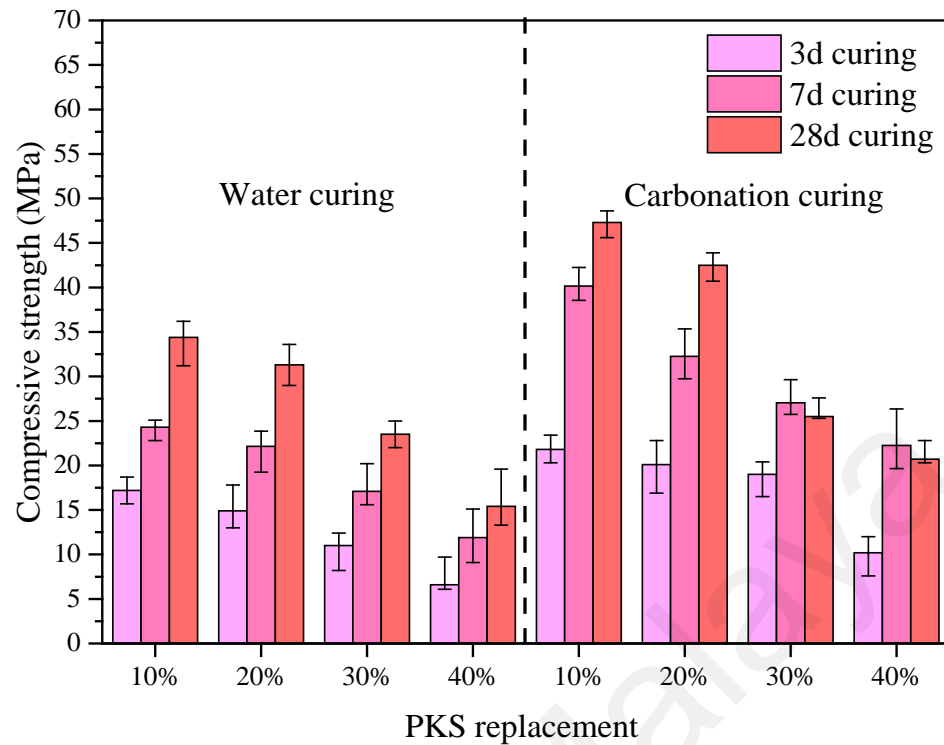


Figure 4.19: Compressive strength for PKS-added mortar at 3d, 7d and 28d

Carbonation was seen to enhance the compressive strength of the mortar overall, especially the early day strength. The improvement of strength due to carbonation curing ranges from 26.7 – 87%. Strength at 28 days for 30% and 40% PKS replacement by volume was lower than 7 days carbonation. Over carbonation may lead to a reduction in the strength of mortar. Excessive conversion of portlandite to calcium carbonate may disrupt the ongoing hydration process, which is essential for strength development, causing the mortar to have lower strength. Carbonate products are rigid and less flexible, making the mortar brittle. It can also cause microcracks on the surface of the mortar due to volume changes. These microcracks can propagate over time, leading to further deterioration and compromising the durability of the structure. Figure 4.20 portrays the results for combine curing for PKS-added mortar. While RHB-added mortar did not show

any improvement in strength after combined curing, it was observed that combined curing helped with hydration and slightly improved the strength of PKS-added mortar.

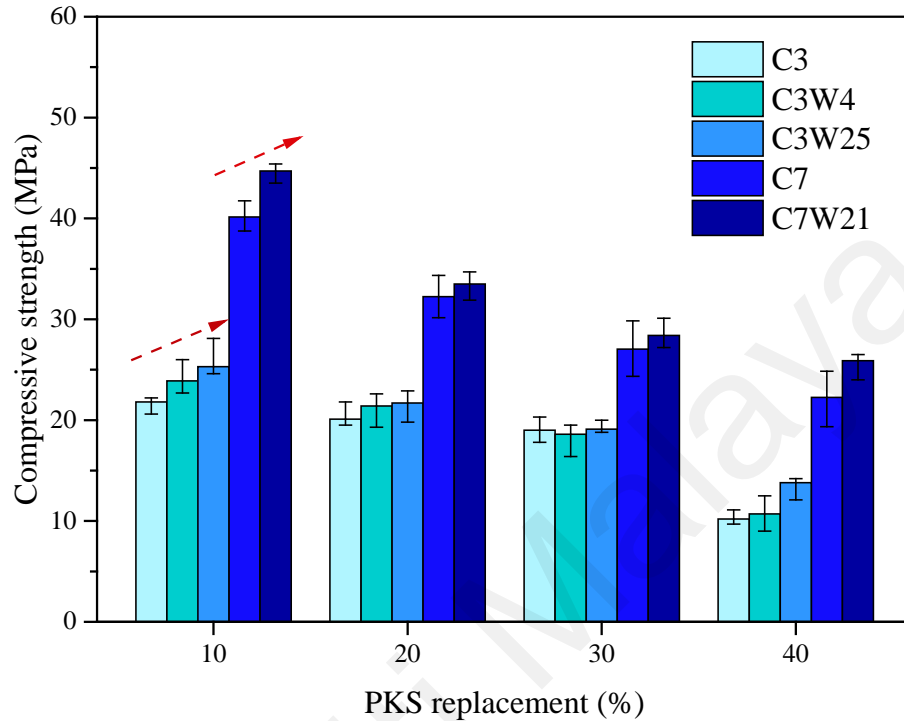


Figure 4.20: Comparison of compressive strength for combined curing of PKS-added mortar

The improvement of strength is true for all dosages of PKS biochar. The difference in the improvement in strength of these two types of biochar may be traced back to the pores, including macro and meso-pores, of the biochar, which governed the porosity of the produced mortar. RHB and PKS biochar had different pore structures, having different interactions that influenced the overall porosity and, consequently, the strength of the mortar. From the porosity test as aforementioned, the porosity of PKS-added mortar is higher than the RHB-added mortar even after carbonation curing. As a result, water could penetrate and diffuse into the mortar, further enhancing hydration. Figure 4.21 compares saturated and unsaturated PKS-added mortar.

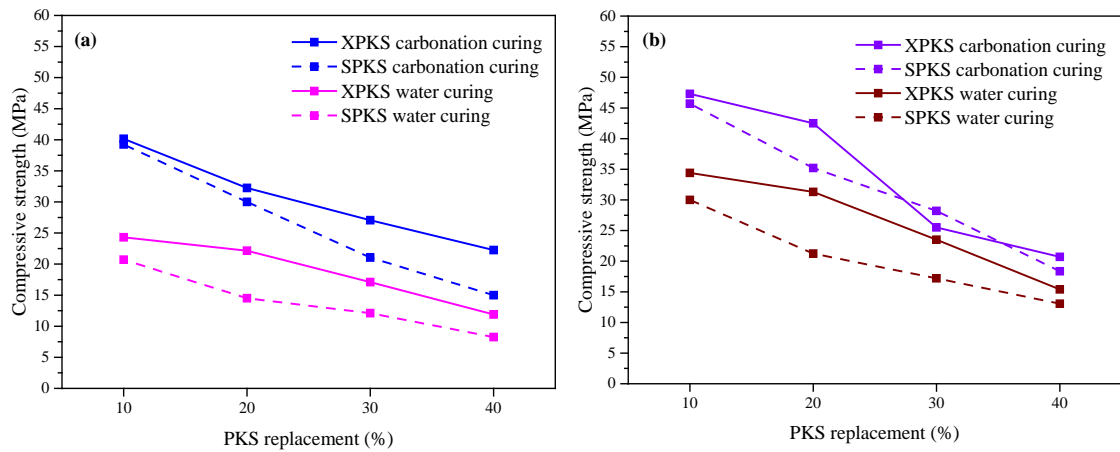


Figure 4.21: Comparison of saturated and unsaturated PKS-added mortar at (a) 7d and (b) 28d curing

Saturated PKS (dotted line graph) showed lower strength as compared to unsaturated PKS for both 7 days and 28 days. This trend corresponded with the strength results of RHB-added mortar. The presence of CO_2 in the pores of the biochar formed carbonic acid which caused deterioration of the binding matrix, compromising the strength. Lower alkalinity of the mix was not conducive for the formation of stable hydration products. Figure 4.22 illustrates the difference in strength of the RHB and PKS-added mortars at replacement of 10% and 20% by volume.

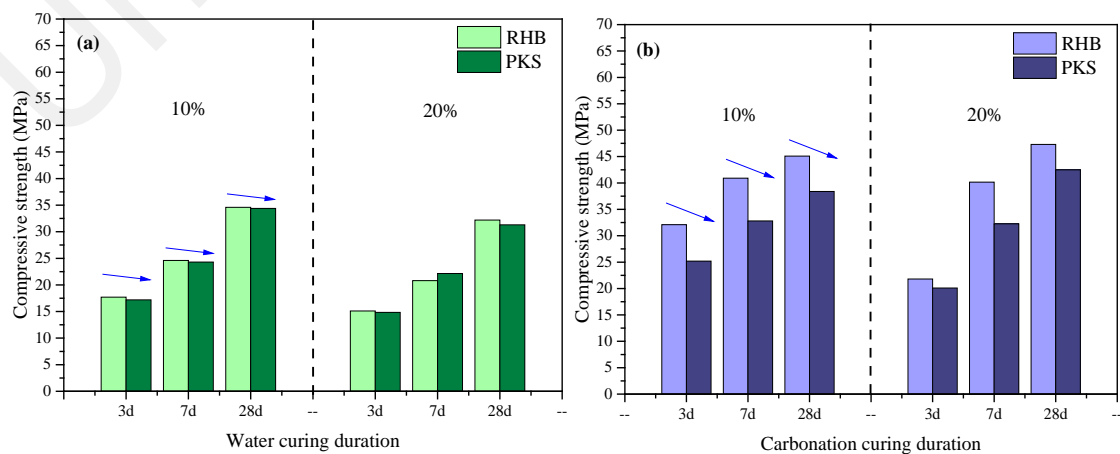


Figure 4.22: Comparison of compressive strength of RHB and PKS-added mortars for (a) water curing and (b) carbonation curing

RHB-added mortars consistently exhibited better strength than PKS-added mortar across all dosages. The strength of the mortar was significantly influenced by the composition and PSD of the biochar. XRF tests revealed that both PKS and OPC contained high Ca content, approximately 74%, but in different forms — OPC as calcium silicates and PKS as calcium carbonates, as observed via XRD. RHB, being high in SiO_2 , may induce a pozzolanic effect, contributing to higher strength while the presence of CaCO_3 in PKS may not contribute to strength for mortar. The porous structure of PKS reduced the strength of the mortar despite good packing and having a smaller surface area compared to OPC. The porosity of PKS hindered effective integration into the mortar matrix, impacting the development of matrix structure and overall strength.

4.5 Carbonation Degree of Biochar-Added Mortar

Figure 4.23 shows the TGA curves highlighting the formation of calcium carbonate from 550 – 950°C.

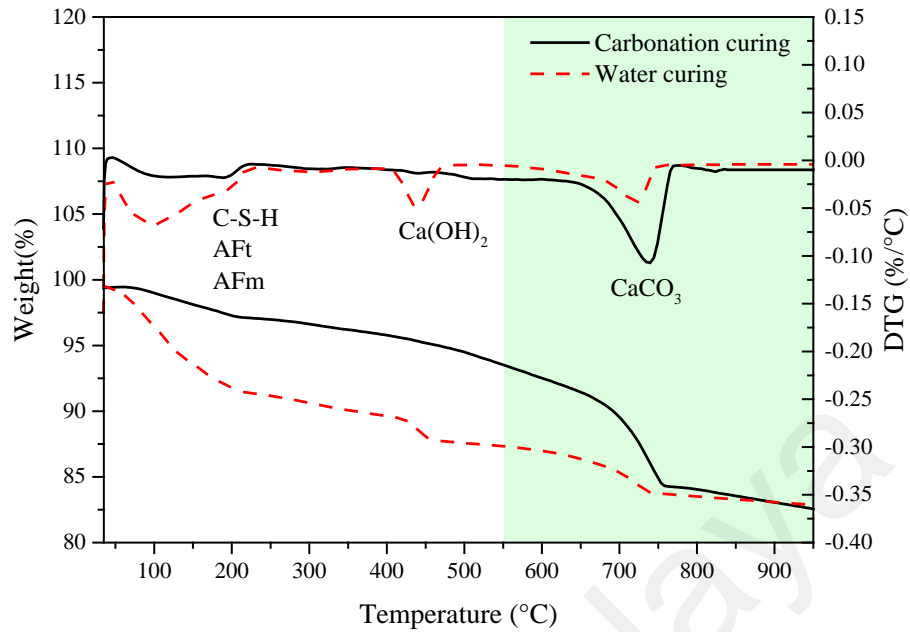


Figure 4.23: Comparison of TGA curves for water cured and carbonation cured control specimens at 7d

The water cured specimens had higher content of C-S-H, ettringites and monosulphates. The presence of portlandite and calcium carbonate was also observed. The carbonation cured specimens had minimal C-S-H and portlandite while more calcium carbonate content. Most of the portlandite was converted to calcium carbonates. Figure 4.24 shows the TGA curves plotted for both RHB and PKS-added mortars.

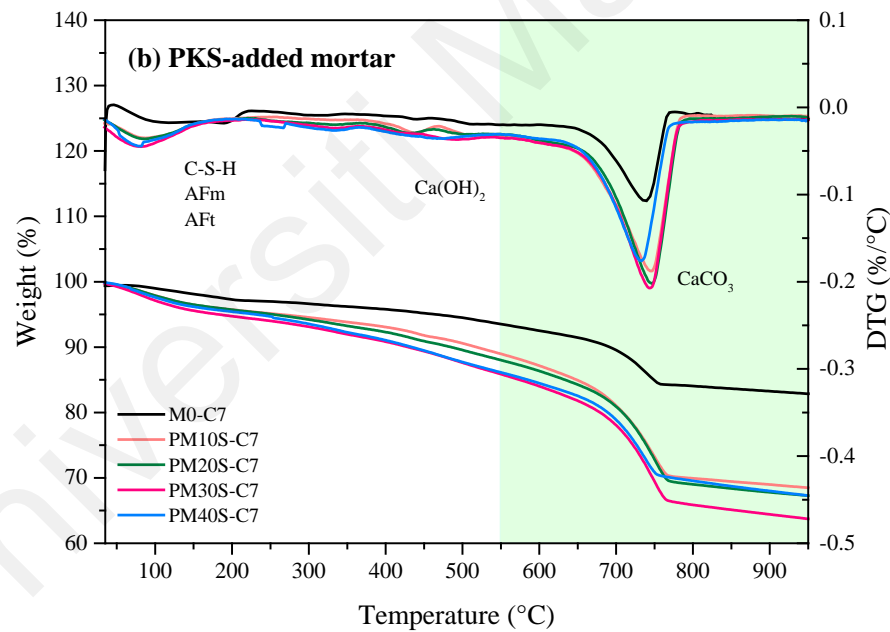
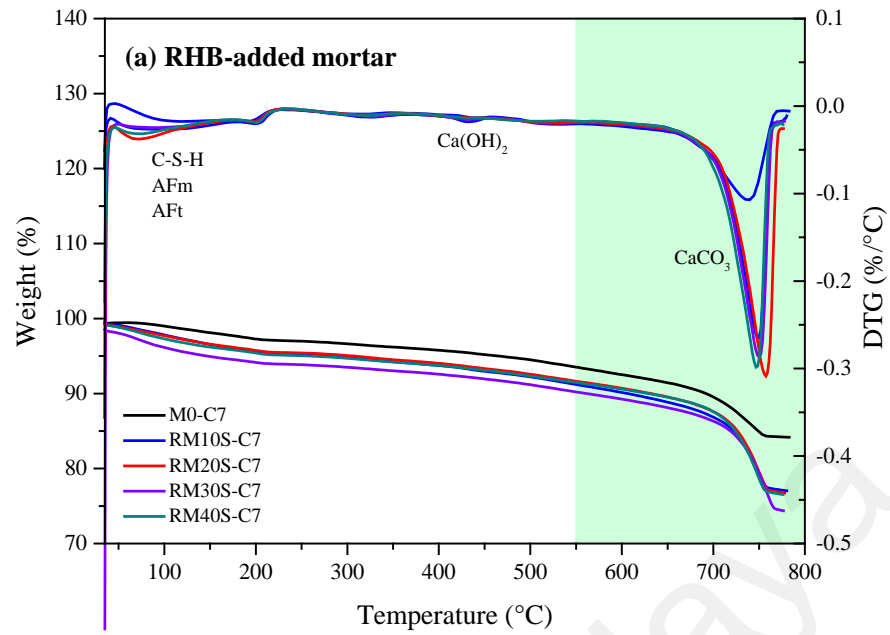


Figure 4.24: TGA curves for (a) RHB-added mortar and (b) PKS-added mortar at 7d carbonation curing

Based on Figure 4.24, high peaks around 750°C indicating high amount of calcium carbonate were formed after subjected to carbonation curing. The DTG curves for RM20S-C7 and PM30S-C7 were observed to be higher than the rest, indicating the

optimum dosage for the respective biochar in terms of formation of calcium carbonate. The degree of carbonation was determined by calculating the amount of calcium carbonate formed and the total CO₂ uptake of the mortars. Results for both biochar were shown in Figure 4.25.

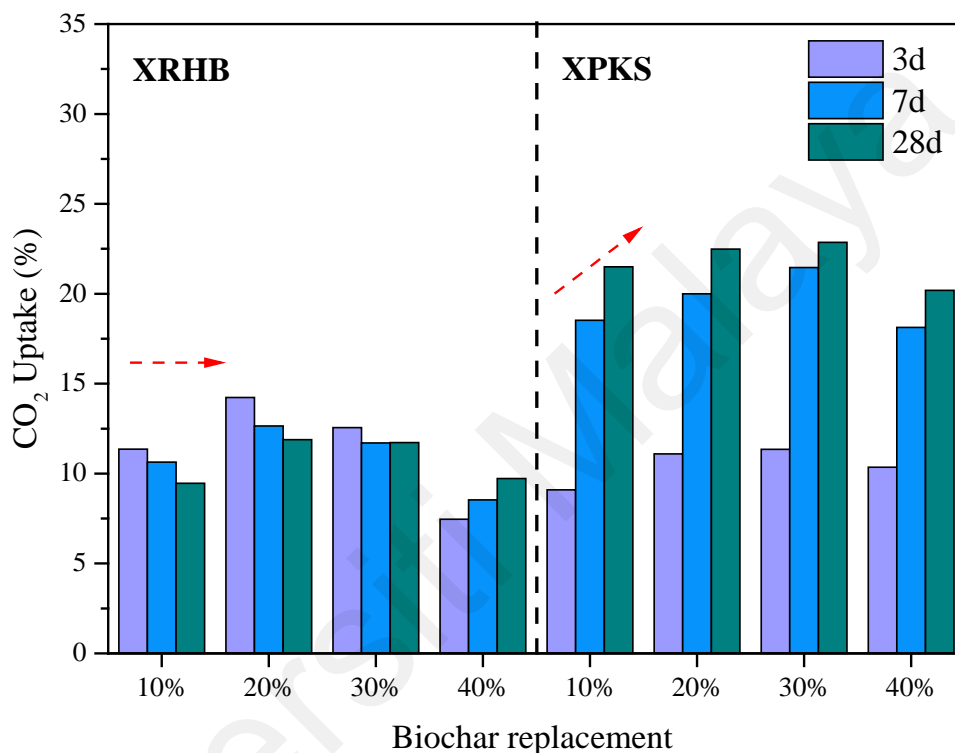


Figure 4.25: CO₂ uptake of RHB and PKS-added mortar at 3d, 7d and 28d carbonation curing

RHB had similar carbon uptake for 3 days, 7 days, and 28 days, indicating that longer duration of carbonation was not beneficial for RHB-added mortars. The calcium carbonate products easily filled the pores on the surface of the mortar, creating a barrier that prevents further CO₂ penetration. This limits the carbonation process over time. On the other hand, PKS-added mortar showed an improvement in CO₂ uptake with longer carbonation duration, even up to 28 days curing. PKS-added mortar was more porous and

allowed the deeper diffusion of CO₂, enabling a more extensive carbonation process. RHB-added mortars had CO₂ uptake of 7.5 – 14.8% while PKS-added mortars had CO₂ uptake of 9.1 – 24.8% for 3 days, 7 days and 28 days carbonation curing. These results were equivalent to an amount of sequestered carbon of 75 – 148 gCO₂/ kg of RHB-added mortar and 91 – 248 gCO₂/ kg of PKS-added mortar.

By comparing the two types of biochar, it was found that PKS-added mortar had higher CO₂ uptake than RHB-added mortar. The results agreed with the calculated CSP in section 4.2.6, where PKS had a better CSP than RHB. In addition to the porous structure of the mortar, the physical and chemical properties of the biochar also affected carbon uptake. The well-developed porous structure and high surface area of PKS were able to adsorb more CO₂. The pores provided sites for CO₂ molecules to adhere to, increasing the overall sequestration capacity. From a chemical perspective, the functional groups on the surface of PKS enhanced its ability to adsorb and interact with CO₂ more effectively as compared to RHB. The carbon content of biochar was also closely related to its carbon sequestration potential; higher carbon content meant more carbon available for sequestration. PKS had a carbon content of 61.59%, while RHB had a carbon content of 33.40%, as reported in section 4.2.5. This finding was consistent with the higher CO₂ uptake observed for PKS-added mortar.

Figure 4.26 illustrates the calculated carbon uptake and calcium carbonate content for both XPKS and SPKS.

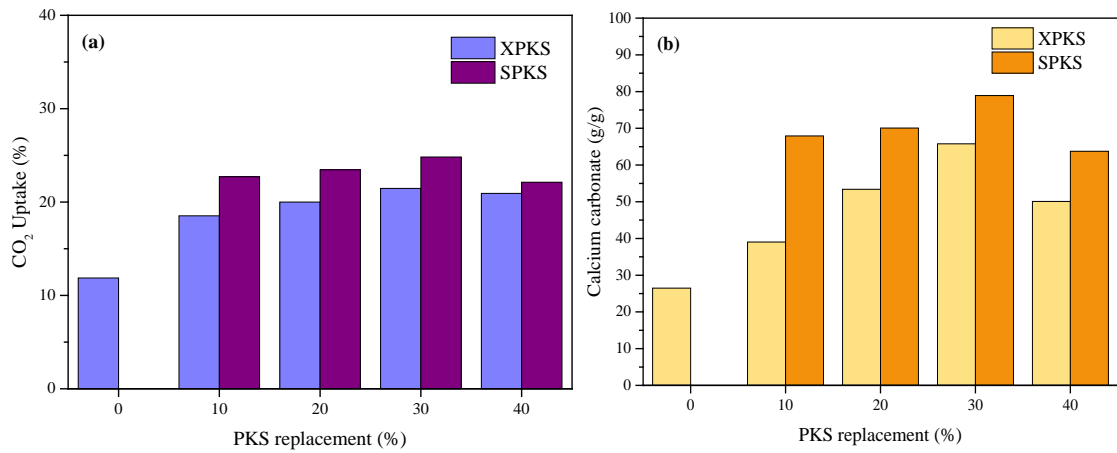


Figure 4.26: CO₂ uptake and calcium carbonate content of saturated and unsaturated PKS at 7d curing

Saturating biochar with CO₂ produced mortars with higher carbon sequestration ability. The SPKS-added mortar showed a higher carbonation degree compared to XPKS. The presence of CO₂ in the pores of SPKS reacted and developed more calcium carbonate and carbon uptake. SPKS had an improvement of CO₂ uptake compared to XPKS by an average of approximately 2.0 – 83.5%. The uncarbonated cement mortar M0-C7 has a carbon uptake of 11.8%. PM30S-C7 has the highest amount of calcium carbonate formed and highest carbon uptake is of 78.9 g/g and 24.8% (i.e. 248 gCO₂/kg PKS-added mortar) respectively, which showed a significant improvement of 110.2% compared to control, which was a doubled uptake of CO₂. The increase in calcium carbonate suggests that PKS facilitate and promote the carbonation cured cement mortar. As Yang and Wang (2021) pointed out, carbonation curing of biochar-added mortar is a viable approach for carbon sequestration in the cement industry. The saturation of biochar with CO₂ before incorporation into cementitious materials was therefore considered beneficial for achieving improved carbonation performance, which is crucial for enhancing material strength.

Chen et al. (2022) obtained CO₂ uptake of approximately 10% for 24h carbonation, with 5% biochar-added mortar having a 5% higher uptake than the control. Other investigations on carbon uptake of biochar-added mortar by TGA calculation ranges from 2–25% (Li & Ling, 2020; Mehdizadeh et al., 2022; Pham et al., 2024; Ren et al., 2022; Tiong et al., 2022). The variations in carbon uptake values observed between studies were attributed to the dependence of carbonation on factors such as the type of biochar used, the percentage of addition, specimen sizes, carbonation parameters, and methods employed for calculating carbon uptake.

Figure 4.27 illustrates the relationship of compressive strength with CO₂ uptake.

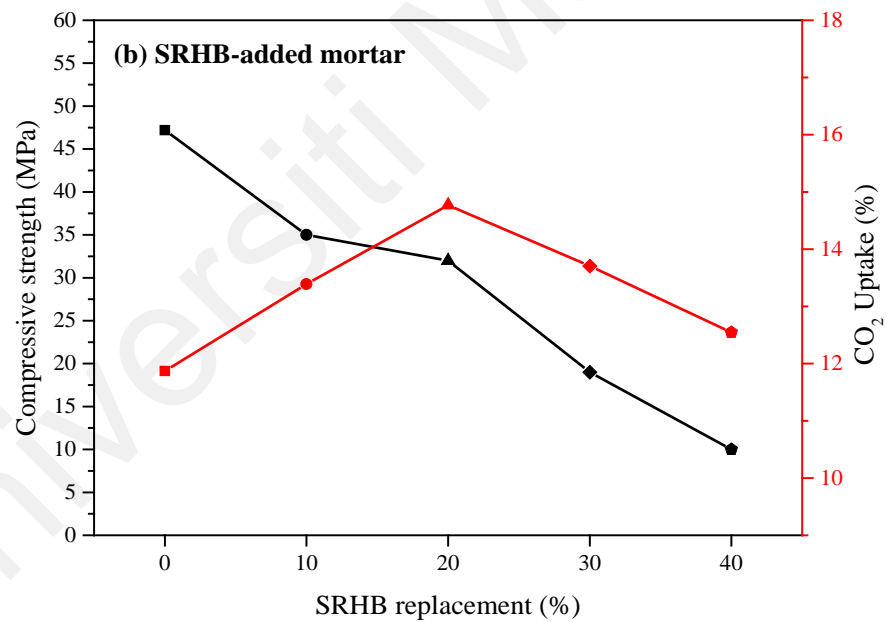
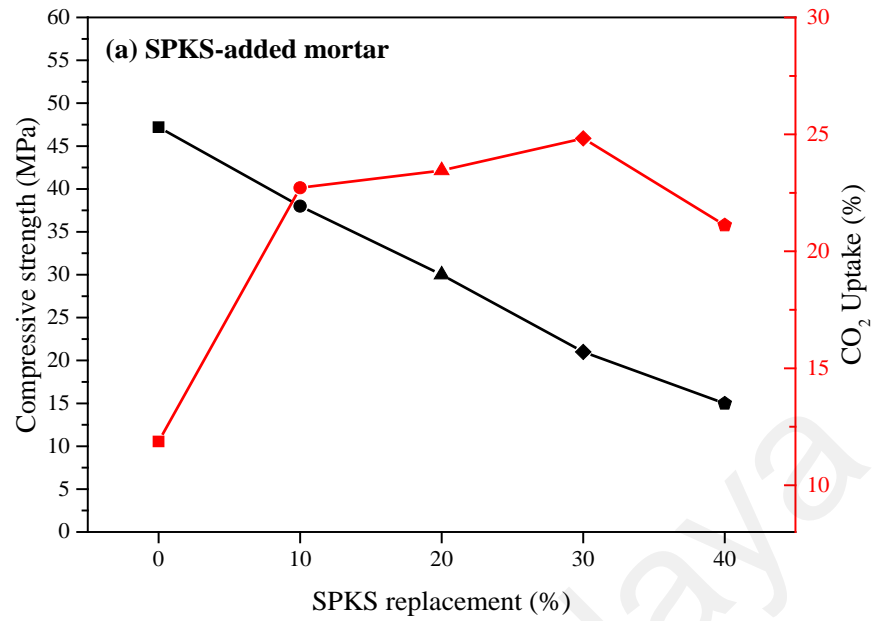


Figure 4.27: Compressive strength versus CO₂ uptake for (a) SPKS- added mortars (b) SRHB-added mortars after full 7d carbonation curing

The hypothesis suggested that increasing the biochar replacement led to a more porous mortar, which facilitated better carbonation. Indeed, the highest CO₂ uptake for RHB

occurred at a 20% replacement by volume, while for PKS, it was at a 30% replacement. However, at replacement levels higher than these, the amount of cement in the mortar decreased, resulting in fewer ingredients available for the carbonation reaction, which led to a lower degree of carbonation. Figure 4.27 provided insights into the potential of PKS- and RHB-added mortars for carbon capture, compared to their strength as concrete products. While higher carbon uptake was achievable, it came at the expense of compressive strength. Therefore, a balance had to be struck between prioritizing strength and maximizing carbon uptake. To minimize compromise on strength while enhancing carbon uptake, the optimal replacement levels were found to be 15% for RHB and 10% for PKS. Mortar designs could be tailored according to specific requirements, whether prioritizing strength or maximizing carbon uptake.

This balance between strength and carbonation potential highlighted the versatility of biochar-modified mortars, offering opportunities for sustainable construction solutions with tailored performance characteristics.

4.6 X-ray Diffraction (XRD) Analysis

XRD analysis is conducted to study the peaks of hydrate products formed and the crystallinity in the specimens. Figure 4.28 presents the XRD patterns for both water and carbonation cured pastes after 28 days of curing.

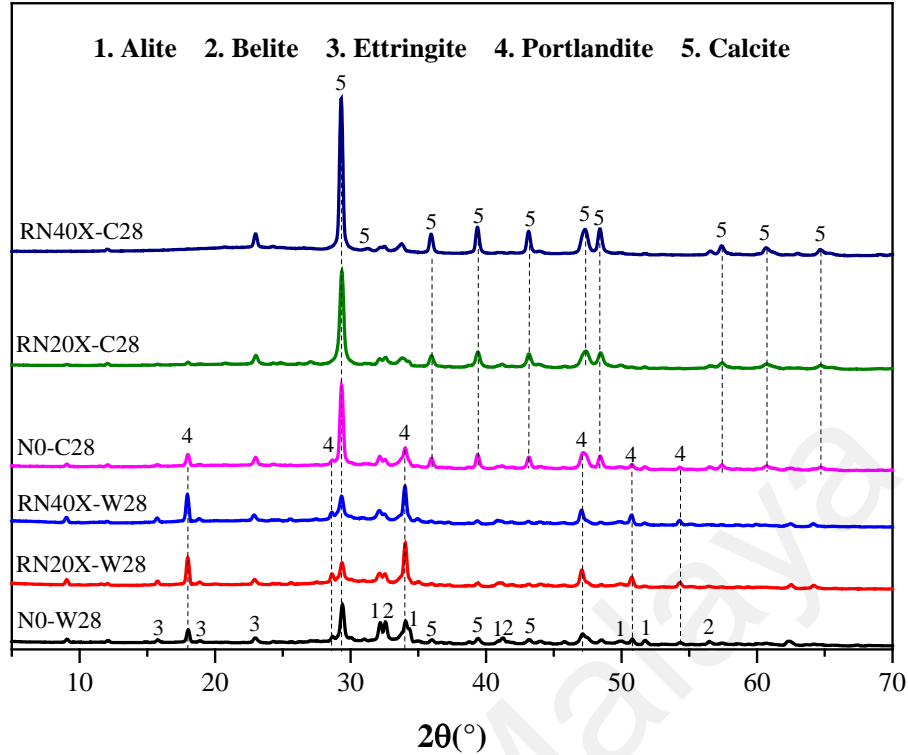


Figure 4.28: XRD patterns of RHB-added mortar

The hydrate products (alite, belite, ettringite, portlandite and calcite) for N0-W28, RN20X-W28 and RN40X-W28 are seen throughout the 2θ range, while for N0-C28, RN20X-C28 and RN40X-C28 mostly calcite is observed. The major peaks of the samples are portlandite ($2\theta = 18.1^\circ, 28.7^\circ, 34.1^\circ, 47.1^\circ, 50.8^\circ, 54.3^\circ$) and calcite ($2\theta = 29.4^\circ, 36.0^\circ, 39.4^\circ, 43.2^\circ, 47.4^\circ, 48.5^\circ, 57.4^\circ, 60.6^\circ, 64.6^\circ$). For water curing, there are unhydrated cement (alite and belite), C-S-H and many portlandite peaks. For carbonation curing, the portlandite compounds react with CO_2 to form calcite. The distinctive peak of calcite at 29.4° is intense and narrow, indicating a high degree of order and crystallinity. N0-C28 has many similarities to those with water curing (P0-W28, P20X-W28 and P40X-W28), having the presence of both portlandite and calcite. The addition of RHB is observed to enhance carbonation, where at higher dosage of RHB at RN20X-C28 and RN40X-C28, no portlandite peak is observed and the alite and belite intensity reduces. This may prove

that all the portlandite and most of the alite and belite are converted into calcite. Thus, the dominant peaks for RN20X-C28 and RN40X-C28 are mainly calcite. The heightened intensity of calcite with increasing RHB suggests the formation of more crystalline calcite, which in turn enhances the strength of the mortar. The XRD findings align well with the improved compressive strength of the carbonated mortars as compared to water cured mortars. Figure 4.29 presents XRD patterns for the PKS-added mortar.

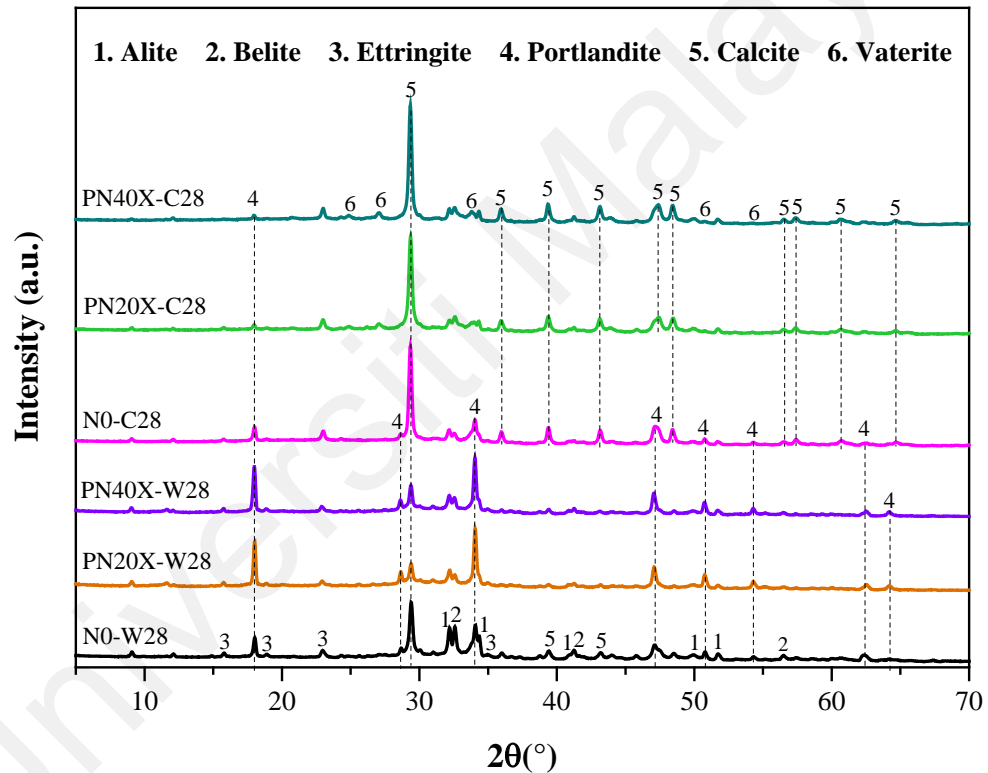


Figure 4.29: XRD patterns for PKS-added mortar

The PKS-added mortar exhibits largely similar XRD patterns compared to the RHB-added mortar. Ettringites are usually seen within the range of $2\theta = 9^{\circ}$ to 35° . The hydrated product of ettringites observed are located at $2\theta = 9.1^{\circ}, 15.8^{\circ}, 18.9^{\circ}, 22.9^{\circ}, 35.0^{\circ}$ for all samples. Alite and belite are observed at $29.4^{\circ}, 32.6^{\circ}, 34.3^{\circ}, 41.3^{\circ}, 49.9^{\circ}, 51.7^{\circ}$ and 32.2° ,

41.1°, 57.4° respectively. High intensity of portlandites is readily identified in wet curing samples at $2\theta = 18.0^\circ, 28.7^\circ, 34.1^\circ, 47.1^\circ, 50.7^\circ, 54.3^\circ, 62.5^\circ, 64.2^\circ$. N0-C28 has both portlandite with lesser intensity and more calcite peaks. As PKS is added into the mortar, seen with PN20X-C28 and PN40X-C28, the carbonation rate improves, and the intensity of calcite becomes higher as more crystalline calcite is formed. The calcites are observed at $2\theta = 29.4^\circ, 35.9^\circ, 39.4^\circ, 43.1^\circ, 47.4^\circ, 48.5^\circ, 56.5^\circ, 57.4^\circ, 60.6^\circ, 64.6^\circ$. A minor portlandite peak is still present at 18.0° of PN20X-C28 and PN40X-C28. Calcium carbonates exist in three polymorphic forms of crystals, which are calcite, aragonite and vaterite. Calcites are more evident due to their strong and distinct peaks. Aragonite and vaterite may be harder to identify due to their weak and diffuse peaks. Some amount of vaterite is detected in the PN40X-C28 sample at $2\theta = 24.8^\circ, 27.1^\circ, 32.7^\circ, 43.6^\circ, 50.1^\circ, 55.7^\circ$. To summarize, the addition of biochar into cement mortar enhances the carbonation process of converting portlandite into calcium carbonates and improves strength of mortar.

4.7 Fourier-Transform Infrared Spectroscopy (FTIR) Analysis

The functional groups of the hydration products and carbonation products are identified through FTIR. Figure 4.30 depicts the results for RHB-added mortar. The fingerprint region of spectrum below 1500 cm^{-1} usually contains the complex absorption patterns unique to the specific samples while the functional group region of spectrum above 1500 cm^{-1} will display characteristic absorption bands of the specific functional group.

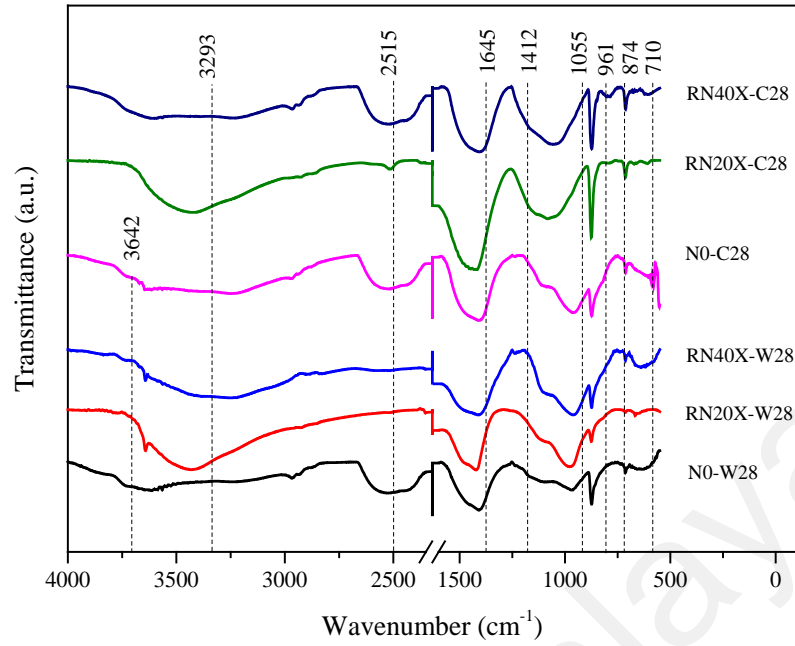


Figure 4.30: FTIR spectra of RHB-added mortar

Findings from FTIR analysis indicate presence of portlandite at 3642 cm^{-1} for all water cured specimens (N0-W28, RN20X-W28, RN40X-W28) and N0-C28 (Huang et al., 2024). At higher RHB replacement of 20% and 40% (RN20X-C28, RN40X-C28), all the portlandite are converted into carbonate products, resulting in the absence of the portlandite peak for these two samples. The bands at 3253 and 1645 cm^{-1} show bending vibration of ν and δ from free water molecules of in the specimens (Z. Ren et al., 2024). Bands at 2515 , 1796 , 1412 , 874 and 710 cm^{-1} are associated with C=O bond from carbonate ions (CO_3^{2-}) from calcium carbonate the formed (Kalkreuth et al., 2024; Salla et al., 2021). The strong band at 1412 cm^{-1} indicates a ν_3 asymmetric stretching of C-O bonds (Xuan et al., 2024). The sharp peak at 874 corresponds to a ν_2 out-of-plane bending of the carbonate ions and the band at 710 cm^{-1} attributes to a ν_4 in-plane bending of the O-C-O angle in the carbonate ions (Saeki et al., 2024). These three peaks of the carbonate ions have higher intensities for the carbonation cured samples indicating the abundance

of calcium carbonate. Hydrate products can be seen at bands 1082 and 961 cm^{-1} due to the symmetric stretching vibration of sulfate group (SO_4^{2-}) in ettringite and an asymmetric stretching vibration of silicate (Si-O-Si) bond in the silicate chains of C-S-H (Huang et al., 2024; Peyvandi et al., 2015). This finding demonstrates that carbonating the mortars improves mechanical strength with the abundant formation of calcium carbonate products. The region 1700-2400 cm^{-1} typically fell within the region associated with organic compounds, thus there are no such bands in the mortar samples. Asymmetric stretch of C=O bond from carbonate ions were shown by band 2515 cm^{-1} . Figure 4.31 shows the FTIR spectra for PKS-added mortar.

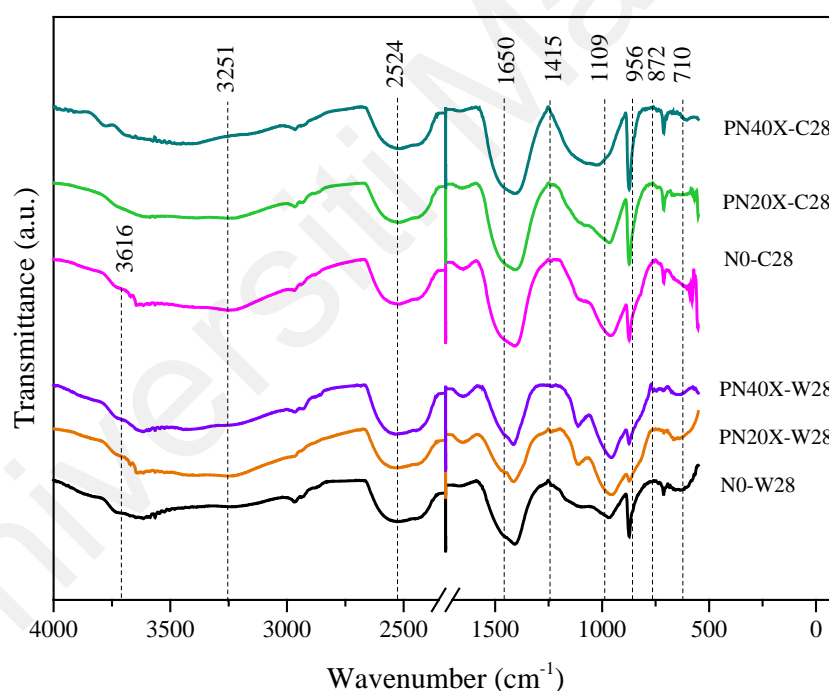


Figure 4.31: FTIR Spectra for PKS-added mortar

The peaks observed in the PKS mortar closely resemble those found in the RHB mortar. The peaks and its related functional groups of both RHB-added mortar and PKS-added mortar are summarized in Table 4.9.

Table 4.9: Summary of FTIR peaks and bands for biochar-added mortar

Wavenumber (cm ⁻¹)	Description
3606-3642	Hydroxyl group -OH stretch from portlandite, Ca(OH) ₂ .
3250-3461	Hydroxyl group -OH ν stretch from free water.
2515-2538	Asymmetric stretch of C=O bond from carbonate ions.
1622-1666	Hydroxyl group -OH δ stretch from free water.
1407-1422	ν_3 asymmetric stretching of C-O bonds from carbonate ions.
1082-1111	Symmetric stretching vibration of sulfate group, SO ₄ ²⁻ .
956-968	Asymmetric stretching vibration of silicate (Si-O-Si) bond.
871-874	ν_2 out-of-plane bending of the carbonate ions.
710-715	ν_4 in-plane bending of the O-C-O angle in the carbonate ions.

4.8 Field Emission Scanning Electron Microscopy – Energy Dispersive X-ray (FESEM-EDS) Analysis

The FESEM images in Figure 4.32 portray the surface morphology of cement-RHB paste as well as the hydrates and carbonates formed. Hydrate products are detected in Figure 4.32 (a)-(d), characterized by the presence of C-S-H gel and ettringite (needle-like hydrates) filling up the pores of the matrix. The filler effect of the biochar particles promotes hydration, resulting in the formation of a dense matrix with fewer capillary voids (Mensah et al., 2021).

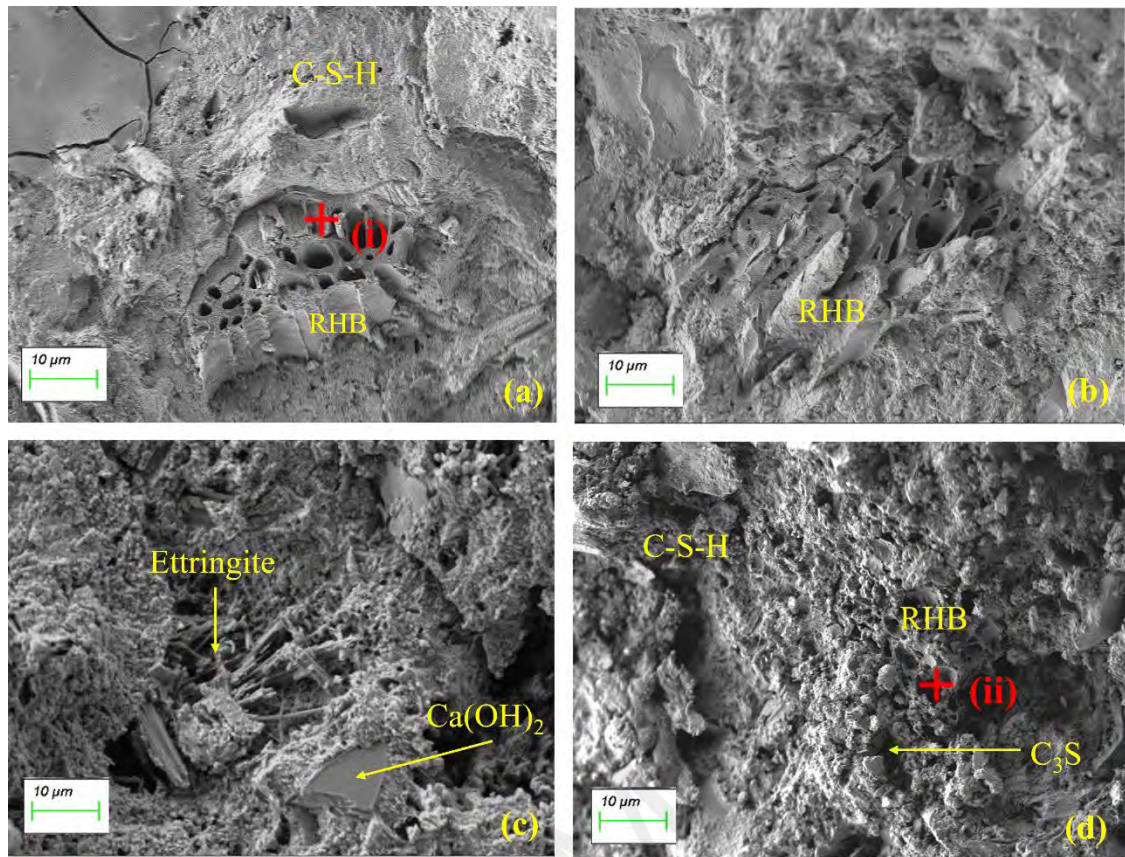


Figure 4.32: FESEM images of (a) RN10X-W28 (b) RN20X-W28 (c) RN30X-W28 (d) RN40X-W28 at 1000x magnification

The morphologies depicted in Figure 4.32 (a) and (b) indicate that at lower levels of P10X-W28 and P20X-W28, the RHB-added mortar has developed a compact and dense microstructure, with abundant presence of C-S-H gels. At higher dosages of P30X-W28 and P40X-W28, as illustrated in Figure 4.32 (c) and (d), the surface structure becomes more porous and less dense. The C-S-H does not appear as smooth surface but irregular and granular. Figure 4.33 are images on the interaction of RHB in the cement paste and the carbonation products.

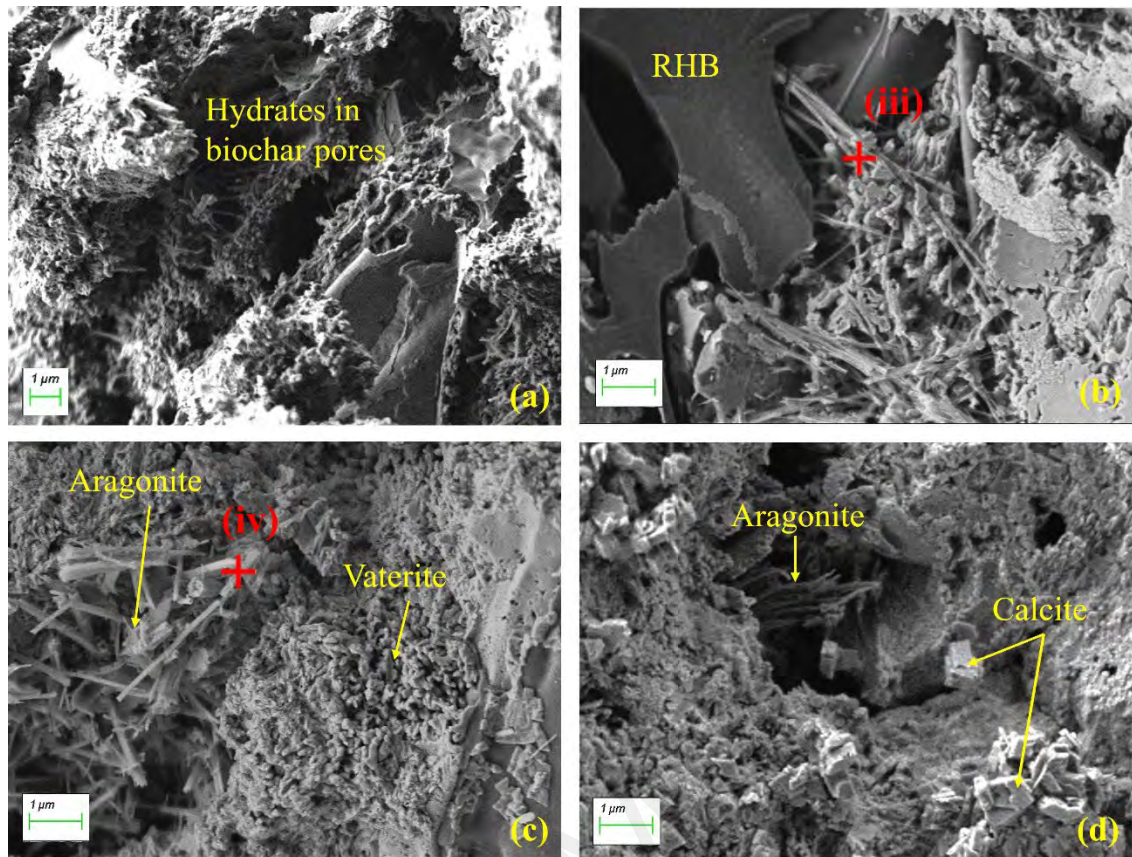


Figure 4.33: (a) RN20X-W28 at magnification 1000x (b, c) RN20X-C28 (d) N0-C28 at magnification 10,000x

In Figure 4.33 (a), the hydrates are seen to form within the pores of RHB where the pores become the site of nucleation for the hydration products. The carbonate products are seen to be in the pores of the RHB and at the interface of the RHB and cement in Figure 4.33 (b). Hydrates are larger in size and can be detected at lower magnification of 1000x while the carbonates are much smaller and can be observed only at magnifications of 10,000x and larger. Carbonation promotes development of a more refined and uniform microstructure within the mortar, filling up the pores, resulting in improved compressive strength. As shown in Figure 4.33 (c) and (d), different types of polymorphs of calcium carbonate are observed in the cement paste after undergoing carbonation curing, namely aragonite (elongated prismatic crystals), vaterite (spherical or amorphous crystals), and calcite (rhombohedral crystals).

The elemental composition of spot (i)-(iv) in Figure 4.32 and 4.33 were analyzed through EDS spectrum as shown in Figure 4.34. The EDS results are used to identify and analyse the hydrates and carbonates in the FESEM images. Spot (i) indicates that the formations within the pores of the RHB are hydrates, showing a high amount for Ca, O, C, some amount of Al and Si. 20.13% of C comes from the RHB. The calcium-to-silicon (Ca/Si) ratio for spot (ii) of P40X-W28 is calculated as 3.72 which is considered high, thus resulting in spherical and uneven C-S-H. Spot (iii) and (iv) show the composition of the carbonated products surrounding the RHB, which are high in calcium content.

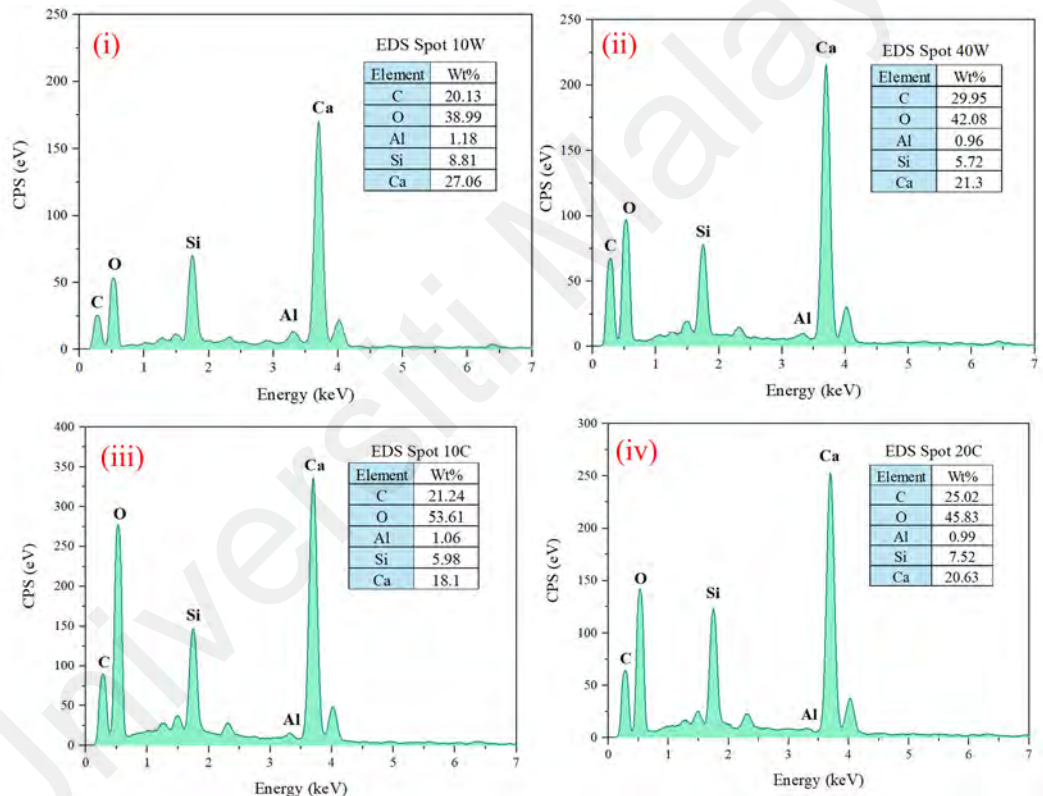


Figure 4.34: EDS elemental spectrum of FESEM spots in Figure 4.33 and 4.34

The FESEM images for PKS-added mortar are presented in Figure 4.35. Images of Figure 4.35 (a) and (b) is water cured for 3 days while (c) – (f) is water cured for 28 days. It can be observed that the addition of PKS into cement paste forms a cement matrix that is porous and has many voids at 3 days of wet curing. Many ettringites were formed at

this initial stage of hydration. After 28 days of curing, very little amount of ettringite is noticeable as continual hydration occurs and it forms into a more stable hydrate.

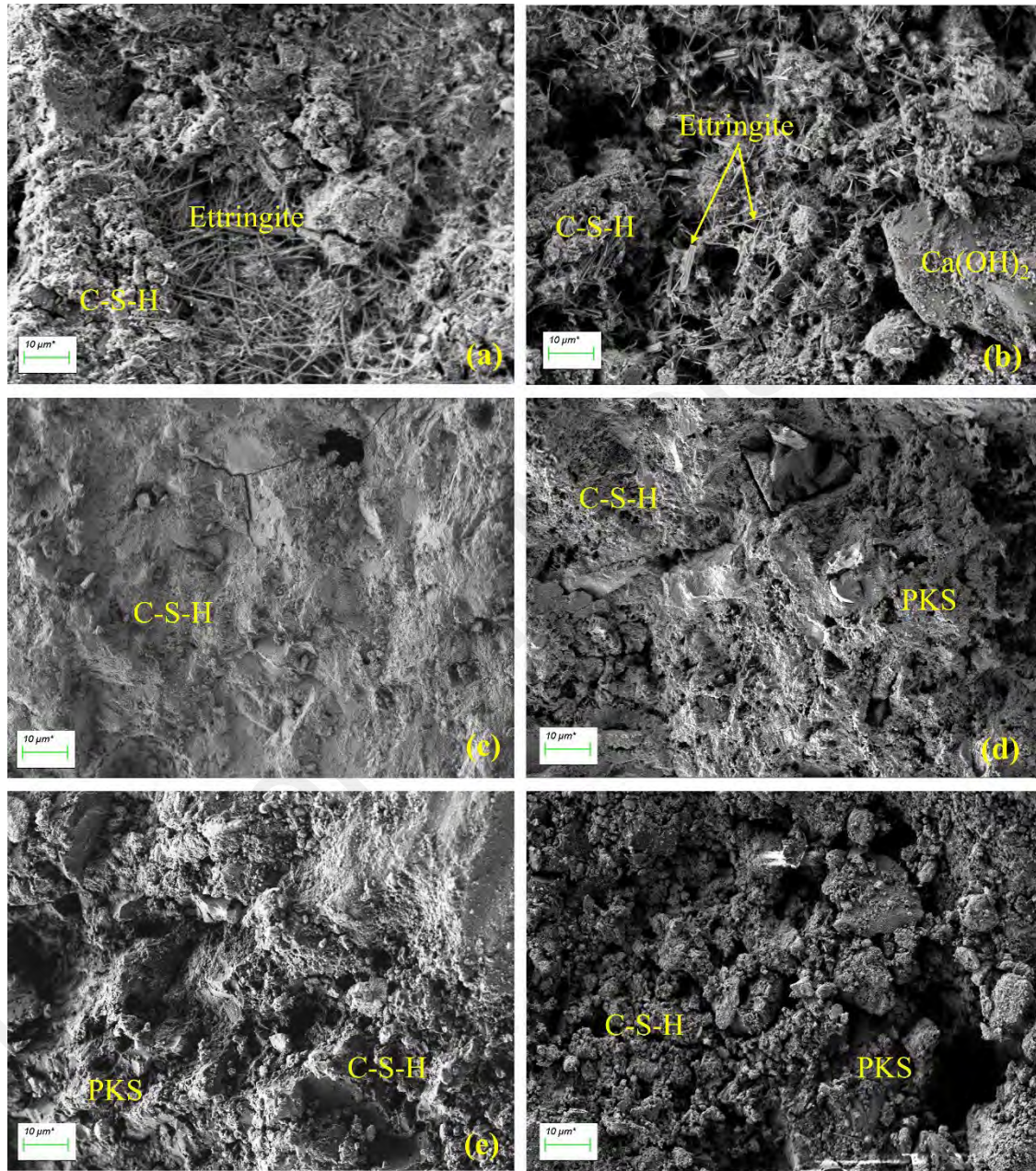


Figure 4.35: (a) N0-W3 (b) PN20X-W3 (c) N0-W28 (d) PN20X-W28 (e) PN30X-W28 (f) PN40X-W28 at magnification 1000x

The surface of the cement matrix or the C-S-H formation from (c) – (f) becomes granular and ‘popcorn’ like as the PKS replacement increases. The changes in C-S-H

appearance is compared with the EDS results of Ca/Si ratio. The increase in Ca/Si ratio from (c) – (f) is 1.1, 1.6, 3.3 and 5.1, which corresponds to the granular C-S-H which has lesser binding effect and lower strength at high PKS replacement. The results are similar to the addition of RHB into cement paste. Figure 4.36 presents the interface of PKS and cement paste.

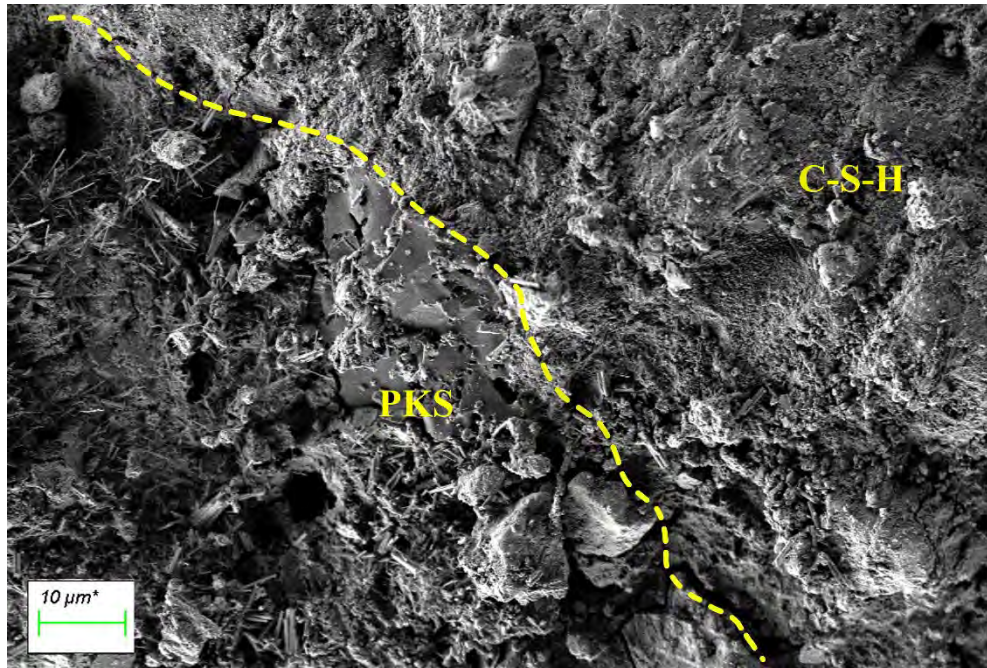


Figure 4.36: PN20X-C28 at magnification 1000x

The needle-like hydrates are more concentrated on the left side of Figure 4.36, where the PKS is located. The hydrates and carbonates are seen to form on the surface and within the pores of the PKS while on the right side only C-S-H is observed. It can be deduced that biochar may promote hydration and carbonation. Figure 4.37 are additional images of hydrates and carbonates in the PKS-added cement paste.

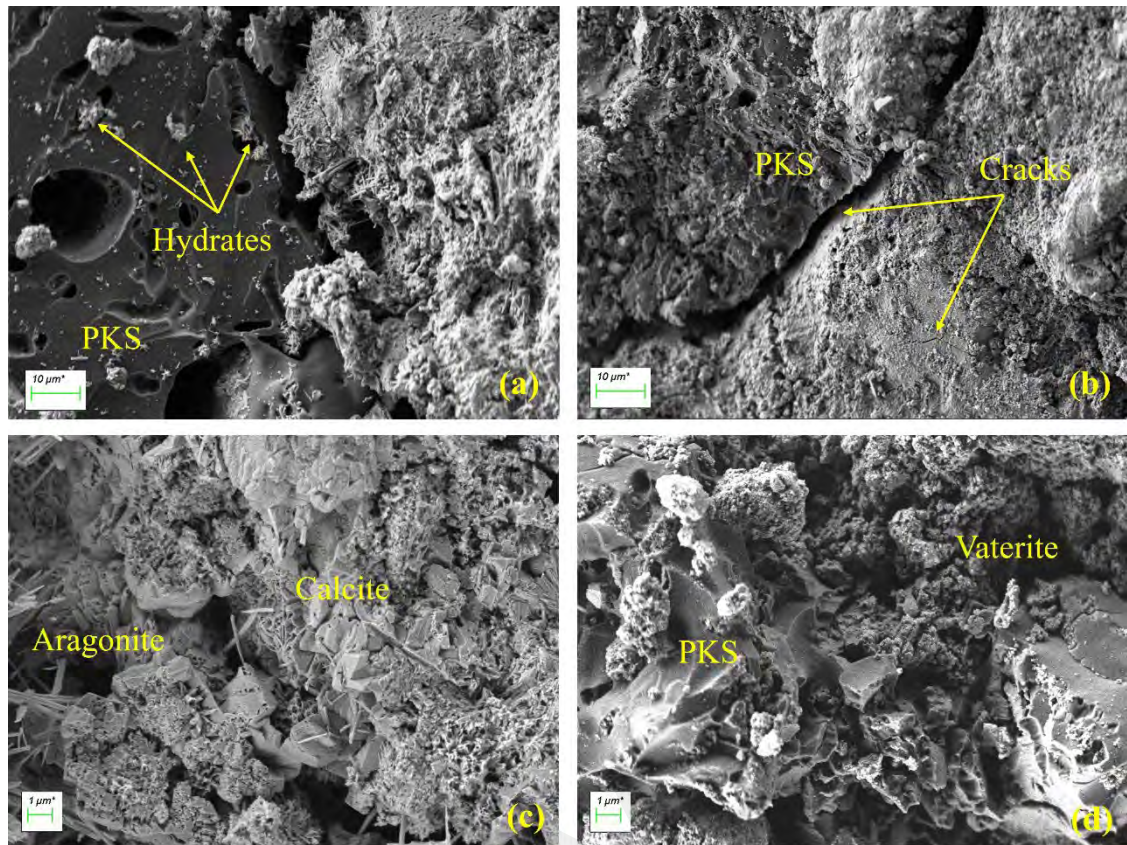


Figure 4.37: (a) PN10X-W28 (b) PN20X-W28 at magnification 1000x (c) N0-C28 (d) PN40X-C28 at magnification 10,000x

Figure 4.37 (a) shows the hydrates formed within the PKS pores. In (b), cracks formed at the interface of biochar and the cement matrix, along with microcracks on the surface of C-S-H, which may indicate weaker bonding with the addition of PKS. Figure 4.37 (c) illustrates different morphologies of calcium carbonates formed on the cement matrix, with a Ca/Si ratio of 6.2 obtained at the calcite spot. Figure 4.37 (d) depicts vaterite formation on the PKS, consistent with XRD patterns indicating the presence of vaterite at 40% PKS replacement, with a Ca/Si ratio of 5.8 for vaterite.

CHAPTER 5: CONCLUSION AND RECOMMENDATIONS

5.1 Conclusion

This research aimed at assessing the carbon sequestration of cement mortar with high volume cement replacement of biochar at 10, 20, 30 and 40%. The incorporation of RHB and PKS into cement mortar influenced the pore structure of the produced cement composite, which impacted on the porosity and microstructure, leading to difference in the properties of compressive strength, porosity and carbonation degree. Based on the experimental results, the following conclusions were drawn, aligning with the research objectives:

- a. Characterization was done for four types of biochar, which were RHB, PKS, CHB and BB to understand the physical and chemical properties of the biochar. The two selected biochar with the highest CSP were RHB and PKS.
- b. The addition of RHB and PKS both produced mortars with high apparent porosity, which was preferable for higher carbon uptake. The apparent porosity of the PKS-added mortars was found to be higher as compared to the RHB-added mortars. Thus, PKS-added mortars were expected to have higher carbon uptake than RHB-added mortars. The apparent porosity of the mortars decreased after carbonation curing, indicating the structural densification due to the formation of carbonation products.
- c. The carbonation depth test through phenolphthalein solution indicates that both RHB and PKS facilitated carbonation. PKS-added mortars showed a higher carbonation rate and carbonated area.
- d. The high replacement of biochar produced porous mortars which had an adverse effect on the compressive strength. The carbonation curing approach improved compressive strength and resolved the low strength issue. Carbonation curing is also utilized for carbon sequestration purposes.

Comparison of both biochar showed that RHB-added mortars have higher compressive strength than PKS-added mortars.

- e. Findings for carbonation degree of the biochar-added mortar indicated that PKS-added mortars achieved the highest CO₂ uptake of 24.8% at replacement of 30% by volume at 7 days carbonation. The PKS-added mortars showed a CO₂ uptake that was double that of the control mortar. The CO₂ uptake for RHB was similar for 3 days, 7 days, and 28 days curing, approximately 7.5 – 14.8% (i.e. 75 – 148 gCO₂/ kg of RHB-added mortar) while the PKS-added mortars had CO₂ uptake of 9.1 – 24.8% (i.e. 91 – 248 gCO₂/ kg of PKS-added mortar).
- f. Microstructure analysis of FTIR, XRD, FESEM-EDS corresponds to the results showing that the portlandites were carbonated into large amount calcium carbonates and the increase in biochar replacement improves carbonation.
- g. Saturated biochar-added mortars generally had lower strength compared to the unsaturated ones. This is true for both types of biochar. In terms of carbonation depth and degree, saturated mortars exhibit a higher carbonation rate and greater CO₂ uptake than unsaturated mortars, which is more beneficial for carbon footprint reduction. Saturated biochar-added mortars had an improvement of CO₂ uptake of up to 83.5% as compared to unsaturated biochar-added mortars. Thus, the technique for saturating biochar with CO₂ before being deployed into building material must be carefully planned to obtain the desired strength performance and carbon sequestration capacity.

Overall, PKS showed better carbon capture performance as compared to RHB, with CO₂ uptake double that of RHB-added mortars. The combination of the integration of biochar and carbonation curing produced mortars with enhanced strength and high carbon

sequestration. PKS has great potential in capturing and storing carbon permanently in construction material. The application of PKS as a green material in construction represents a sustainable alternative to conventional concrete. It reduces GHG emissions, enhances resource efficiency while supporting effective carbon sequestration. The PKS-added mortar successfully achieves the aim of waste valorization while also facilitating good CO₂ uptake.

5.2 Recommendations

Integrating biochar into cement composites indeed offers a promising path toward sustainable construction practices. However, based on the findings gained from this study, several areas for future research have been identified. The following sections outline specific areas for further investigation:

- i. The carbon sequestration ability of biochar can be further enhanced through surface modification of biochar to enhance its adsorption properties. Physical and chemical modifications can be applied to activate and maximize the CO₂ adsorption. The activation of biochar can be further explored.
- ii. Investigation on the aggregate replacement by biochar is recommended. This method can potentially allow for the replacement of a much higher percentage, producing porous and lightweight mortar without significantly compromising the compressive strength compared to cement replacement.
- iii. A comprehensive life cycle assessment can be carried out to quantify the overall environmental impact of using biochar in mortars, including its potential benefits in reducing carbon emissions and improving sustainability.

REFERENCES

- Agarwal, R., Pawar, N., Supriya, Rawat, P., Rai, D., Kumar, R., & Naik B, S. (2023). Thermo-mechanical behavior of cementitious material with partial replacement of Class-II biochar with Accelerated Carbonation Curing (ACC). *Industrial Crops and Products*, 204. <https://doi.org/10.1016/j.indcrop.2023.117335>
- Ahmad, M., Ahmad, M., Usman, A. R. A., Al-Faraj, A. S., Abduljabbar, A., Ok, Y. S., & Al-Wabel, M. I. (2019). Date palm waste-derived biochar composites with silica and zeolite: synthesis, characterization and implication for carbon stability and recalcitrant potential. *Environmental Geochemistry and Health*, 41(4), 1687–1704. <https://doi.org/10.1007/s10653-017-9947-0>
- Ahmad, S., Assaggaf, R. A., Maslehuddin, M., Al-Amoudi, O. S. B., Adekunle, S. K., & Ali, S. I. (2017). Effects of carbonation pressure and duration on strength evolution of concrete subjected to accelerated carbonation curing. *Construction and Building Materials*, 136, 565–573. <https://doi.org/10.1016/j.conbuildmat.2017.01.069>
- Akinyemi, B. A., & Adesina, A. (2020). Recent advancements in the use of biochar for cementitious applications: A review. *Journal of Building Engineering*, 32. <https://doi.org/10.1016/j.jobbe.2020.101705>
- Aman, A. M. N., Selvarajoo, A., Lau, T. L., & Chen, W. H. (2022). Biochar as Cement Replacement to Enhance Concrete Composite Properties: A Review. *Energies*, 15(20). <https://doi.org/10.3390/en15207662>
- Bao, J., Zhang, B., Abd, W., Qadr, A., Wan-Mohtar, I., Khalid, N. I., Hafiz, M., Rahim, A., Amru, A., Luthfi, I., Solehah, N., Zaini, M., Akmal, N., Din, S., & Aqilah, N. (2023). *Fermentation Underutilized Malaysian Agro-Industrial Wastes as Sustainable Carbon Sources for Lactic Acid Production*. <https://doi.org/10.3390/fermentation>
- Barbhuiya, S., Bhusan Das, B., & Kanavaris, F. (2024). Biochar-concrete: A comprehensive review of properties, production and sustainability. *Case Studies in Construction Materials*, 20. <https://doi.org/10.1016/j.cscm.2024.e02859>
- Beskopylny, A. N., Stel'makh, S. A., Shcherban', E. M., Mailyan, L. R., Meskhi, B., Smolyanichenko, A. S., Varavka, V., Beskopylny, N., & Dotsenko, N. (2022). Influence of Electromagnetic Activation of Cement Paste and Nano-Modification by Rice Straw Biochar on the Structure and Characteristics of Concrete. *Journal of Composites Science*, 6(9). <https://doi.org/10.3390/jcs6090268>
- Bolan, N., Hoang, S. A., Beiyuan, J., Gupta, S., Hou, D., Karakoti, A., Joseph, S., Jung, S., Kim, K. H., Kirkham, M. B., Kua, H. W., Kumar, M., Kwon, E. E., Ok, Y. S., Perera, V., Rinklebe, J., Shaheen, S. M., Sarkar, B., Sarmah, A. K., Van Zwieten, L. (2022). Multifunctional applications of biochar beyond carbon storage. *International Materials Reviews*, 67(2), 150–200. <https://doi.org/10.1080/09506608.2021.1922047>

- Boumaaza, M., Belaadi, A., Bourchak, M., Juhany, K. A., Jawaïd, M., Marvila, M. T., & de Azevedo, A. R. G. (2023). Optimization of flexural properties and thermal conductivity of *Washingtonia* plant biomass waste biochar reinforced bio-mortar. *Journal of Materials Research and Technology*, 23, 3515–3536. <https://doi.org/10.1016/j.jmrt.2023.02.009>
- CarbonCure Technology. (2024). *A Win-Win Solution*. <https://www.carboncure.com/>
- Cha, J. S., Park, S. H., Jung, S. C., Ryu, C., Jeon, J. K., Shin, M. C., & Park, Y. K. (2016). Production and utilization of biochar: A review. *Journal of Industrial and Engineering Chemistry*, 40, 1–15. <https://doi.org/10.1016/j.jiec.2016.06.002>
- Chen, T., & Gao, X. (2019). Effect of carbonation curing regime on strength and microstructure of Portland cement paste. *Journal of CO₂ Utilization*, 34, 74–86. <https://doi.org/10.1016/j.jcou.2019.05.034>
- Chen, T., Zhao, L., Gao, X., Li, L., & Qin, L. (2022). Modification of carbonation-cured cement mortar using biochar and its environmental evaluation. *Cement and Concrete Composites*, 134. <https://doi.org/10.1016/j.cemconcomp.2022.104764>
- Dalton, S., Fariz Mohamed, A., & Ogboo Chikere, A. (2017). Status Evaluation of Palm Oil Waste Management Sustainability in Malaysia. *OIDA International Journal of Sustainable Development*, 10, 12. <https://oidaijsd.com/wp-content/uploads/2019/02/10-12-05.pdf>
- Danesh, P., Niaparast, P., Ghorbannezhad, P., & Ali, I. (2023). Biochar Production: Recent Developments, Applications, and challenges. *Fuel*, 337. <https://doi.org/10.1016/j.fuel.2022.126889>
- El-Hassan, H., Shao, Y., & Ghouleh, Z. (2013). Effect of Initial Curing on Carbonation of Lightweight Concrete Masonry Units. *Materials Journal*, 110(4), 441–450.
- Ello, A. S., De Souza, L. K. C., Trokourey, A., & Jaroniec, M. (2013). Development of microporous carbons for CO₂ capture by KOH activation of African palm shells. *Journal of CO₂ Utilization*, 2, 35–38. <https://doi.org/10.1016/j.jcou.2013.07.003>
- Feliz Florian, G., Ragoubi, M., Leblanc, N., Taouk, B., & Abdelouahed, L. (2024). Biochar Production and Its Potential Application for Biocomposite Materials: A Comprehensive Review. *Journal of Composites Science*, 8(6), 220. <https://doi.org/10.3390/jcs8060220>
- Ferrara, G., Belli, A., Keulen, A., Tulliani, J. M., & Palmero, P. (2023). Testing procedures for CO₂ uptake assessment of accelerated carbonation products: Experimental application on basic oxygen furnace steel slag samples. *Construction and Building Materials*, 406. <https://doi.org/10.1016/j.conbuildmat.2023.133384>
- Flórez, E., Acelas, N., Ramirez, A. P., Giraldo, S., Rodriguez, B., Correa, E., & Echeverria, F. (2019). Small additions of activated Biochar from palm oil shells to Portland cement mortar. *Journal of Physics: Conference Series*, 1247(1). <https://doi.org/10.1088/1742-6596/1247/1/012052>

- Foundation for Food & Agriculture Research. (2022). *Producers and Researchers Agree, Scale Up of a Sustainable Biochar Industry is Critical to Meet Climate Targets, and Build Agricultural Resilience and Soil Health*. <https://foundationfar.org/news/producers-and-researchers-agree-scale-up-of-a-sustainable-biochar-industry-is-critical-to-meet-climate-targets-and-build-agricultural-resilience-and-soil-health/>
- Gabhane, J. W., Bhange, V. P., Patil, P. D., Bankar, S. T., & Kumar, S. (2020). Recent trends in biochar production methods and its application as a soil health conditioner: a review. *SN Applied Sciences*, 2(7). <https://doi.org/10.1007/s42452-020-3121-5>
- Golden Agri-Resources. (2018). *How it works: Zero waste in palm oil production*. <https://www.goldenagri.com.sg/>
- Gong, J., Niu, R., Liu, J., Chen, X., Wen, X., Mijowska, E., Sun, Z., & Tang, T. (2014). Simultaneously improving the thermal stability, flame retardancy and mechanical properties of polyethylene by the combination of graphene with carbon black. *RSC Advances*, 4(64), 33776–33784. <https://doi.org/10.1039/c4ra04623d>
- González, B., & Manyà, J. J. (2020). Activated olive mill waste-based hydrochars as selective adsorbents for CO₂ capture under postcombustion conditions. *Chemical Engineering and Processing - Process Intensification*, 149. <https://doi.org/10.1016/j.cep.2020.107830>
- Guo, S., Li, Y., Wang, Y., Wang, L., Sun, Y., & Liu, L. (2022). Recent advances in biochar-based adsorbents for CO₂ capture. *Carbon Capture Science and Technology*, 4. <https://doi.org/10.1016/j.ccst.2022.100059>
- Guo, Y., Tan, C., Sun, J., Li, W., Zhang, J., & Zhao, C. (2020). Biomass ash stabilized MgO adsorbents for CO₂ capture application. *Fuel*, 259. <https://doi.org/10.1016/j.fuel.2019.116298>
- Gupta, S. (2021). Carbon sequestration in cementitious matrix containing pyrogenic carbon from waste biomass: A comparison of external and internal carbonation approach. *Journal of Building Engineering*, 43, 102910. <https://doi.org/10.1016/j.jobbe.2021.102910>
- Gupta, S., & Kashani, A. (2021). Utilization of biochar from unwashed peanut shell in cementitious building materials – Effect on early age properties and environmental benefits. *Fuel Processing Technology*, 218. <https://doi.org/10.1016/j.fuproc.2021.106841>
- Gupta, S., Kashani, A., & Mahmood, A. H. (2022). Carbon sequestration in engineered lightweight foamed mortar – Effect on rheology, mechanical and durability properties. *Construction and Building Materials*, 322. <https://doi.org/10.1016/j.conbuildmat.2022.126383>
- Gupta, S., Kashani, A., Mahmood, A. H., & Han, T. (2021). Carbon sequestration in cementitious composites using biochar and fly ash – Effect on mechanical and durability properties. *Construction and Building Materials*, 291. <https://doi.org/10.1016/j.conbuildmat.2021.123363>

- Gupta, S., Krishnan, P., Kashani, A., & Kua, H. W. (2020). Application of biochar from coconut and wood waste to reduce shrinkage and improve physical properties of silica fume-cement mortar. *Construction and Building Materials*, 262. <https://doi.org/10.1016/j.conbuildmat.2020.120688>
- Gupta, S., & Kua, H. W. (2017). Factors Determining the Potential of Biochar As a Carbon Capturing and Sequestering Construction Material: Critical Review. *Journal of Materials in Civil Engineering*, 29(9). [https://doi.org/10.1061/\(asce\)mt.1943-5533.0001924](https://doi.org/10.1061/(asce)mt.1943-5533.0001924)
- Gupta, S., Kua, H. W., & Low, C. Y. (2018). Use of biochar as carbon sequestering additive in cement mortar. *Cement and Concrete Composites*, 87, 110–129. <https://doi.org/10.1016/j.cemconcomp.2017.12.009>
- Gupta, S., Kua, H. W., & Pang, S. D. (2018). Biochar-mortar composite: Manufacturing, evaluation of physical properties and economic viability. *Construction and Building Materials*, 167, 874–889. <https://doi.org/10.1016/j.conbuildmat.2018.02.104>
- Gupta, S., Kua, H. W., & Pang, S. D. (2020). Effect of biochar on mechanical and permeability properties of concrete exposed to elevated temperature. *Construction and Building Materials*, 234. <https://doi.org/10.1016/j.conbuildmat.2019.117338>
- Gupta, S., Muthukrishnan, S., & Kua, H. W. (2021). Comparing influence of inert biochar and silica rich biochar on cement mortar – Hydration kinetics and durability under chloride and sulfate environment. *Construction and Building Materials*, 268. <https://doi.org/10.1016/j.conbuildmat.2020.121142>
- Haider, F. U., Coulter, J. A., Cai, L., Hussain, S., Cheema, S. A., Wu, J., & Zhang, R. (2022). An overview on biochar production, its implications, and mechanisms of biochar-induced amelioration of soil and plant characteristics. *Pedosphere*, 32(1), 107–130. [https://doi.org/10.1016/S1002-0160\(20\)60094-7](https://doi.org/10.1016/S1002-0160(20)60094-7)
- Haris Javed, M., Ali Sikandar, M., Ahmad, W., Tariq Bashir, M., Alrowais, R., & Bilal Wadud, M. (2022). Effect of various biochars on physical, mechanical, and microstructural characteristics of cement pastes and mortars. *Journal of Building Engineering*, 57. <https://doi.org/10.1016/j.jobbe.2022.104850>
- Harvey, O. R., Kuo, L. J., Zimmerman, A. R., Louchouart, P., Amonette, J. E., & Herbert, B. E. (2012). An index-based approach to assessing recalcitrance and soil carbon sequestration potential of engineered black carbons (biochars). *Environmental Science and Technology*, 46(3), 1415–1421. <https://doi.org/10.1021/es2040398>
- Haryati, Z., Loh, S. K., Kong, S. H., & Bachmann, R. T. (2018). Pilot scale biochar production from palm kernel shell (PKS) in a fixed bed allothermal reactor. *Journal of Oil Palm Research*, 30(3), 485–494. <https://doi.org/10.21894/jopr.2018.0043>
- Hidayat, Rahmat, A., Nissa, R. C., Sukanto, Nuraini, L., Nurtanto, M., & Ramadhani, W. S. (2023). Analysis of rice husk biochar characteristics under different

pyrolysis temperature. *IOP Conference Series: Earth and Environmental Science*, 1201(1). <https://doi.org/10.1088/1755-1315/1201/1/012095>

- Hidayu, A. R., Sukor, M. Z., Mohammad, N. F., Elham, O. S. J., Azri, N. I., Azhar, M. A. I., & Jalil, M. J. (2019). Preparation of activated carbon from palm kernel shell by chemical activation and its application for β -carotene adsorption in crude palm oil. *Journal of Physics: Conference Series*, 1349(1). <https://doi.org/10.1088/1742-6596/1349/1/012103>
- Huang, G., Lv, Y., Ren, S., Liao, Y., Wang, X. Y., Guo, R., & Lin, R. S. (2024). Production of low-CO₂ ternary binder using red sandstone, cement, and granulated blast furnace slag: A comprehensive performance analysis. *Construction and Building Materials*, 431. <https://doi.org/10.1016/j.conbuildmat.2024.136576>
- International Energy Agency. (2022). *CO₂ Emissions in 2022*. <https://www.iea.org/reports/co2-emissions-in-2022>
- Jagadeesh, N., & Sundaram, B. (2023). Adsorption of Pollutants from Wastewater by Biochar: A Review. *Journal of Hazardous Materials Advances*, 9, 100226. <https://doi.org/10.1016/j.hazadv.2022.100226>
- Joseph, S., Cowie, A. L., Van Zwieten, L., Bolan, N., Budai, A., Buss, W., Cayuela, M. L., Graber, E. R., Ippolito, J. A., Kuzyakov, Y., Luo, Y., Ok, Y. S., Palansooriya, K. N., Shepherd, J., Stephens, S., Weng, Z., & Lehmann, J. (2021). How biochar works, and when it doesn't: A review of mechanisms controlling soil and plant responses to biochar. *GCB Bioenergy* 13(11), 1731–1764. <https://doi.org/10.1111/gcbb.12885>
- Jung, S., Park, Y. K., & Kwon, E. E. (2019). Strategic use of biochar for CO₂ capture and sequestration. *Journal of CO₂ Utilization*, 32, 128–139. <https://doi.org/10.1016/j.jcou.2019.04.012>
- Kaliyavaradhan, S. K., & Ling, T. C. (2017). Potential of CO₂ sequestration through construction and demolition (C&D) waste - An overview. *Journal of CO₂ Utilization*, 20, 234–242. <https://doi.org/10.1016/j.jcou.2017.05.014>
- Kaliyavaradhan, S. K., Ling, T. C., & Mo, K. H. (2020). CO₂ sequestration of fresh concrete slurry waste: Optimization of CO₂ uptake and feasible use as a potential cement binder. *Journal of CO₂ Utilization*, 42. <https://doi.org/10.1016/j.jcou.2020.101330>
- Kalkreuth, J., Ullrich, A., Garbev, K., Merz, D., Stemmermann, P., & Stapf, D. (2024). Accelerated carbonation of hardened cement paste: Quantification of calcium carbonate via ATR infrared spectroscopy. *Journal of the American Ceramic Society*, 107(4), 2627–2640. <https://doi.org/10.1111/jace.19546>
- Khan, S., Irshad, S., Mehmood, K., Hasnain, Z., Nawaz, M., Rais, A., Gul, S., Wahid, M. A., Hashem, A., Abd_Allah, E. F., & Ibrar, D. (2024). Biochar Production and Characteristics, Its Impacts on Soil Health, Crop Production, and Yield Enhancement: A Review. *Plants*, 13(2). <https://doi.org/10.3390/plants13020166>

- Kong, S. H., Loh, S. K., Bachmann, R. T., Zainal, H., & Cheong, K. Y. (2019). Palm kernel shell biochar production, characteristics and carbon sequestration potential. *Journal of Oil Palm Research*, 31(3), 508–520. <https://doi.org/10.21894/jopr.2019.0041>
- Kua, H. W., & Tan, S. M. H. (2023). Novel typology of accelerated carbonation curing: using dry and pre-soaked biochar to tune carbon capture and mechanical properties of cementitious mortar. *Biochar*, 5(1). <https://doi.org/10.1007/s42773-023-00234-w>
- Li, J., Cao, L., Yuan, Y., Wang, R., Wen, Y., & Man, J. (2018). Comparative study for microcystin-LR sorption onto biochars produced from various plant- and animal-wastes at different pyrolysis temperatures: Influencing mechanisms of biochar properties. *Bioresource Technology*, 247, 794–803. <https://doi.org/10.1016/j.biortech.2017.09.120>
- Li, X., & Ling, T. C. (2020). Instant CO₂ curing for dry-mix pressed cement pastes: Consideration of CO₂ concentrations coupled with further water curing. *Journal of CO₂ Utilization*, 38, 348–354. <https://doi.org/10.1016/j.jcou.2020.02.012>
- Lin, X., Li, W., Guo, Y., Dong, W., Castel, A., & Wang, K. (2023). Biochar-cement concrete toward decarbonisation and sustainability for construction: Characteristic, performance and perspective. *Journal of Cleaner Production*, 419. <https://doi.org/10.1016/j.jclepro.2023.138219>
- Liu, J., Liu, G., Zhang, W., Li, Z., Xing, F., & Tang, L. (2022). Application potential analysis of biochar as a carbon capture material in cementitious composites: A review. *Construction and Building Materials*, 350. <https://doi.org/10.1016/j.conbuildmat.2022.128715>
- Liu, W., Li, K., & Xu, S. (2022). Utilizing bamboo biochar in cement mortar as a bio-modifier to improve the compressive strength and crack-resistance fracture ability. *Construction and Building Materials*, 327. <https://doi.org/10.1016/j.conbuildmat.2022.126917>
- Liu, Z., & Meng, W. (2021). Fundamental understanding of carbonation curing and durability of carbonation-cured cement-based composites: A review. *Journal of CO₂ Utilization*, 44. <https://doi.org/10.1016/j.jcou.2020.101428>
- Lu, S., & Zong, Y. (2018). Pore structure and environmental serves of biochars derived from different feedstocks and pyrolysis conditions. *Environmental Science and Pollution Research*, 25(30), 30401–30409. <https://doi.org/10.1007/s11356-018-3018-7>
- Ma, Z., Chen, D., Gu, J., Bao, B., & Zhang, Q. (2015). Determination of pyrolysis characteristics and kinetics of palm kernel shell using TGA-FTIR and model-free integral methods. *Energy Conversion and Management*, 89, 251–259. <https://doi.org/10.1016/j.enconman.2014.09.074>
- Maljaee, H., Paiva, H., Madadi, R., Tarelho, L. A. C., Morais, M., & Ferreira, V. M. (2021). Effect of cement partial substitution by waste-based biochar in mortars

properties. *Construction and Building Materials*, 301. <https://doi.org/10.1016/j.conbuildmat.2021.124074>

- Manyà, J. J., García-Morcate, D., & González, B. (2020). Adsorption performance of physically activated biochars for postcombustion CO₂ capture from dry and humid flue gas. *Applied Sciences (Switzerland)*, 10(1). <https://doi.org/10.3390/app10010376>
- Manyà, J. J., González, B., Azuara, M., & Arner, G. (2018). Ultra-microporous adsorbents prepared from vine shoots-derived biochar with high CO₂ uptake and CO₂/N₂ selectivity. *Chemical Engineering Journal*, 345, 631–639. <https://doi.org/10.1016/j.cej.2018.01.092>
- Mehdizadeh, H., Cheng, X., Mo, K. H., & Ling, T. C. (2022). Upcycling of waste hydrated cement paste containing high-volume supplementary cementitious materials via CO₂ pre-treatment. *Journal of Building Engineering*, 52. <https://doi.org/10.1016/j.jobbe.2022.104396>
- Mehdizadeh, H., Shao, X., Mo, K. H., & Ling, T. C. (2022). Enhancement of early age cementitious properties of yellow phosphorus slag via CO₂ aqueous carbonation. *Cement and Concrete Composites*, 133. <https://doi.org/10.1016/j.cemconcomp.2022.104702>
- Mensah, R. A., Shanmugam, V., Narayanan, S., Razavi, S. M. J., Ulfberg, A., Blanksvärd, T., Sayahi, F., Simonsson, P., Reinke, B., Försth, M., Sas, G., Sas, D., & Das, O. (2021). Biochar-added cementitious materials—a review on mechanical, thermal, and environmental properties. *Sustainability (Switzerland)*, 13(16). <https://doi.org/10.3390/su13169336>
- Mishra, G., Danoglidis, P. A., Shah, S. P., & Konsta-Gdoutos, M. S. (2023). Carbon capture and storage potential of biochar-enriched cementitious systems. *Cement and Concrete Composites*, 140. <https://doi.org/10.1016/j.cemconcomp.2023.105078>
- MPOB. (2024). *Overview of the Malaysian Oil Palm Industry in 2023*. <https://bepi.mpob.gov.my/>
- Mulabagal, V., Baah, D. A., Egiebor, N. O., & Chen, W.-Y. (2015). Biochar from Biomass: A Strategy for Carbon Dioxide Sequestration, Soil Amendment, Power Generation, and CO₂ Utilization. *Handbook of Climate Change Mitigation and Adaptation*, 1–31. https://doi.org/10.1007/978-1-4614-6431-0_80-1
- Muthukrishnan, S., Gupta, S., & Kua, H. W. (2019). Application of rice husk biochar and thermally treated low silica rice husk ash to improve physical properties of cement mortar. *Theoretical and Applied Fracture Mechanics*, 104. <https://doi.org/10.1016/j.tafmec.2019.102376>
- Muzyka, R., Misztal, E., Hrabak, J., Banks, S. W., & Sajdak, M. (2023). Various biomass pyrolysis conditions influence the porosity and pore size distribution of biochar. *Energy*, 263. <https://doi.org/10.1016/j.energy.2022.126128>

- Navaratnam, S., Wijaya, H., Rajeev, P., Mendis, P., & Nguyen, K. (2021). Residual stress-strain relationship for the biochar-based mortar after exposure to elevated temperature. *Case Studies in Construction Materials*, 14. <https://doi.org/10.1016/j.cscm.2021.e00540>
- Nguyen, M. V., & Lee, B. K. (2016). A novel removal of CO₂ using nitrogen doped biochar beads as a green adsorbent. *Process Safety and Environmental Protection*, 104, 490–498. <https://doi.org/10.1016/j.psep.2016.04.007>
- Park, J. H., Kim, Y. U., Jeon, J., Yun, B. Y., Kang, Y., & Kim, S. (2021). Analysis of biochar-mortar composite as a humidity control material to improve the building energy and hygrothermal performance. *Science of the Total Environment*, 775. <https://doi.org/10.1016/j.scitotenv.2021.145552>
- Pavlova, P. L., Minakov, A. V., Platonov, D. V., Zhigarev, V. A., & Guzei, D. V. (2022). Supercritical Fluid Application in the Oil and Gas Industry: A Comprehensive Review. *Sustainability (Switzerland)*, 14(2). <https://doi.org/10.3390/su14020698>
- Peyvandi, A., Holmes, D., Soroushian, P., & Balachandra, A. M. (2015). Monitoring of Sulfate Attack in Concrete by Al²⁷ and Si²⁹ MAS NMR Spectroscopy. *Journal of Materials in Civil Engineering*, 27(8). [https://doi.org/10.1061/\(asce\)mt.1943-5533.0001175](https://doi.org/10.1061/(asce)mt.1943-5533.0001175)
- Pham, B. T., Wang, M., Luo, S., & Ling, T.-C. (2024). Addressing workability issue and performance of CO₂-mixed cement pastes. *Construction and Building Materials*, 436, 136800. <https://doi.org/10.1016/j.conbuildmat.2024.136800>
- Praneeth, S., Guo, R., Wang, T., Dubey, B. K., & Sarmah, A. K. (2020). Accelerated carbonation of biochar reinforced cement-fly ash composites: Enhancing and sequestering CO₂ in building materials. *Construction and Building Materials*, 244. <https://doi.org/10.1016/j.conbuildmat.2020.118363>
- Precedence Research. (2023). *Biochar Market Size, Share and Trends 2024-2034*. <https://www.precedenceresearch.com/biochar-marke>
- Promraksa, A., & Rakmak, N. (2020). Biochar production from palm oil mill residues and application of the biochar to adsorb carbon dioxide. *Heliyon*, 6(5). <https://doi.org/10.1016/j.heliyon.2020.e04019>
- Ren, P., Ling, T. C., & Mo, K. H. (2022). CO₂ pretreatment of municipal solid waste incineration fly ash and its feasible use as supplementary cementitious material. *Journal of Hazardous Materials*, 424. <https://doi.org/10.1016/j.jhazmat.2021.127457>
- Ren, Z., Wang, L., Wang, H., Li, M., Liu, S., & Wan, L. (2024). Carbonation behavior of solidified/stabilized cadmium in phosphogypsum slag-based cementitious materials. *Construction and Building Materials*, 437. <https://doi.org/10.1016/j.conbuildmat.2024.136848>
- Restuccia, L., Ferro, G. A., Suarez-Riera, D., Sirico, A., Bernardi, P., Belletti, B., & Malcevschi, A. (2020). Mechanical characterization of different biochar-based

cement composites. *Procedia Structural Integrity*, 25, 226–233. <https://doi.org/10.1016/j.prostr.2020.04.027>

- Roberts, K. G., Gloy, B. A., Joseph, S., Scott, N. R., & Lehmann, J. (2010). Life cycle assessment of biochar systems: Estimating the energetic, economic, and climate change potential. *Environmental Science and Technology*, 44(2), 827–833. <https://doi.org/10.1021/es902266r>
- Sackey, E. A., Song, Y., Yu, Y., & Zhuang, H. (2021). Biochars derived from bamboo and rice straw for sorption of basic red dyes. *PLoS ONE*, 16(7 July). <https://doi.org/10.1371/journal.pone.0254637>
- Saeki, N., Cheng, L., Kurihara, R., Ohkubo, T., Teramoto, A., Suda, Y., Kitagaki, R., & Maruyama, I. (2024). Natural carbonation process in cement paste particles in different relative humidities. *Cement and Concrete Composites*, 146. <https://doi.org/10.1016/j.cemconcomp.2023.105400>
- Sahoo, S. S., Vijay, V. K., Chandra, R., & Kumar, H. (2021). Production and characterization of biochar produced from slow pyrolysis of pigeon pea stalk and bamboo. *Cleaner Engineering and Technology*, 3. <https://doi.org/10.1016/j.clet.2021.100101>
- Saleem, H., Ahmad, M., Rashid, J., Ahmad, M., Al-wabel, M. I., & Amin, M. (2022). Carbon potentials of different biochars derived from municipal solid waste in a saline soil. *Pedosphere*, 32(2), 283–293. [https://doi.org/10.1016/S1002-0160\(21\)60073-5](https://doi.org/10.1016/S1002-0160(21)60073-5)
- Salla, S. R., Modhera, C. D., & Babu, U. R. (2021). An experimental study on various industrial wastes in concrete for sustainable construction. *Journal of Advanced Concrete Technology*, 19(2), 133–148. <https://doi.org/10.3151/jact.19.133>
- Šavija, B., & Luković, M. (2016). Carbonation of cement paste: Understanding, challenges, and opportunities. *Construction and Building Materials*, 117, 285–301. <https://doi.org/10.1016/j.conbuildmat.2016.04.138>
- Schmidt, H. P. (2012). 55 Uses of Biochar. *Ithaka Journal*, 1, 286–289. <https://www.terrapreta.bioenergylists.org/files/e082012-55-uses-of-bc.pdf>
- SEDA Malaysia. (2021). *Malaysia Renewable Energy Road Map: Pathway towards Low Carbon Energy System*. <https://www.seda.gov.my/reportal/myrer/>
- Senadheera, S. S., Gupta, S., Kua, H. W., Hou, D., Kim, S., Tsang, D. C. W., & Ok, Y. S. (2023). Application of biochar in concrete – A review. *Cement and Concrete Composites*, 143. <https://doi.org/10.1016/j.cemconcomp.2023.105204>
- Shaaban, M., Van Zwieten, L., Bashir, S., Younas, A., Núñez-Delgado, A., Chhajro, M. A., Kubar, K. A., Ali, U., Rana, M. S., Mehmood, M. A., & Hu, R. (2018). A concise review of biochar application to agricultural soils to improve soil conditions and fight pollution. *Journal of Environmental Management*, 228, 429–440. <https://doi.org/10.1016/j.jenvman.2018.09.006>

- Shafawi, A. N., Mohamed, A. R., Lahijani, P., & Mohammadi, M. (2021). Recent advances in developing engineered biochar for CO₂ capture: An insight into the biochar modification approaches. *Journal of Environmental Chemical Engineering*, 9(6). <https://doi.org/10.1016/j.jece.2021.106869>
- Shi, C., He, P., Tu, Z., & Cao, Z. (2014). Effect of Preconditioning on Process and Microstructure of Carbon Dioxide Cured Concrete. *Journal of the Chinese Ceramic Society*.
- Shi, Q., Zhang, H., Shahab, A., Zeng, H., Zeng, H., Bacha, A. U. R., Nabi, I., Siddique, J., & Ullah, H. (2021). Efficient performance of magnesium oxide loaded biochar for the significant removal of Pb²⁺ and Cd²⁺ from aqueous solution. *Ecotoxicology and Environmental Safety*, 221. <https://doi.org/10.1016/j.ecoenv.2021.112426>
- Sikora, P., Woliński, P., Chougan, M., Madraszewski, S., Węgrzyński, W., Papis, B. K., Federowicz, K., Ghaffar, S. H., & Stephan, D. (2022). A systematic experimental study on biochar-cementitious composites: Towards carbon sequestration. *Industrial Crops and Products*, 184. <https://doi.org/10.1016/j.indcrop.2022.115103>
- Sirico, A., Belletti, B., Bernardi, P., Malcevski, A., Pagliari, F., Fornoni, P., & Moretti, E. (2020). Effects of biochar addition on long-term behavior of concrete. *Theoretical and Applied Fracture Mechanics*, 122. <https://doi.org/10.1016/j.tafmec.2022.103626>
- Spokas, K. A., Koskinen, W. C., Baker, J. M., & Reicosky, D. C. (2009). Impacts of woodchip biochar additions on greenhouse gas production and sorption/degradation of two herbicides in a Minnesota soil. *Chemosphere*, 77(4), 574–581. <https://doi.org/10.1016/j.chemosphere.2009.06.053>
- Supriya, Chaudhury, R., Sharma, U., Thapliyal, P. C., & Singh, L. P. (2023). Low-CO₂ emission strategies to achieve net zero target in cement sector. *Journal of Cleaner Production*, 417. <https://doi.org/10.1016/j.jclepro.2023.137466>
- Tang, W., Zhan, B., Wu, C., & Kou, S. cong. (2021). Experimental investigation and mathematical modelling of the carbon dioxide sequestration of cement pastes during pressurized CO₂ curing. *Construction and Building Materials*, 302. <https://doi.org/10.1016/j.conbuildmat.2021.124383>
- Tiong, M., Li, X., Mo, K. H., & Ling, T. C. (2022). Effects of moulding pressure and w/c induced pore water saturation on the CO₂ curing efficiency of dry-mix cement blocks. *Construction and Building Materials*, 335. <https://doi.org/10.1016/j.conbuildmat.2022.127509>
- Uday, V., Harikrishnan, P. S., Deoli, K., Zitouni, F., Mahlnecht, J., & Kumar, M. (2022). Current trends in production, morphology, and real-world environmental applications of biochar for the promotion of sustainability. *Bioresource Technology*, 359. <https://doi.org/10.1016/j.biortech.2022.127467>
- UNFCCC. (2015). *Paris Agreement*. <https://unfccc.int/process-and-meetings/the-paris-agreement>

- United Nation. (2023). *Progress towards the Sustainable Development Goals*. <https://unstats.un.org/sdgs/report/2023/>
- Vogler, N., Drabetzki, P., Lindemann, M., & Kühne, H. C. (2022). Description of the concrete carbonation process with adjusted depth-resolved thermogravimetric analysis. *Journal of Thermal Analysis and Calorimetry*, 147(11), 6167–6180. <https://doi.org/10.1007/s10973-021-10966-1>
- Wang, D., Noguchi, T., & Nozaki, T. (2019). Increasing efficiency of carbon dioxide sequestration through high temperature carbonation of cement-based materials. *Journal of Cleaner Production*, 238. <https://doi.org/10.1016/j.jclepro.2019.117980>
- Wang, J., Xu, H., Xu, D., Du, P., Zhou, Z., Yuan, L., & Cheng, X. (2019). Accelerated carbonation of hardened cement pastes: Influence of porosity. *Construction and Building Materials*, 225, 159–169. <https://doi.org/10.1016/j.conbuildmat.2019.07.088>
- Wang, L., Chen, L., Tsang, D. C. W., Guo, B., Yang, J., Shen, Z., Hou, D., Ok, Y. S., & Poon, C. S. (2020). Biochar as green additives in cement-based composites with carbon dioxide curing. *Journal of Cleaner Production*, 258. <https://doi.org/10.1016/j.jclepro.2020.120678>
- Wang, L., Deng, J., Yang, X., Hou, R., & Hou, D. (2023). Role of biochar toward carbon neutrality. *Carbon Research*, 2(1). <https://doi.org/10.1007/s44246-023-00035-7>
- Wei, H., Deng, S., Hu, B., Chen, Z., Wang, B., Huang, J., & Yu, G. (2012). Granular Bamboo-Derived Activated Carbon for High CO₂ Adsorption: The Dominant Role of Narrow Micropores. *ChemSusChem*, 5(12), 2354–2360.
- Xuan, M. Y., Guo, R., Lin, R. S., Wang, X., & Wang, X. Y. (2024). Mechanism of fineness and content of quartz powder on the improvement of carbonation curing efficiency. *Cement and Concrete Composites*, 150. <https://doi.org/10.1016/j.cemconcomp.2024.105570>
- Yang, J., Yue, L., Hu, X., Wang, L., Zhao, Y., Lin, Y., Sun, Y., DaCosta, H., & Guo, L. (2017). Efficient CO₂ Capture by Porous Carbons Derived from Coconut Shell. *Energy and Fuels*, 31(4), 4287–4293. <https://doi.org/10.1021/acs.energyfuels.7b00633>
- Yang, X., Igalavithana, A. D., Oh, S. E., Nam, H., Zhang, M., Wang, C. H., Kwon, E. E., Tsang, D. C. W., & Ok, Y. S. (2018). Characterization of bioenergy biochar and its utilization for metal/metalloid immobilization in contaminated soil. *Science of the Total Environment*, 640–641, 704–713. <https://doi.org/10.1016/j.scitotenv.2018.05.298>
- Yang, X., & Wang, X. Y. (2021). Strength and durability improvements of biochar-blended mortar or paste using accelerated carbonation curing. *Journal of CO₂ Utilization*, 54. <https://doi.org/10.1016/j.jcou.2021.101766>
- Zeidabadi, Z. A., Bakhtiari, S., Abbaslou, H., & Ghanizadeh, A. R. (2018). Synthesis, characterization and evaluation of biochar from agricultural waste biomass for

use in building materials. *Construction and Building Materials*, 181, 301–308.
<https://doi.org/10.1016/j.conbuildmat.2018.05.271>

Zhan, B. J., Xuan, D. X., Poon, C. S., & Shi, C. J. (2016). Effect of curing parameters on CO₂ curing of concrete blocks containing recycled aggregates. *Cement and Concrete Composites*, 71, 122–130.
<https://doi.org/10.1016/j.cemconcomp.2016.05.002>

Zhang, C., Ji, Y., Li, C., Zhang, Y., Sun, S., Xu, Y., Jiang, L., & Wu, C. (2023). The Application of Biochar for CO₂ Capture: Influence of Biochar Preparation and CO₂ Capture Reactors. *Industrial and Engineering Chemistry Research*, 62(42), 17168–17181. <https://doi.org/10.1021/acs.iecr.3c00445>

Zhang, D., Ghoulah, Z., & Shao, Y. (2017). Review on carbonation curing of cement-based materials. *Journal of CO₂ Utilization*, 21, 119–131.
<https://doi.org/10.1016/j.jcou.2017.07.003>

Zhang, D., Li, V. C., & Ellis, B. R. (2018). Optimal Pre-hydration Age for CO₂ Sequestration through Portland Cement Carbonation. *ACS Sustainable Chemistry and Engineering*, 6(12), 15976–15981.
<https://doi.org/10.1021/acssuschemeng.8b03699>

Zhang, D., & Shao, Y. (2016). Early age carbonation curing for precast reinforced concretes. *Construction and Building Materials*, 113, 134–143.
<https://doi.org/10.1016/j.conbuildmat.2016.03.048>